CATÓLICA
ESCOLA SUPERIOR DE BIOTECNOLOGIA
PORTO

FLOW-BASED METHODS FOR IODINE AND IRON QUANTIFICATION IN FOOD-RELATED, WATER, AND BLOOD SERUM SAMPLES

Thesis submitted to *Universidade Católica Portuguesa* to attain the degree of PhD in Biotechnology, with specialization in Chemistry

Joana Lopes Abreu Miranda

December 2021

CATÓLICA
ESCOLA SUPERIOR DE BIOTECNOLOGIA
PORTO

FLOW-BASED METHODS FOR IODINE AND IRON QUANTIFICATION IN FOOD-RELATED, WATER, AND BLOOD SERUM SAMPLES

Thesis submitted to *Universidade Católica Portuguesa* to attain the degree of PhD in Biotechnology, with specialization in Chemistry

Joana Lopes Abreu Miranda

Supervisor: António O. S. S. Rangel, Full Professor
Co-supervisor: Raquel B. R. Mesquita, Ph.D.

December 2021

To those who never let me give up and inspired it,

Artur, Sérgio, Mariana and João

Abstract

Abstract

In this thesis, the use of different flow systems was exploited for developing new methodologies for miniaturization of the analysis of complex matrix samples (food-related, water and biological samples). The main purpose was to devise methodologies able to perform in-line the necessary sample treatment operations, reducing the operator influence and reagents manipulation, and tentatively using greener processes.

Under this program, a flow-based spectrofluorimetric chip manifold method for the iodine determination in food-related samples, was developed. The use of a multi-syringe enabled the automation of the Sandell-Kolthoff reaction, leading to a lower operator influence and reagents consumption and manipulation. An in-line oxidation process was implemented to analyse samples with organo-iodine containing compounds; this implied to eliminate interferences and decomposition of organo-iodine compounds in supplement pills and seaweed samples (Chapter 3). The developed method was effectively applied to the iodine determination in salt, food supplements (algae), seaweed and pharmaceutical samples, which are examples of intake forms of iodine. The proposed manifold, combined with the fluorometric reaction, made this method more sensitive than the classic approach of the Sandell-Kolthoff reaction and presents some advantageous over previously described flow methods, namely in terms of a wider dynamic concentration range. The method allowed to determine iodine within a range of 0.20 – 4.0 µmol/L, with or without the in-line UV digestion, with a limit of detection of 0.028 µmol/L and 0.025 µmol/L, respectively.

In Chapter 4, an hexadentate 3-hydroxy-4-pyridinone (3,4–HPO) ligand was used as a chromogenic reagent for the spectrophotometric quantification of iron(III) in fresh and sea waters. A method based on a micro sequential injection lab-on-valve (µSI-LOV) system in a solid phase spectrometry (SPS) mode, is described. To implement SPS, a packed column of nitrilotriacetic acid superflow resin (NTA) in the flow cell, was used, consequently eliminating the sample matrix. Furthermore, the possibility to perform of an analytical curve resorting to just one standard was demonstrated. The consumption of the hexadentate 3,4–HPO ligand was about 30 µg per determination and the effluent production lower than 2.5 mL. The dynamic concentration range was 0.45 – 9.0 µmol/L, with a limit of detection of 0.13 µmol/L and limit of quantification 0.43 µmol/L. The proposed µSI-LOV-SPS methodology was successfully applied to river, ground, estuarine, tap, and sea waters.

The evaluation of the analytical performance of different 3,4–HPO bidentate chelators, as chromogenic reagents in the determination of iron(III), using a µSI system, in aqueous samples, was described in Chapter 5.

In Chapter 6, a bidentate 3-hydroxy-4-pyridinone ligand was anchored to sepharose beads and used as chromogenic reagent for the spectrophotometric quantification of non-transferrin-bound

iron (NTBI). By employing a micro sequential injection lab-on-valve (μSI-LOV) system with a SPS technique, it was possible to eliminate the interference of the sample matrix and quantify iron(III) directly on the beads surface. The dynamic concentration range was 1.62 – 7.16 μmol/L, with a limit of detection of 0.49 μmol/L and limit of quantification 1.62 μmol/L. The proposed μSI-LOV-SPS method, in Chapter 6, was a contribution to the development of an automated method for the quantification of the NTBI in serum samples.

Keywords: Iodine, Iron, Flow based systems, 3,4–hydroxypyridinone ligands, food and biological samples.

Resumo

Resumo

Nesta tese de doutoramento foi explorada a utilização de diferentes sistemas de fluxo para o desenvolvimento de novas metodologias para a miniaturização da análise de amostras com matrizes complexas (amostras alimentares, águas naturais e biológicas). O objetivo principal era desenvolver metodologias capazes de realizar, em linha, os tratamentos de amostra necessários, reduzindo a influência do operador e a manipulação de reagentes, e tentativamente usando processos mais verdes.

No âmbito deste programa doutoral, foi desenvolvido um método de fluxo espectrofluorimétrico, utilizando um "chip", para a determinação de iodo em amostras alimentares. Para a automatização da reação de Sandell-Kolthoff, utilizou-se uma multi-seringa, possibilitando uma menor influência do operador, consumo e manipulação de reagentes. Foi implementado um processo de oxidação em linha para a análise de amostras contendo compostos iodo-orgânicos, implicando a eliminação de interferências e decomposição de compostos iodo-orgânicos em comprimidos de suplemento e amostras de algas (Capítulo 3). O método desenvolvido foi aplicado na determinação de iodo em amostras de sal, suplementos (algas), algas e amostras farmacêuticas, enquanto exemplos de formas de ingestão de iodo. O sistema proposto, combinado com a reação fluorimétrica, tornou este método mais sensível do que a abordagem clássica da reação de Sandell-Kolthoff e apresentou algumas vantagens em relação aos métodos de fluxo descritos anteriormente, nomeadamente em termos de intervalo de determinação, apresentado um intervalo amplo. O método permitiu determinar o conteúdo em iodo no intervalo de 0,20 - 4,0 µmol/L, com um limite de deteção de 0,028 µmol/L e 0,025 µmol/L, com ou sem a digestão-UV em linha, respetivamente.

No Capítulo 4 foi utilizado um ligando de 3-hidroxi-4-piridinona (3,4–HPO) hexadentado como reagente cromogénico para a quantificação espectrofotométrica de ferro(III) em águas doces e marinhas. O método descrito foi desenvolvido para um micro-sistema de injeção sequencial lab-on-valve (µSI-LOV) utilizando espectrofotometria de fase sólida (SPS). Para a implementação da SPS, foi utilizada uma coluna compactada de resina de ácido nitrilotriacético (NTA) na célula de fluxo, possibilitando a eliminação da matriz da amostra. Além disso, foi demonstrada a possibilidade de realização de uma curva de calibração recorrendo a apenas um padrão. O consumo de ligando 3,4-HPO hexadentado foi de cerca de 30 µg por determinação e a produção de efluente inferior a 2,5 mL. O intervalo de determinação foi de 0,45 - 9,0 µmol/L de ferro(III), com limite de deteção de 0,13 µmol/L e limite de quantificação de 0,43 µmol/L. A metodologia µSI-LOV-SPS proposta foi aplicada com sucesso a amostras de águas de rios, subterrâneas, estuarinas, de torneira e do mar.

No Capítulo 5 foi descrita a utilização de um sistema μSI para a avaliação do desempenho analítico de diferentes quelantes bidentados de 3,4–HPO, como reagentes cromogénicos para a determinação de ferro(III), em amostras aquosas.

No Capítulo 6, um ligando bidentado de 3-hidroxi-4-piridinona foi ancorado a esferas de sefarose e utilizado como reagente cromogénico para a quantificação espectrofotométrica de ferro não ligado à transferrina (NTBI). Utilizando um micro-sistema de injeção sequencial lab-on-valve (μSI-LOV) com a técnica de SPS, foi possível eliminar a interferência da matriz da amostra e quantificar o ferro diretamente na superfície das esferas funcionalizadas de sefarose. O intervalo de determinação foi de 1,62 - 7,16 μmol/L, com um limite um de deteção de 0,49 μmol/L e um limite de quantificação de 1,62 μmol/L. O método μSI-LOV-SPS, proposto no Capítulo 6, foi uma contribuição para o desenvolvimento de um método automatizado para a quantificação do NTBI em amostras de soro.

Palavras-chave: Iodo, ferro, sistemas de fluxo, ligandos 3,4–hidroxipiridinona, amostras alimentares e biológicas

Acknowledgements

Acknowledgements

To Escola Superior de Biotecnologia – Universidade Católica Portuguesa for receiving me first as a graduation student, as master student and then as a PhD student, providing the necessary conditions to complete the work I developed and for giving me the opportunity of teaching undergraduated students, what was an enrichment experience.

To Fundo Social Europeu for the financial support and for the grant NORTE-08-5369-FSE-000007_BD_1, to accomplish this important mark on my professional life.

To my supervisor, Professor Doutor António Rangel, my special thanks for the knowledge and scientific guidance, which was crucial for my professional growth. I would also like to express my gratefulness for the sincere friendship and all the support, patience, care and advice.

To my co-supervisor, Doutora Raquel Mesquita, who guided and oriented me throughout the work developed during this PhD experience.

To Professor Doutor Víctor Cerdà, for receiving me in his group in University of the Balearic Islands, Spain, my special thanks for the friendship and support during my stay abroad.

To Professor Doutor José M. Estela and Doutor Edwin Palacio, for guiding me during my stay in the University of the Balearic Islands, Spain.

To Ana Machado and André Silva who kindly provided samples whenever requested.

To Susana Vidigal for all the support and friendship.

To all the colleagues and friends that shared a workplace with me, with whom I had the pleasure of sharing with me your time and had taught me something every day.

To Tânia (Tânocas) for being always my person, my friend, for giving me strength, support, and guidance when I needed. Even a bad day would turn into a goofy and special one. Thank you for helping me grow professionally and individually.

To my friends (Inês Santos, Ana Laly, Ana Luísa Oliveira and Rita Costa) who encourage me through this crazy time.

To my godmother, Ilva, that always have an encouraging word in the most difficult times and supports me through all my life decisions.

To my mother for being always by my side, no matter what. The person that made me keep fighting for my dreams when everyone said that it would probably never happen. Thank you for keep pushing me to always be better and more. To my father for the patience and understanding of my difficult temper in the more stressed occasions, that were a lot during this PhD experience. Thank you both for raising me and making me the person that I am today.

To my husband Sérgio, that inspired all the PhD theme, my case study. Thank you for all the patience during all these years, for being always by my side. Thank you for the sacrifices you made to make this possible. Without your love none of this would be possible.

To my baby boy, Artur, who fulfilled my life, gave me a new meaning and willingness to my ambitions and dreams.

Table of Contents

Table of Contents

Chapter 2 – General Materials and Methods

Chapter 3 - Chip-based spectrofluorimetric determination of iodine in a multi-syringe flow platform with and without in-line digestion – application to salt and algae samples

Chapter 4 – Measurement of iron(III) in waters by microsequential injection solid phase spectrometry using an hexadentate 3-hydroxy-4-pyridinone chelator as reagent

Chapter 5 – New hydrophilic 3-hydroxy-4-pyridinone chelators with ether-derived substituents: synthesis and evaluation of analytical performance in the determination of iron in waters

List of Abbreviations

List of Abbreviations

μSI – Micro sequential injection

μSIA – Micro sequential injection analysis

μSI – LOV – Micro sequential injection Lab-on-valve

3,4–HPO – 3-hydroxy-4-pyridinones

AAS – Atomic absorption spectroscopy

AC – Analytical curve

BI – Bead injection

BSA – Bovine serum albumin

C – Carrier

CCD – Charged coupled device

CP256 – Hexadentate 3-hydroxy-4-pyridinone chelator

F – irradiation

FC – Flow cell

FIA – Flow injection analysis

HC – Holding coil

ICP-MS – Inductively coupled plasma mass spectrometry

ID – Iron deficiency

IDA – Iron deficiency anaemia

IV – Injection valve

LOD – Limit of detection

LOQ – Limit of quantification

LOV – Lab-on-valve

MQW – Milli-Q water

NIS – Na^+/I^- symporter

NTA – Nitrilotriacetic acid

NTBI – Non-transferrin-bound iron

OF – Optical fibers

P – Pump

PMMA – Poly(methyl methacrylate)

PTFE – Polytetrafluoroethylene

R_i – Reagents

RSD – Relative standard deviation

S_i /SP– Syringe pumps

SD – Standard deviation

SIA – Sequential injection analysis

SPE – Solid phase extraction

SPS – Solid phase spectrometry

SV – Selection valve

RC – Reaction coil

RD – Relative deviation

T3 – Triiodothyronine

T4 – Thyroxine

TPO – Thyroid peroxidase

TSH – Thyroid-stimulating hormone

TRF – Thyrotropin-releasing factor

V_i – Solenoid valve

W – Waste

Chapter 1

General Introduction

The increasing demand for new analytical methods involving more automatic and less expensive techniques, made flow methodologies potentially useful tools to fulfil these needs. In addition, the concept of green chemistry is receiving more attention, as one more contribution to minimize environmental pollution, from industry to research. Due to the above-mentioned reasons, new flow methodologies are required. These novel methods aim at achieving miniaturization, lower consumption of samples and reagents, and lower waste production. Portability of the associated equipment in flow systems is also an important asset for field analysis. All these characteristics make flow methodologies a good candidate to respond to the need for the automation of the analysis of complex matrices, such as biological samples, in which the available volume is often limited. To analyse these complex biological samples, several pre-treatments are required, namely dilution, pre-concentration, and elimination of interferences, normally carried out in a conventional manual way. Flow methodologies have privileged characteristics to analyse complex samples, preventing the need for off-line pre-treatments steps by enabling to do in-line the required treatments. In this scenario, the work on this thesis is a contribution to developing novel methods for health-related parameters.

In this general introduction section, the framework of the methodologies/applications to be developed, as well as the main topics addressed in this thesis, are presented. The details about the background of each developed method are presented in the respective chapters.

1.1 Iodine and iron in biological and environmental matrices

1.1.1 Iodine

Iodine can be found in abundance in the oceans, as iodide, being present in the aquatic environment of the earth, but is rare in most parts of the terrestrial environment. This absence leads to iodine deficiency in plants, animals grown on these soils and consequently in populations in such areas (1,2).

Iodine is a nutrient and a component of the thyroid hormones essential for human growth and development (3). Iodide, in both inorganic and organically bound forms, is rapidly and efficiently absorbed from the gastrointestinal tract (within 30 minutes), and little is lost in the stool. In the body, iodide is confined mainly to the extracellular fluid, but it is also found in red blood cells and is concentrated in the intraluminal fluids of the gastrointestinal tract, particularly the saliva and gastric juice, from which it is reabsorbed, re-entering the extracellular fluid.

Iodide uptake is a critical first step in thyroid hormone synthesis. Ingested iodine is normally bound to serum proteins, particularly albumin, being extracted by the thyroid gland from the circulation in a highly efficient manner. Unbound iodine is excreted in the urine, being excreted more than 90% of ingested iodine (4,5).

The thyroid gland develops during the third week of gestation. Thyroxine (T4) structure contains four iodine atoms and, after deiodination, leads to the formation of the hormone triiodothyronine (T3), or the inactive hormone reverse T3.

The uptake mechanism for iodide is mediated and regulated by the Na^+/I^- symporter (NIS), which is expressed at the basolateral membrane of thyroid follicular cells. This is a transport mechanism highly regulated, permitting the adaptation to variations in dietary supply, increasing or suppressing the amount of NIS, however, is high or low iodine levels. Still, this requires the daily thyroidal uptake of sufficient iodide and its oxidation by thyroid peroxidase (TPO) to allow the synthesis of the thyroid hormones (5).

The processes in the thyroid are differently activated during low and high iodine intakes, possibly making the type of disease that dominates thyroid pathology in populations different, depending on the level of iodine intake. In an individual, the risk of having a thyroid disease will depend on the level of iodine intake and on fluctuations in iodine intake, the genetics of the individual, as well as exposure to other environmental factors.

A normal thyroid gland can adapt and keep thyroid hormone production within the normal range even in less severe iodine deficiency. The thyroid gland contains enough stored hormone to last for

about two months, permitting a constant amount of hormone despite significant variations in the availability of iodine. However, if the deficiency is prolonged, the reservoirs of thyroxine can be depleted. Prolonging thyroid hyperactivity associated with such adaptation leads to thyroid growth. Studies now indicate that just a small change in the level of iodine intake will lead to a frequency decrease of some thyroid disorders, but other types of disease will become more common (1).

The intake of iodine is crucial for nervous system function throughout life, but particularly during fetus development, as it is required for thyroid hormone synthesis. The lack of the adequate iodine intake can lead to maternal hypothyroidism and hypothyroxinaemia, being associated with adverse psychomotor development, correlated to attention deficit, hyperactivity disorders and autism, influencing mood and behaviour (6). The increase in thyroid hormone production, in pregnant and lactating women's, make iodine requirements increase by 50% (7).

As iodine can be found mainly in the aquatic environment of the earth, the intake of iodine in Portugal was neglected due to the proximity of the ocean. Recently, some major concerns have arisen from the observation of iodine deficiency in Portuguese pregnant women (8). Furthermore, studies in the scholar age Portuguese population concluded that we are close to the lower limit of the recommended iodine intake (9). In Portugal, results point to an inadequate iodine intake in pregnant women (8), being recommended an iodine supplementation during pregnancy with 150-200 µg/day (10).

Iodine deficiency is now a major public health concern in Europe, as it seems to be re-emerging since iodine deficient is affecting a significant part of the population (11). When assessed iodine nutrition during pregnancy, two-thirds of the countries reported inadequate iodine intakes (7).

Marine foodstuffs, fish, shellfish, algae, and sea salt are the main sources of iodine, in the human diet (12). More than 120 countries around the world had implemented salt iodization programmes and many of them have successfully eliminated iodine deficiency disorders or made progress in their control (13,14). Salt iodization is a highly cost-effective strategy to prevent iodine deficiency (14). Most of Europe has remained iodine deficient, even though, over the past four decades, occurred a major global expansion of salt iodization (15). Many countries tackle the worldwide iodine deficiency problem with different approaches. Some only use fortified household salt, whereas others use iodisation in all consumed salt or salt for specific products, such as bread.

An alternative to iodized salt is the use of naturally iodized salt (marine salt) and seaweed as an iodine source. In Portugal, marine salt, by itself, contains a naturally high amount of iodine. Even though this high quantity of iodine is in marine salt, it is still required to fortify it, to be used as an effective alternative to fight iodine insufficiency (12).

A considerable amount of consumers in the world consume natural products over artificial ones (16). In several Asian countries, eatable seaweed products are normally and abundantly consumed, as they are low in calories and full of nutrients (17). The use of iodine-rich seaweed for

consumption is a method largely used by Japan, being the only population in the world with excessive intake of iodine (1). Iodine is accumulated from seawater into seaweeds making them a good dietary source of iodine. Disorders resulted from iodine deficiency can be eliminated with adequate consumption of seaweed (17).

In conclusion, iodine enters the food chain following its incorporation by plants (soil), water and animals because of evaporation and deposition from the ocean. Iodine can also enter the body via medications, diagnostic agents, dietary supplements, and food additives. Ultimately, the diet is its most important source (18).

Therefore, the World Health Organization released a combination of different studies of urinary iodine concentration from 6-to 12-year-old children, expressed as the median in mg/L, being used to classify a population's iodine status. The median urinary iodine concentrations used to assess iodine nutrition in the population are: for levels of insufficient intake within <0.16 to 0.78 µmol/L, adequate levels of 0.79 to 1.57 µmol/L, above requirement levels 1.58 to 2.36 µmol/L and excessive levels ≥2.36 µmol/L of iodine (13,19).

In this scenario, in this thesis, a new method for the quantification of the iodide present in possible food supplement samples is presented. The current methods for the determination of this parameter are stated in the introduction of chapter 3 as well as the innovation to be proposed in this thesis.

1.1.2 Iron

Iron is essential for human health because of its role in oxygen transport in the body and participation in redox reactions. In the body, the iron is in the form of iron-containing compounds, and they are grouped into two categories: metabolic or enzymatic functions and iron storage and transport.

Most of the iron in the body is found within the erythrocyte cycle. The main iron-containing protein is haemoglobin in erythrocytes and it is about two-thirds of the body iron. Erythrocytes are continually produced in the bone marrow (lasting 120 days) and most of the iron comes from the breakdown of old erythrocytes and only a small portion comes from the absorption of food iron (20). Body iron homeostasis main step is intestinal iron absorption because of low iron excretion (21). It is absorbed mostly in the duodenum by an active process that transports iron from the gut lumen into the mucosal cell, where it is transferred across the cell into the circulation when needed.

The major iron storage compounds are ferritin and hemosiderin. Large quantities of ferritin are present in iron storage tissue such as the liver, spleen, and bone marrow. Can be also small quantities present in human serum.

Transferrin is a specific carrier protein, responsible for the extracellular transport of iron within the body. Transferrin accounts for only about 0.1% of the total body iron and its movement through the plasma compartment is controlled by the number of transferrin receptors, on the surface of body cells. The synthesis of transferrin receptors is upregulated when a cell senses a need for iron, allowing it to compete more effectively for circulating transferrin iron (20). When iron intake is lower than iron requirements, iron is mobilized from the iron stores in the body. This stage is characterized by a decrease in the concentration of serum ferritin. Then, occurs a decrease in transported iron. In serum, iron concentrations decrease, transferrin (total iron-binding capacity) levels increase, and hence transferrin saturation (serum iron/total iron-binding capacity) is reduced (22).

When iron intake is higher than iron requirements, there is free, unbound iron, being incompatible with either plasma iron transport (precipitate) or with intracytosolic iron circulation (damaging the cellular environment). Consequently, iron must be bound with appropriate ligands (23).

This means that iron homeostasis is tightly regulated, avoiding in one hand, iron deficiency and excess on the other hand. A critical situation happens when there is the need to excrete iron, as there is no active mechanism to do it, in case of systemic iron overload.

Iron overload is developed when the mechanisms responsible for regulating the iron absorption are altered (genetic mutations, ineffective erythropoiesis) or bypassed (red blood cell transfusion, intravenous iron application) (24).

Non-transferrin-bound iron (NTBI) appears when iron influx into the plasma compartment exceeds iron efflux, in iron overload, ineffective erythropoiesis, or decreased transferrin iron clearance in erythroid hypoplasia (22). The term NTBI denotes the forms of iron in serum that are bound to ligands other than transferrin. These biomolecules are loosely bound to iron, in such a way that it retains its ability to catalyse the formation of reactive oxygen species. They represent iron bound to serum albumin, citrate and other undefined negatively charged ligands (25).

Several clinical stages of NTBI have been reported, such as thalassemia, hemochromatosis and in patients receiving chemotherapy (26).

Hemochromatosis is a homochromatic genetic disease, that is characterized by an overload of hepatic iron. The disease can have different characteristics, be hereditary, increase transferrin saturation, deposition of iron and alterations in the production, regulation, or activity of hepcidin. Hepcidin is a hepatic peptide responsible for the iron metabolism function regulation, inhibiting the excretion of the iron from cells, to guarantee iron homeostasis (27). It is estimated that, on average, around 1:260 of the Caucasian population is affected by hereditary hemochromatosis type I, being a common human genetic disease (90% of the cases correspond to the type I of hemochromatosis) (27–29). It is characterized by a mutation on the HFE gene (C282Y), affecting indirectly the hepcidin function.

The origin of this mutation was probably in the north of Europe, as it has a higher expression in this area. It is frequent in individuals with Nordic and Celtic ancestry, with a prevalence of one case in every 220-250 people (29). In Portugal, it is also present, mainly in the north of the territory, possibly linked to the invader origins, from the Celtic and Swabians. Thought, the south of the country was occupied for a long time by the Moors, justifying the reduced incidence of this mutation. Also, the fact that the malaria disease incidence was superior in the south of Portugal, translated into a disadvantage and worked as a natural selection for these individuals with the C282Y mutation (27,29).

As it is a disease with a high prevalence in the population, it is important to have methods that can quantify the NTBI. Plasma NTBI is detectable when transferrin saturation exceeds 75%. Quantifying NTBI value is important to understand its emergence, under different pathophysiological settings, but can also be potentially useful in the management of iron-overloaded patients (22).

One of the guidance parameters for the evaluation of iron overload is normally done with the quantification of the serum ferritin (when it is equal to or higher than 1000 ng/mL). The current

guidelines for treatment methodologies recommend the use of oral iron chelates (using deferiprone or deferasirox) or phlebotomy procedure, for removing iron from the body (24).

There are also health problems with iron deficiency, affecting the cognitive development in childhood, immune function and pregnancy outcomes (18).

During pregnancy, iron requirements increase; the same happens with iodine. Low maternal iron levels induce preterm delivery, low birth weight and iron deficiency in children (30).

Iron deficiency, particularly and iron deficiency anaemia (IDA), remains a severe nutritional deficiency and it is also associated with alterations in many metabolic processes, such as the effects on thyroid metabolism (20). Anaemia is a result of an extensive variety of causes, but it is commonly assumed that approximately half of the reported cases are due to iron deficiency. It is estimated that this deficiency often co-exists with iodine deficiency (18).

In this scenario, in this thesis, new methods for the determination of iron with new low toxicity chromogenic reagents, are presented. Although the final aim was to develop a method for the NTBI determination based on an hydroxypyridinone, an option was made to firstly develop a method for the determination of iron in water samples. In principle, this application would be simpler, and the results could be further used to extend to the NTBI assessment in blood serum. The current methods for the determination of this parameter are presented in the introduction of chapters 4, 5 and 6, as well as the innovation to be proposed in this thesis.

1.1.3 Iron and iodine and their Influence on thyroid hormones production

Thyroid hormones are transferred from mother to fetus, being the initial of fetal thyroid function, so it is important the maternal thyroid sufficiency in early pregnancy (31). The first steps of thyroid hormones biosynthesis depend on thyroid peroxidase (TPO), that is a glycosylated heme protein that catalyses the iodination of thyroglobulin, to produce T4 and T3 hormones (32). This heme protein bound to ferriprotoporphyrin IX is necessary for thyroid peroxidase function (31).

Thyroid peroxidase (TPO) is also an autoantigen in several autoimmune thyroid disorders, so antibodies are produced against it. These disorders, such as Hashimoto's thyroiditis and Graves' disease, consist in immune responses towards thyroid proteins. The sera from patients are routinely tested to quantify the presence of antibodies to TPO to indicate the differential diagnosis of thyroid disorders (33).

The significant decrease of TPO activity in iron deficiency anaemia suggests that thyroid status alterations could be due to a deficiency in iron-dependent enzymes, considering the crucial role of heme in TPO activity, that interfere with iodine and thyroid metabolism (34,35). So, considering the crucial role of heme in TPO activity, IDA could lower TPO activity and thereby interfere with iodine and thyroid metabolism (35).

The synthesis process of the thyroid hormones production, in the thyroid gland, is controlled and stimulated by the thyroid-stimulating hormone (TSH). Therefore, this hormone is essential to human development as it is responsible for regulating the body metabolism. In response to an increase or decrease in the concentration of thyroid hormones, TSH production is either inhibited or elevated (36).

The excess of iron in the body due to the presence of NTBI can lead to a defective TSH secretion. The accumulation of iron in the pituitary gland and its effects on its size and functions have been reported in many studies. In some patients have been reported iron deposition in the thyroid gland, which can suggest being responsible for the thyroid damage, dysfunction and, eventually, failure (37).

So, there is evidence that the deficiency or overload of iron, leads to different alterations in the thyroid hormone synthesis (Figure 1.1), leading to thyroid dysfunction.

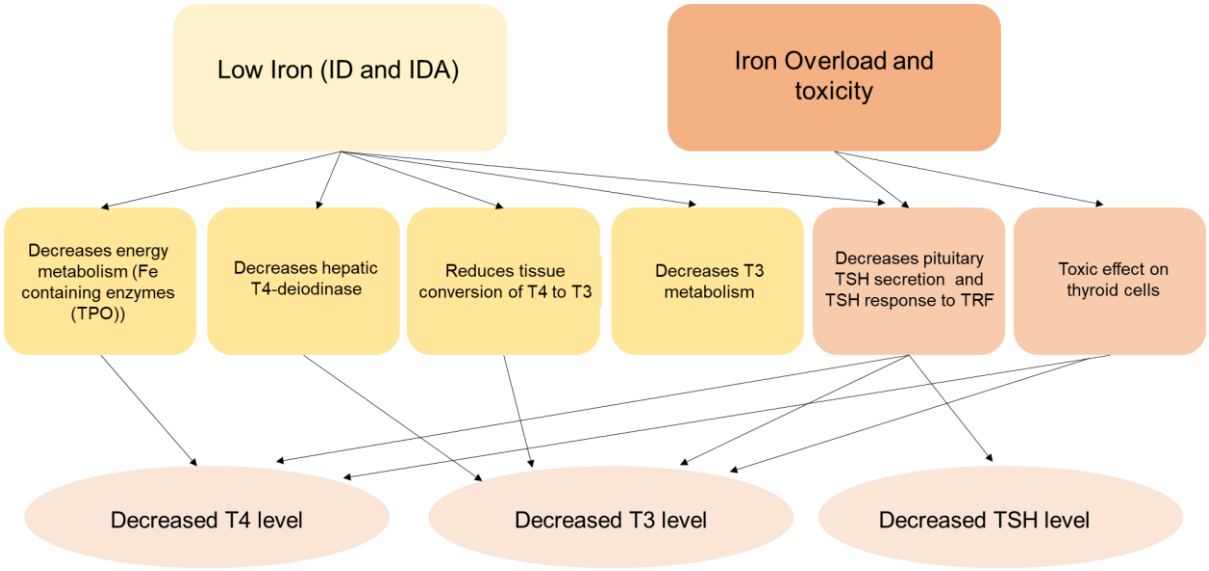

Figure - 1.1 Mechanisms of thyroid dysfunction in iron deficiency or overload: ID, iron deficiency; IDA, iron deficiency anemia; T3, triiodothyronine; T4, thyroxine; TSH, thyroid-stimulating hormone; TPO, thyroid peroxidase; TRF, Thyrotropin-releasing factor - Adapted from Soliman *et al*. Acta Biomed. 2017 (37).

There is evidence of a strong interaction between iron and iodine and thyroid metabolism. Randomised controlled intervention trials have shown that providing iron along with iodine either as an iron supplement or as dual fortification of salt, can benefit the iodine prophylaxis programme, resulting also in significant improvement of thyroid metabolism (18,38).

There is the need to monitor the amount of iron present in the serum to prevent the disruption of the iron homeostasis in the human body. In this way, supplementation or chelate therapy is needed to rebalance the iron status in the body. Adequate correlation with nutrition and early diagnosis and management of thyroid dysfunction can improve the outcome of several patients (37).

1.1.4 Hydroxypyridinones as chromogenic reagents for iron

Aiming for less toxic reagents to be used for the iron determination, hydroxypyridinones were used in this thesis as chromogenic reagents. A wide variety of hydroxypyridinones can be synthesized from hydroxypyranones, which in a large number occur in the plant kingdom, to have the main function of forming complexes with most metal cations. Hydroxypyridinones and their complexes have been applied in several areas of diagnosis and therapy of some diseases, as ex. chelation therapy. These ligands are composed of hydroxylic and ketonic oxygen atoms at appropriate positions on the heterocyclic rings becoming potentially chelating ligands, as their anions form stable complexes with a range of metal ions. This group of ligands includes: 3-hydroxy-2-pyranones, 3-hydroxy-4-pyranones, and the closely related 3-hydroxy-2-pyridinones, 3-hydroxy-4-pyridinones, and 1-hydroxy-2-pyridinones (39).

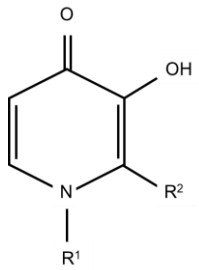

Figure - 1.2 General formulae for 3-hydroxy-4-pyridinones.

The synthesis of 3-hydroxy-4-pyridinones (3,4–HPO) ligands (Figure 1.2) and their complexes with M(II) and M(III) metal ions have been studied for several applications (40). The 3,4–HPO ligands form stable complexes with metal ions, particularly with a high capacity to trap iron(III) (41). The assessment of iron is frequently performed by molecular absorption spectrometry using relatively toxic reagents, as bathophenanthroline, thiocyanate, 1,10-phenantroline, 2,2-bipyridyl, eriochrome cyanine R and cetyltrimethylammonium (42). The 3,4–HPO ligands, known for their biomedical applications, could be particularly attractive as a less toxic chromogenic reagent for the same purpose. The possibility of tailoring these ligands structure, allowing hydrophilic/lipophilic balance without significantly changing its chelating properties, is an advantage (41). The structures are synthetically versatile, allowing to develop bidentate and hexadentate chelators. The last is based on a tetrahedral structure, consisting in three bidentate 3,4–HPO chelating units, linked via amide bonds. This ligand has high affinity for iron, providing a 1:1 stoichiometry and a lower kinetic lability (43,44). The use of the 3,4–HPO as a ”more sustainable” alternative and less toxic chromogenic

and selective reagent was studied, for the determination of iron in water (40,41,44,45). The application of these ligands as chromogenic reagents using flow analysis techniques was firstly proposed in a collaboration between our group and a group in bioinorganic chemistry from REQUIMTE, Universidade do Porto (40,41,44,45), with a large experience in synthesis and characterization of the above-mentioned ligands. The possibility of tailoring a 3,4–HPO ligand to have the required characteristics for iron determination in complex matrices is an advantage when the analysis of biological samples, as the quantification of NTBI in serum, is intended.

1.2 Flow Analysis Systems

1.2.1 Flow Injection Analysis

The first flow injection analysis (FIA) system was described over 40 years ago (46). It consisted of a new approach for the quantification of an analyte, based on a continuous flow of solutions. The sample is injected in this flow, reagents are added in confluences and the product is directed to the detector (Figure 1.3).

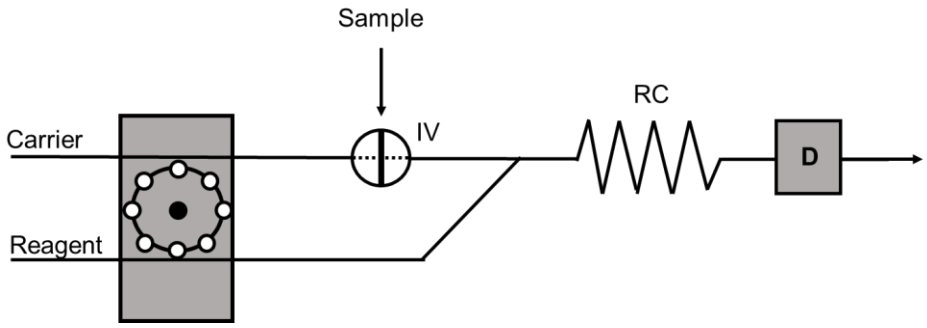

Figure - 1.3 – Schematic representation of a flow injection analysis generic manifold; IV: injection valve; RC: reaction coil; D: detector.

The main principle was that no physical and chemical equilibria must be attained, as long as the conditions are the same for samples and standards. This principle is radically different from previous automation approaches (Segmented Flow Analysis, (47)) and from conventional methods based on steady-state measurements.

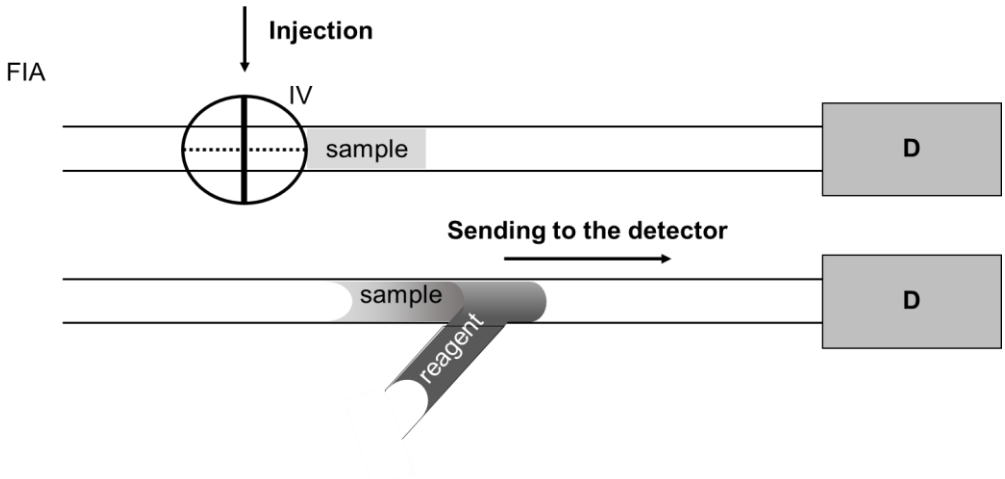

Figure - 1.4 Schematic representation of sample introduction and mixture in FIA: IV, injection valve; D: detector.

The mechanisation of chemical analysis allowed the execution of a high number of repetitive experiments and prevented the operator from handling hazardous materials. Samples and reagents are mixed (Figure 1.4) and can have a variety of intermediate implemented operations, incorporating continuous (in-line) sample preparation units (as dialysis, extractors, digestors, etc) (47).

1.2.2 Sequential Injection Analysis

Several flow analysis modes were proposed since the first flow injection analysis system described in the previous section. Aiming to overcome some limitations attributed to flow injection systems, namely a continuous consumption of reagents, and the need for one manifold for each analyte, the Sequential Injection Analysis (SIA) technique was proposed (48).

Although SIA is based on the same principles (non-equilibrium, controlled dispersion) of the FIA, the differences are mainly related with the dispersion patterns inside the systems.

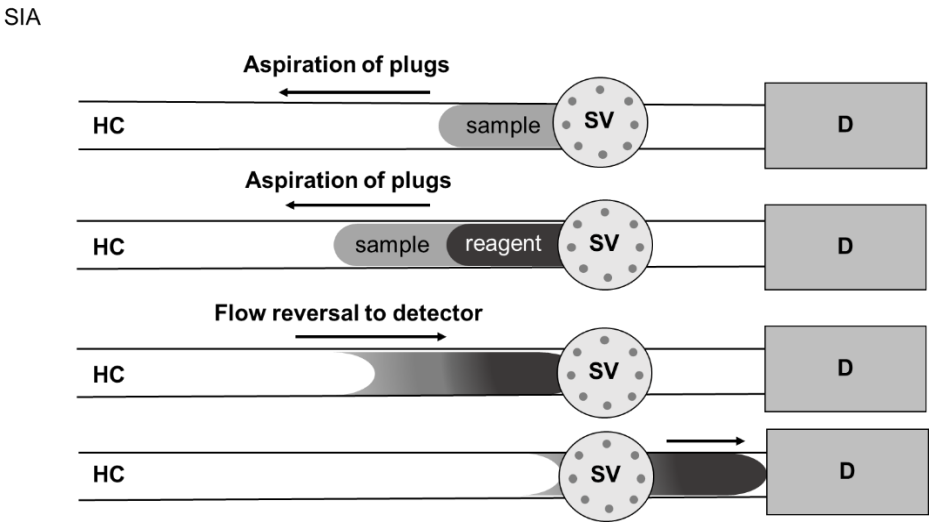

Figure - 1.5 Schematic representation of sample introduction and mixture in SIA system: HC: holding coil; SV: selection valve; D: detector.

Unlike what happens in FIA technique, in which the sample is injected in the system through an injection valve and mixed with the continuous flow of reagents in confluence points, resulting in a concentration gradient (Figure 1.4), in SIA, samples and reagents are placed in each port of a selection valve and aspirated, in a specific order, to the holding coil tube. Then, solutions are propelled in the reverse direction, promoting the mixture on the way to the detector (Figure 1.5).

Both methods allow to analyse samples in real-time, but computer-control is essential in SIA in order to control the pump and synchronise the pump and valve movements (Figure 1.5).

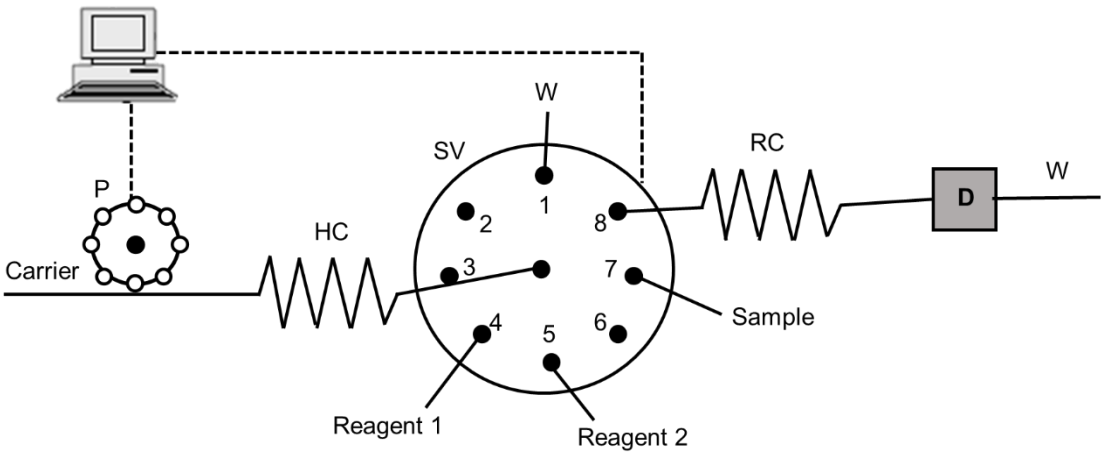

Figure - 1.6 Schematic representation of a Sequential Injection Analysis (SIA) system: P: propulsion device; HC: holding coil; RC: reaction coil; SV: eight port selection valve; D: detector; W: waste.

One of the advantages of the SIA is that the volume of dispensed reagents is just the required amount. Additionally, the carrier is not pumped continuously, leading to a low effluent production.

1.2.2.1 Micro Sequential Injection Analysis

Aiming at downscaling the SIA apparatus, a new version was presented, and was named Micro Sequential Injection (Figure 1.7, A).

All the SIA system components are packed in a box, making it an easily portable system.

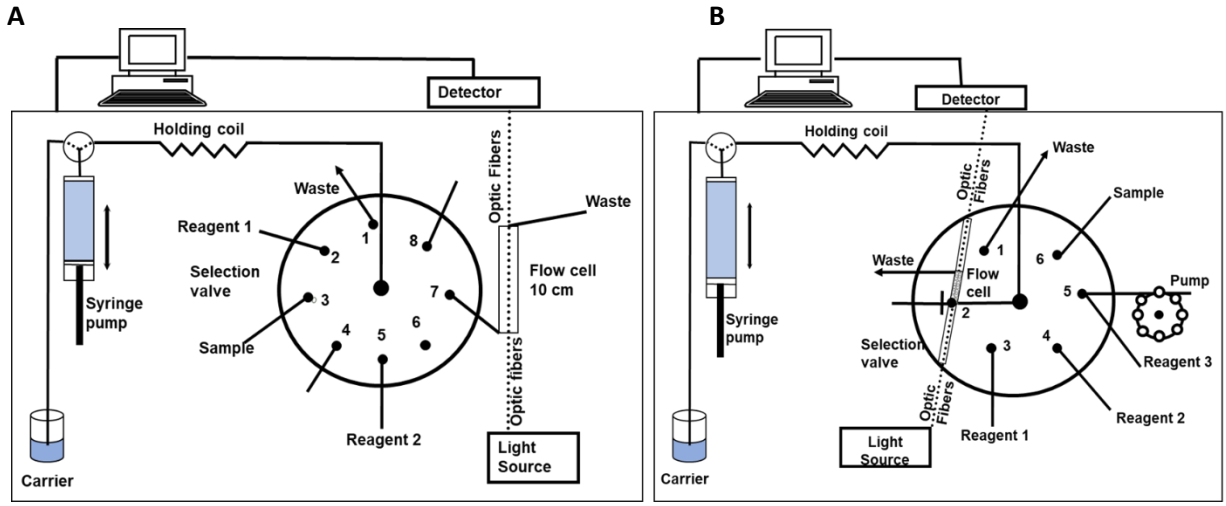

Figure - 1.7 - Schematic representation of a Micro Sequential Injection (μSI) (**A**) and Lab-on-Valve (μSI-LOV) System (**B**).

A Lab-on-valve (LOV) part can be settled in a μSI selection valve head (49). The LOV allows the detection to be carried out directly in the selection valve. This is so because the optical fibers can be coupled directly through the flow cell (Figure 1.7, B), permitting also to extend and reduce the optical path length as required. The flow cell provides versatility to manage fluids in the μSI-LOV format, including the possibility of handling solid particles, such as beads of resin (50,51). The fibres can be set in different positions, configured for absorption or fluorescence detection. The μSI-LOV system, called the third generation of the flow injection techniques, was developed with the intent of minimizing the samples and reagents consumption.

The merge of all these characteristics, make the μSI-LOV a potential system to analyse complex matrices, especially when analysis of biological samples is intended.

1.2.3 Multi-syringe Flow Analysis

Trying to associate the robustness of the SIA methods to the FIA technique, a technique was presented by Cerdà and co-workers (52), based on using various syringes coupled to multicommutation valves, as propulsion system. The use of syringes manufactured by Crison, as opposed to the peristaltic pumps, was intended to solve the flow rate problems related to the deterioration of the flexible tubing used in FIA techniques.

This multi-syringe propulsion system allows the possibility of combining the multichannel operation of the syringes with a constant pulseless, by a single motor, and exact known volume delivery (47). All is controlled by computer software. On the head of each syringe, a two-way commutation valve

is set, allowing to connect or disconnect from the manifold lines, for dispense or pickup movements, enabling to have flexibility and save reagents.

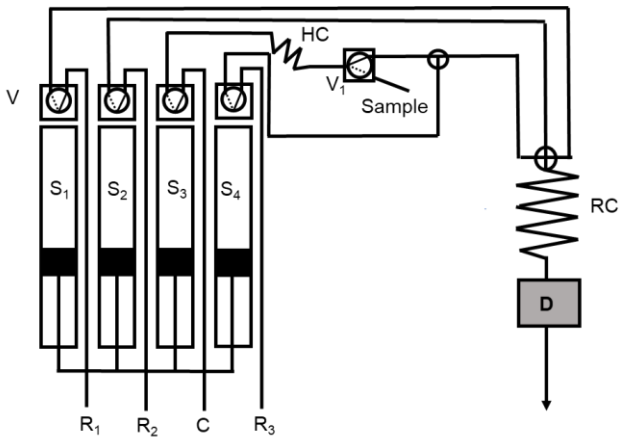

Figure - 1.8 Schematic representation of a multi-syringe generic manifold. It comprises a multiple channel piston pump, composed of four syringes. Each syringe is equipped with a solenoid valve (V) that connects the syringe to the flow system: R: reagents; C: carrier; S_1–S_3: syringe pumps; V_i: two-way solenoid valve; HC: holding coil; RC: reaction coil; D: detector.

This technique requires confluences and/or solenoid valves for solutions mixing and a detector. As in other above mentioned flow systems, different reactors and in-line treatment devices can be employed. As depicted in Figure 1.8, the sample can be introduced by a time-based approach, by its aspiration to the HC and then propulsion to the detector. Alternatively, a volume-based strategy can be used with two commutation valves to define a loop. One of the possible limitations of these systems is the need to stop the forward movement to reload the syringes, thus decreasing sampling analyses frequency.

1.3 Flow-based Solid Phase Extraction

Spectrophotometric methods are often used as a relatively low-cost alternative for the quantitative analysis of chemical components in solution. The selectivity and sensitivity of these methods are often insufficient for today's analytical demands. To overcome these limitations, solid phase extraction can be done before the spectrophotometric determination (50). This technique potentially allows to preconcentrate the analyte and remove the interferents from the sample.

Solid phase extraction (SPE) has been gaining importance over liquid-liquid extraction due to the possibility of avoiding some toxic solvents and potentially allow a better precision. It basically

involves a sorbent material that somehow retains the analyte or then potential interfering agents. So, it has been used with two main objectives: either preconcentrating the analyte or as sample clean-up procedure.

The solid phase can be immobilized in a column device or be added in batch mode. The limitation of the batch approach is the need to pack and extract the solid phase manually. The precision associated with this process is impaired by the manual handling of human operators. These limitations can be minimized if the process is automated in a flow-based analysis system.

The big advantage of the use of flow-based methods is that the SPE can be performed directly in the system. These procedures comprise two main approaches. The solid phase is either reused for several analytical runs, by using packed-bed reactor or disk-phased reactors which are placed somewhere in the flow manifold. However, the implementation of permanent solid phase in flow systems can be difficult, as the solid phase can become too much packed and increase overpressure. Additionally, if it is not renewed, it might become saturated, carry-over effects can be noticed, and the surface can become contaminated with an irreversible sorption of interfering agents. Alternatively, the solid phase can be discharged after each run. In these conditions, the surface can be renewed in each cycle, and have a real-time monitoring of the sensor system. Basically, in both approaches the following sequence are used:

REUSABLE

- sample loading;
- analyte retention
- matrix elimination;
- analyte elution;
- signal measurement;
- reconditioning.

RENEWABLE

- sample loading;
- baseline setting
- analyte retention;
- on surface detection;
- physical renovation.

In the first approach, a column device can be settled in the system to perform SPE, preconcentrating the analyte and removing matrix interference. After the analyte elution and signal measurement, there is the need for sensor chemical regeneration (sensor surface is renewed). This approach is necessary, as the reconditioning steps at each cycle, to increase the lifetime of the solid material (50,51).

In the second approach, there is the possibility of renewing the solid material, performing physical regeneration (beads are discharged after measurement), in an approach called bead injection (BI) method. It consists in the manipulation of a precise volume of suspended beads, serving as a solid phase carrier for reagents, reactive groups or even cells (47). The solid phase is renewed, as the beads are discharged after each measurement (50). Moreover, this method can be applied in the quantification of samples with complex matrices, without pre-treatments or even to be used as a sample clean-up prior to quantification (50). Although in BI no interference from species accumulation is observed, it turns out to be a quite expensive technique, due to a high resin consumption.

The solid surface can have two main functions, as it can just retain the analyte (SPE) or accommodate the chemical reaction directly in the beads surface (Solid Phase Spectrometry (SPS)). In the SPS technique, the light passes directly through the packed solid phase, and for each measurement, the signal can be carried out on the surface of the adsorbent particles trapped in the flow cell.

The SI format, in particular μSI-LOV format, allows to have a solid phase packed automatically and in the flow cell with the possibility of extending and reducing the optical path, depending on the size of column intended (Figure 1.9, B and C).

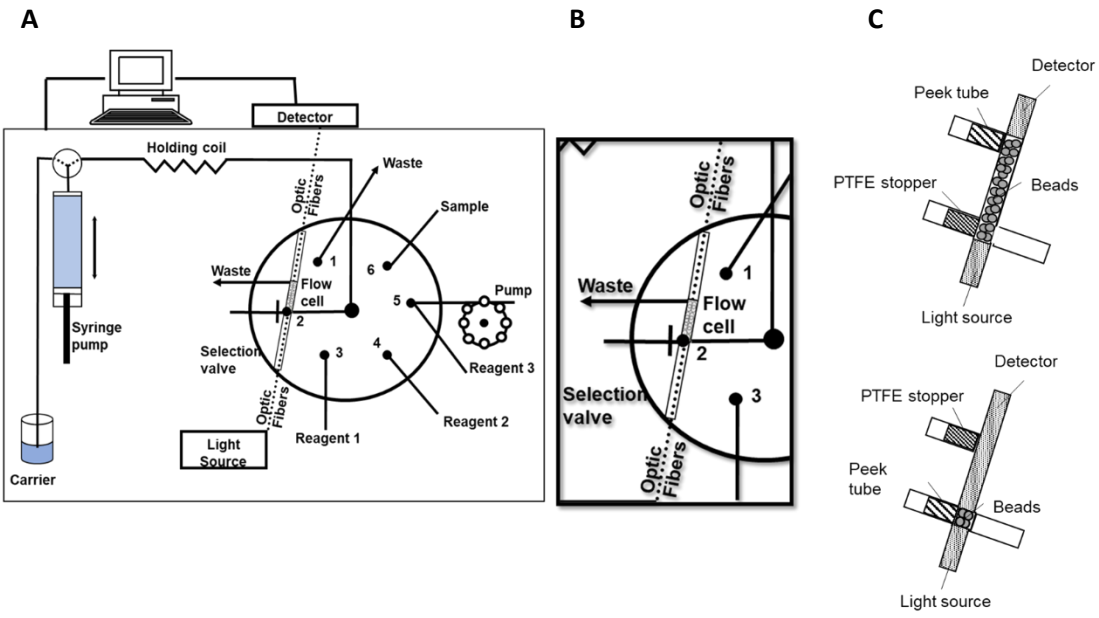

Figure - 1.9 Micro Sequential Injection Lab-on-Valve Solid Phase Spectrometry (μSI-LOV-SPS) manifold **(A)** and flow cell detail, scheme of resin column (beads) packed between the two optical fibers **(B)**, 10 and 1.5 mm optical path **(C)**.

In summary, the μSI-LOV format allows to do solid phase extraction (SPE), solid phase spectrometry (SPS) or bead injection (BI) techniques. All three techniques are based in analyte retention on a solid support. A LOV system incorporating a renewable column is an attractive approach to separate and preconcentrate trace metals, especially when a complex sample matrix is processed. (53) These characteristics make the μSI-LOV an excellent system to use a small volume of reagents and samples, when one or both are limited, as for example, biological samples. This possibility can be essential when working with complex samples, as biological samples, to eliminate matrix components that could interfere with the quantification of the analyte. The quantification can also be performed directly in the beads surface, with an immobilized reagent in a solid phase material (for example functionalized beads).

In this thesis, a spectrofluorimetric method for iodine quantification is presented, using a miniaturized chip-based flow manifold. The method consisted of a multi-syringe module for solutions propulsion and a chip manifold for solutions handling and integrated spectrofluorimetric detection. The determination of this parameter is stated in chapter 3 as well as the innovation to be proposed in this thesis.

New methods based on μSI systems for iron determination using new low toxicity chromogenic reagents are presented in this thesis. Firstly, a μSI-LOV method was developed, using an SPS approach, for iron determination in water samples (Chapter 4). In Chapter 5, a method using a μSI system was developed for the characterisation study of 3,4-HPO ligands. The results were further used in the method development, using a μSI-LOV-SPS for the NTBI determination, in serum samples, based on a ligand functionalised solid phase. The current methods for the determination of this parameter are presented in the introduction of chapters 4,5 and 6 as well as the innovation to be proposed in this thesis.

1.4 Objectives

The main objective of this PhD thesis was to contribute to the development of robust, automatic, reliable, and miniaturized methods for the determination of iodine and iron in biological, food-related and water samples. The methodologies to be developed should be able to provide an effective tool to study the relationship between the assessed parameters in thyroid-related disorders.

To achieve the above-mentioned purpose, flow techniques based on different flow modes, and coupled to different in-line treatments (eg solid phase extraction) would be the main tools to be resorted to in this thesis. The idea was to develop methods, and corresponding apparatus, as simple as possible, and minimize sample treatment off the manifolds. Additionally, the use of low toxicity reagents, and the minimization of samples and reagents consumption, was also targeted.

1.5 Structure of the thesis

This PhD thesis is organized in seven chapters.

In Chapter 1, a general introduction about iodine and iron in biological and environmental matrices is presented. The main concepts of flow analysis systems are also discussed, as well as their potential for performing some in-line sample treatment processes.

In Chapter 2, the reagents and equipment used throughout the experimental work are presented. The optimization procedures and statistical methods to assess the results quality, used in the development of the flow manifolds, are also presented.

The following four chapters (from Chapter 3 to Chapter 6) describe the flow systems and the corresponding developed methods, including the results obtained and their discussion. Chapters 4 and 5 contributed to the development of analytical tools for water analysis and, in chapters 3 and 6, to food and biological samples analysis, respectively.

The information presented in Chapters 4 and 5 of this thesis corresponds to the one already published in international peer-reviewed journals. However, to facilitate reading, it was transposed to the thesis format, instead of the direct presentation of the journal's pdf document.

The final chapter of this thesis (Chapter 7) contains the general conclusions of the developed work during this thesis. In addition, some suggestions for a possible future work are presented.

References

1. Laurberg P, Cerqueira C, Ovesen L, Rasmussen LB, Perrild H, Andersen S, et al. Iodine intake as a determinant of thyroid disorders in populations. Best Pract Res Clin Endocrinol Metab. 2010;24(1):13–27.

2. Hess SY. The impact of common micronutrient deficiencies on iodine and thyroid metabolism: the evidence from human studies. Best Pract Res Clin Endocrinol Metab. 2010;24(1):117–132.

3. Zimmermann MB. Iodine Deficiency. Endocr Rev. 2009;30(4):376–408.

4. Santana Lopes M, Jácome De Castro J, Marcelino M, Oliveira MJ, Carrilho F, Limbert E. Iodo e Tiróide: O que o clínico deve saber. Acta Med Port. 2012;25(3):174–8.

5. Jameson JL. Harrison's endocrinology. 2nd ed. McGraw-Hill Medical; 2010.

6. Costeira MJ, Oliveira P, Santos NC, Ares S, Saenz-Rico B, De Escobar GM, et al. Psychomotor development of children from an iodine-deficient region. J Pediatr. 2011;159(3):447–453.

7. Garnweidner-Holme L, Aakre I, Lilleengen AM, Brantsæter AL, Henjum S. Knowledge about iodine in pregnant and lactating women in the Oslo area, Norway. Nutrients. 2017;9(5).

8. Limbert E, Prazeres S, São Pedro M, Madureira D, Miranda A, Ribeiro M, et al. Iodine intake in Portuguese pregnant women: results of a countrywide study. Eur J Endocrinol. 2010;163(4):631–635.

9. Limbert E, Prazeres S, São Pedro M, Madureira D, Miranda A, Ribeiro M, et al. Aporte do Iodo nas Crianças das Escolas em Portugal. Acta Med Port. 2012;25(1):29–36.

10. Lopes MS, Castro JJ de, Marcelino M, Oliveira MJ, Carrilho F, Limbert E. Iodine and Thyroid: What a Clinic Should Know. Acta Med Port. 2012;25(3):174–178.

11. Henjum S, Lilleengen AM, Aakre I, Dudareva A, Gjengedal ELF, Meltzer HM, et al. Suboptimal iodine concentration in breastmilk and inadequate iodine intake among lactating women in Norway. Nutrients. 2017;9(7):643.

12. Lobato CB, Machado A, Mesquita RBR, Lima L, Bordalo AA. Can non-fortified marine salt cover human needs for iodine? Int J Food Sci Nutr. 2019;70(3):349–354.

13. Andersson M, Karumbunathan V, Zimmermann MB. Global iodine status in 2011 and trends over the past decade. J Nutr. 2012;142(4):744–750.

14. Hess SY, Ouédraogo CT, Young RR, Bamba IF, Stinca S, Zimmermann MB, et al. Urinary

iodine concentration identifies pregnant women as iodine deficient yet school-aged children as iodine sufficient in rural Niger. Public Health Nutr. 2017;20(7):1154–1161.

15. Zimmermann MB, Andersson M. Prévalence du déficit iodé en Europe en 2010. Ann Endocrinol (Paris). 2011;72(2):164–166.

16. Aquaron R, Delange F, Marchal P, Lognoné V, Ninane L. Bioavailability of seaweed iodine in human beings. Cell Mol Biol (Noisy-le-grand). 2002;48(5):563–569.

17. Yeh TS, Hung NH, Lin TC. Analysis of iodine content in seaweed by GC-ECD and estimation of iodine intake. J Food Drug Anal. 2014;22(2):189–196.

18. Larsen P. Williams Textbook of Endocrinology. 10th ed. Elsevier. Elsevier; 2003.

19. World Health Organization. Urinary iodine concentrations for determining iodine status in populations. Vitamin and Mineral Nutrition Information System. WHO/NMH/NHD/EPG/13.1. 2013.

20. World Health Organization. Iron Deficiency Anaemia: Assessment, Prevention and Control. Geneva: World Health Organization. Geneva, Switzerland: World Health Organization. 2001.

21. Theil EC, Chen H, Miranda C, Janser H, Elsenhans B, Núñez MT, et al. Absorption of iron from ferritin is independent of heme iron and ferrous salts in women and rat intestinal segments. J Nutr. 2012 Mar 1;142(3):478–483.

22. Garbowski MW, Ma Y, Fucharoen S, Srichairatanakool S, Hider R, Porter JB. Clinical and methodological factors affecting non-transferrin-bound iron values using a novel fluorescent bead assay. Transl Res. 2016 Nov 1;177:19-30.e5.

23. Brissot P, Ropert M, Le Lan C, Loréal O. Non-transferrin bound iron: A key role in iron overload and iron toxicity. Vol. 1820, Biochimica et Biophysica Acta - General Subjects. Biochim Biophys Acta; 2012. p. 403–410.

24. Franke GN, Kubasch AS, Cross M, Vucinic V, Platzbecker U. Iron overload and its impact on outcome of patients with hematological diseases. Mol Aspects Med. 2020;75:100868.

25. Patel M, Ramavataram DVSS. Non transferrin bound iron: Nature, manifestations and analytical approaches for estimation. Indian J Clin Biochem. 2012;27(4):322–332.

26. Gosriwatana I, Loreal O, Lu S, Brissot P, Porter J, Hider RC. Quantification of non-transferrin-bound iron in the presence of unsaturated transferrin. Anal Biochem. 1999;273(2):212–220.

27. Matos LC, Batista P, Monteiro N, Heriques P, Girão F, Carvalho A de. Genetic Diseases Associated with Iron Overload. Med Interna - Rev Soc Port Med Interna. 2012;48–56.

28. European Association for the Study of the Liver. EASL clinical practice guidelines for HFE hemochromatosis. J Hepatol. 2010;53(1):3–22.

29. Gouveia S, Ribeiro C, Carrilho F. Sobrecarga de ferro e diabetes mellitus. Rev Port Endocrinol Diabetes e Metab. 2014;9(1):74–78.

30. Habimana L, Twite KE, Wallemacq P, De Nayer P, Daumerie C, Donnen P, et al. Iodine and iron status of pregnant women in Lubumbashi, Democratic Republic of Congo. Public Health Nutr. 2013;16(8):1362–1370.

31. Ipek IÖ, Kaçmaz E, Bozaykut A, Sezer RG, Seren L, Paketçi C. The effect of iron deficiency anemia on plasma thyroid hormone levels in childhood. Turk Pediatr Ars. 2011;46(2):129–132.

32. Fayadat L, Niccoli-Sire P, Lanet J, Franc JL. Role of heme in intracellular trafficking of thyroperoxidase and involvement of H2O2 generated at the apical surface of thyroid cells in autocatalytic covalent heme binding. J Biol Chem. 1999;274(15):10533–10538.

33. Fan JL, Patibandla SA, Kimura S, Rao TN, Desai RK, Seetharamaiah GS, et al. Purification and characterization of a recombinant human thyroid peroxidase expressed in insect cells. J Autoimmun. 1996;9(4):529–536.

34. Eftekhari MH, Mozaffari-Khosravi H, Shidfar F. The relationship between BMI and iron status in iron-deficient adolescent Iranian girls. Public Health Nutr. 2009;12(12):2377–2381.

35. Hess SY, Hurrell RF, Zimmermann MB, Delange F. Interactions between Iodine and iron deficiencies. Vol. PhD, Institute of Food Science, Laboratory for Human Nutrition. 2003.

36. Choi S, Hwang J, Lee S, Lim DW, Joo H, Choo J. Quantitative analysis of thyroid-stimulating hormone (TSH) using SERS-based lateral flow immunoassay. Sensors Actuators, B Chem. 2017;240:358–364.

37. Soliman AT, De Sanctis V, Yassin M, Wagdy M, Soliman N. Chronic anemia and thyroid function. Acta Biomed. 2017;88(1):119–127.

38. Zimmermann MB, Zeder C, Chaouki N, Saad A, Torresani T, Hurrell RF. Dual fortification of salt with iodine and microencapsulated iron: A randomized, double-blind, controlled trial in Moroccan schoolchildren. Am J Clin Nutr. 2003;77(2):425–432.

39. Burgess J, Rangel M. Hydroxypyranones, hydroxypyridinones, and their complexes. Vol. 60, Advances in Inorganic Chemistry. 2008. 167–243 p.

40. Mesquita RBR, Moniz T, Miranda JLA, Gomes V, Silva AMN, Rodriguez-Borges JE, et al. Synthesis and characterization of a 3-hydroxy-4-pyridinone chelator functionalized with a polyethylene glycol (PEG) chain aimed at sequential injection determination of iron in

natural waters. Polyhedron. 2015;101:171–178.

41. Mesquita RBR, Suárez R, Cerdà V, Rangel M, Rangel AOSS. Exploiting the use of 3,4-HPO ligands as nontoxic reagents for the determination of iron in natural waters with a sequential injection approach. Talanta. 2013;108:38–45.

42. Marczenko Z, Balcerzak M. Separation, preconcentration, and spectrophotometry in inorganic analysis. First Edit. Elsevier. Netherlands; 2000.

43. Nunes A, Podinovskaia M, Leite A, Gameiro P, Zhou T, Ma Y, et al. Fluorescent 3-hydroxy-4-pyridinone hexadentate iron chelators: Intracellular distribution and the relevance to antimycobacterial properties. J Biol Inorg Chem. 2010;15(6):861–877.

44. Miranda JLA, Mesquita RBR, Nunes A, Rangel M, Rangel AOSS. Iron speciation in natural waters by sequential injection analysis with a hexadentate 3-hydroxy-4-pyridinone chelator as chromogenic agent. Talanta. 2016;148:633–640.

45. Suárez R, Mesquita RBR, Rangel M, Cerdà V, Rangel AOSS. Iron speciation by microsequential injection solid phase spectrometry using 3-hydroxy-1(H)-2-methyl-4-pyridinone as chromogenic reagent. Talanta. 2015;133:15–20.

46. Ruzicka J, Hansen EH. Flow injection analyses. Part I. A new concept of fast continuous flow analysis. Anal Chim Acta. 1975;78(1):145–157.

47. SEGUNDO M, Rangel A. Flow Analysis: A Critical View of Its Evolution and Perspectives. J flow Inject Anal. 2002;19(1):3–8.

48. Ruzicka J, Marshall GD. Sequential injection: a new concept for chemical sensors, process analysis and laboratory assays. Anal Chim Acta. 1990;237(C):329–343.

49. Ruzicka J. Lab-on valve: Universal microflow analyzer based on sequential and bead injection. Analyst. 2000;125(6):1053–1060.

50. Vidigal SSMP, Tóth I V., Rangel AOSS. Sequential injection lab-on-valve platform as a miniaturisation tool for solid phase extraction. Anal Methods. 2013;5(3):585–597.

51. Santos IC, Mesquita RBR, Rangel AOSS. Micro solid phase spectrophotometry in a sequential injection lab-on-valve platform for cadmium, zinc, and copper determination in freshwaters. Anal Chim Acta. 2015;891:171–178.

52. Cerdà V, Estela JM, Forteza R, Cladera A, Becerra E, Altimira P, et al. Flow techniques in water analysis. Talanta. 1999 Nov 15;50(4):695–705.

53. Yu YL, Jiang Y, Chen ML, Wang JH. Lab-on-valve in the miniaturization of analytical systems and sample processing for metal analysis. TrAC - Trends Anal Chem. 2011;30(10):1649–1658.

Chapter 2

General Materials and Methods

2.1. Introduction

The general considerations related with reagents and sample preparation are described in this chapter.

A general description of the characteristics and components of the developed flow-based manifolds is also presented in this chapter, including the computer software programs.

Additionally, several aspects of optimization procedures used in the development of the flow methods and statistical treatment used to assess the quality of the results, are also described in this chapter.

2.2. Reagents and Solutions

All solutions were prepared with analytical grade chemicals and MilliQ water (resistivity > 18MΩ cm, Millipore, USA).

When required, a combined glass pH electrode (Crison) and a potentiometer (Crison model micro pH 2002), Spain was used to measure the pH of the solutions.

2.3. Sample Collection

In chapter 3, a total of 13 marine salt samples from different sources, two pharmaceutical samples, two iodine supplement pills (dried algae) samples and one dried seaweed sample, were selected for accuracy assessment.

Water samples, in chapter 4, were collected in the Northwest area of Portugal, consisting of river, ground, estuarine, tap, and sea waters. After acidification to pH 2 with nitric acid, they were kept refrigerated until analysis.

Human serum samples, in chapter 6, were provided by a partner group from Requimte, Universidade do Porto. Blood was collected by venesection using serum vacutainer tubes with no additive. The blood was allowed to clot for 20 minutes at room temperature and was then centrifuged at 3,000 rpm for 20 minutes, after which the serum was decanted and immediately frozen at –80 ºC for storage until required.

2.4. Flow-Based System Components

The methodologies presented in this thesis involved three types of systems, a multi-syringe flow platform with a chip-based reactor (in chapter 3), a micro sequential injection (μSI) system (in chapter 5) and a μSI with an incorporated Lab-on-valve part (μSI – LOV) (in chapters 4 and 6).

The principal components are described below.

2.4.1. Propulsion Devices

A multi-syringe pump (Crison, Spain) was used, in chapter 3, as a propulsion device (Figure 2.1, A). This device provided the movement of aspiration and propelling solutions and samples through the system tubing. The multi-syringes were controlled by an AutoAnalysis Station 5.0 computer software (Sciware, Spain).

The FIAlab 3500 system from FIAlab Instruments Medina, WA, USA (used in chapters 4 and 6), displayed a high resolution bi-directional micro syringe pump with a glass syringe (Cravo) of 2500 μL of volume (Figure 2.1, B_1). This syringe was connected to the multiposition valve, propelling, or aspirating to or from the holding coil. The peristaltic pump was used as an auxiliar propulsion device to make the circulation of the bead injection suspension (chapter 6) (Figure 2.1, C).

The micro sequential injection system in chapter 5 consisted in a MicroSIA of FIAlab (FIAlab Instruments, USA), with a bidirectional syringe pump of 2.5 mL (Figure 2.1, B_2), connected to a selection valve through a central channel tube.

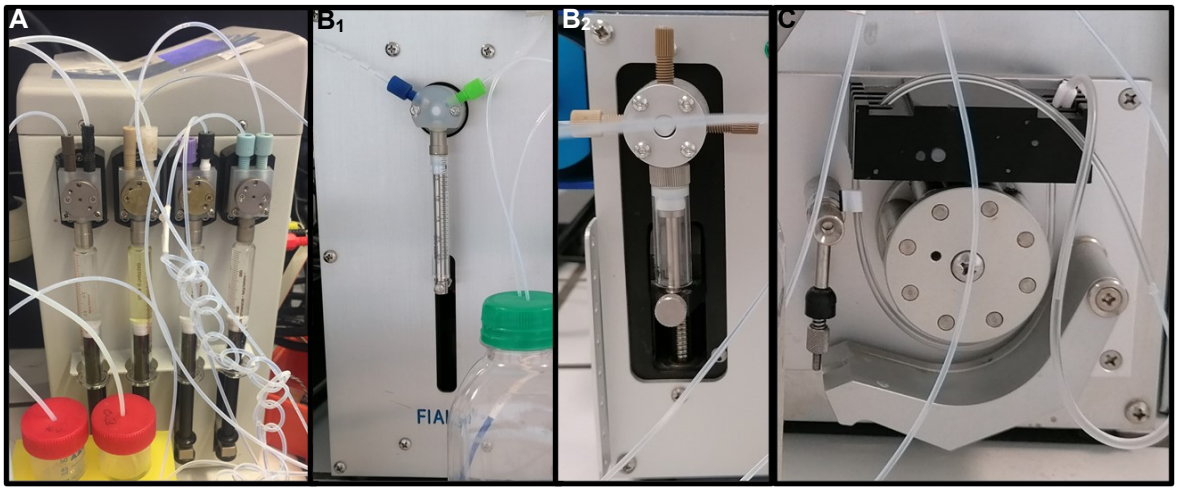

Figure - 2.1 Photographs of the propulsion devices: **A)** Multi-syringe pump; **B_1)** Syringe pump; **B_2)** Syringe pump; **C)** Peristaltic pump.

2.4.2. Valves

A solenoid valve (Figure 2.2) was added to perform sample injection in the multi-syringe flow platform with a chip-based reactor, in chapter 3.

Figure - 2.2 Photograph of the solenoid valve used in the flow system developed in chapter 3.

In chapters 4, 5 and 6, the micro sequential injection systems had a two-way commutation valve placed on the top of the syringe pumps (Figure 2.1, B_1 and B_2) as it occurred on the top of each burette in the multi-syringe used in chapter 3 (Figure 2.1, A).

In chapters 4 and 6, a six-port selection valve multi-position from VICI Cheminert (19P-0272L) was used (Figure 2.3, B), incorporated in a the FIAlab 3500 system (Figure 2.3, A). A Lab-on-Valve module, a multi-purpose central sample processing unit, is mounted on the place of its stator.

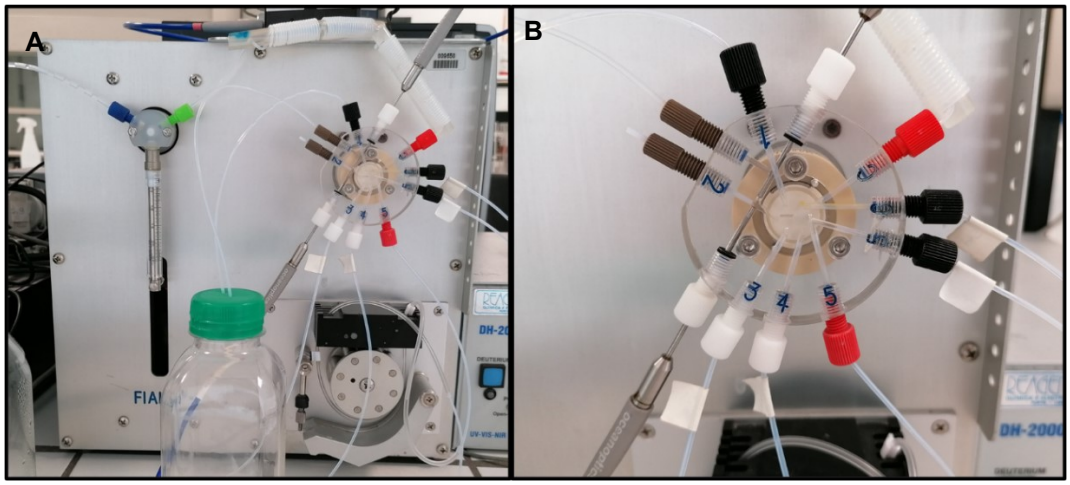

Figure - 2.3. Photographs of: **A)** the FIAlab 3500 system; **B)** a six-port selection valve multi-position with a lab-on-valve head installed.

The micro sequential injection system (Figure 2.4, A) in chapter 5 comprised an eight-port selection valve (Valco VICI Cheminert 170-0317L) (Figure 2.4, B).

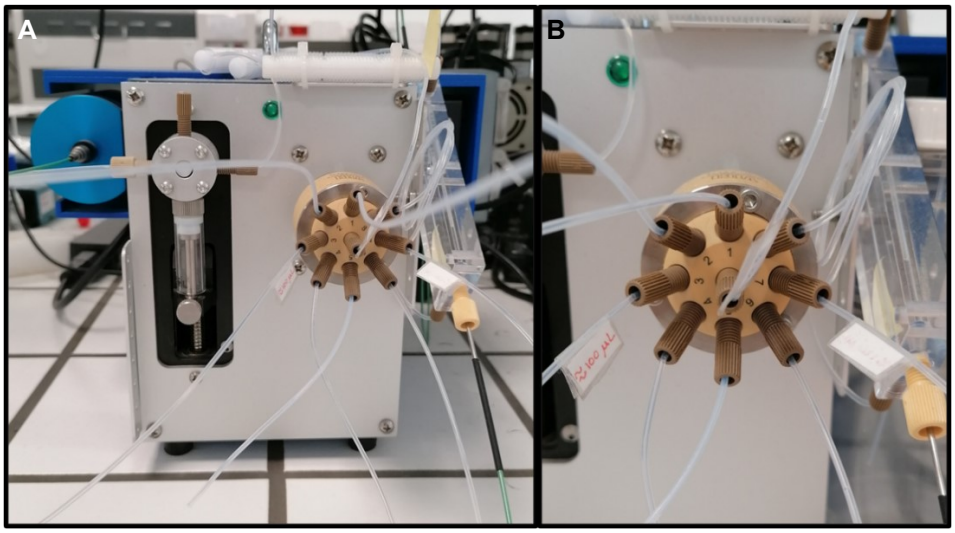

Figure - 2.4 Photographs of: **A)** the micro sequential injection system; **B)** A eight-port selection valve.

The FIAlab systems had the valves placed inside a FIAlab 3500 box in chapters 4 and 6, and a Micro SIA box in chapter 5 (Figures 2.3 and 2.4).

2.4.3. UV Digestor

A heated UV digester (Global FIA, USA) (Figure 2.5, A) was used in chapter 3, to aid the digestion of the samples organic matter. To minimize air bubbles inside the flow tubes, because of the 75˚ C temperature, thus interfering the signal acquisition, a debubbler device (Figure 2.5, B) was added.

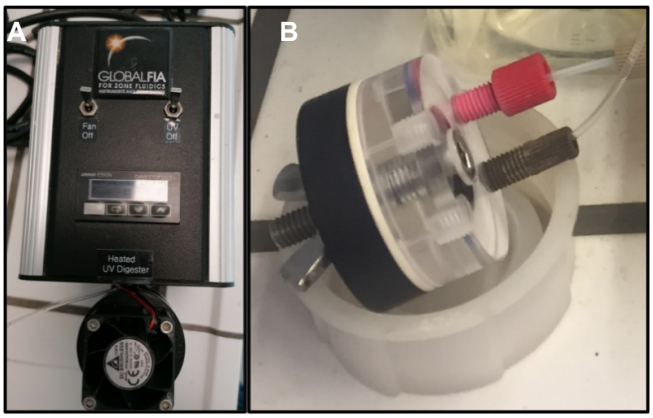

Figure - 2.5 Photograph of: **A)** the Global FIA UV digester; **B)** debubbler device.

2.4.4. Tubes, Connectors and Other Devices

The tubing that connected the components of the flow-based systems were all made of 0.8 mm i.d. PTFE from Ominifit (UK).

In chapter 3, a chip (6.5 mm long, 4.4 mm wide and 1.4 mm height) was used, constructed in poly(methyl methacrylate), PMMA, with a 3D printer (Form1 +, Formlabs, Germany) by using the Rhinoceros software. The chip (Figure 2.6) included a helicoidal microflow-channel (1.2 mm, 520 mm long) and connections for the solutions circulation. This device was constructed in the University of the Balearic Islands, Spain.

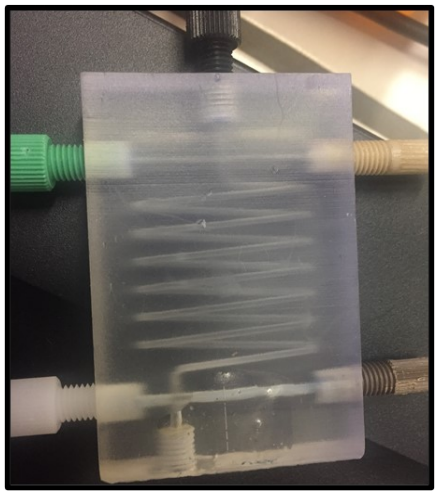

Figure - 2.6 Photograph of the structure of the chip used in chapter 3.

2.4.5. Detection system and computer software program

In chapter 3, the spectrofluorimetric detector was integrated into the structure of the chip (2 mm optical path flow cell with ca. 8 µL internal volume). The two optical fibers (600-µm core) were inserted in the chip, perpendicularly positioned, to irradiate, using a 25W deuterium source (Ocean Optics DH-2000-BAL), the solutions mixture. The emitted radiation was led to a CCD multichannel spectrometer (Ocean Optics HR4000). The Autoanalysis software was employed for the system control and SpectraSuite for data acquisition.

The detection system in chapters 4 and 6 comprised a USB 2000 Ocean Optics (USA) CCD spectrophotometer, fiber optics cables (FIA-P200-SR, 400 mm) and a Mikropack DH-2000-BAL

deuterium halogen light source. For flow programming and data acquisition, a FIAlab for Windows 5.0 software on a personal computer (HP Compaq) was used.

In chapter 5, detection was attained with an Ocean Optics Flame – T – UV– Vis (FLMT01897) charged coupled device (CCD) detector, equipped with a pair of FIA-P600-Fiber cable600 Micron diameter (SMA terminated on one end and PEEK sheath termination on the other end) and an Ocean Optics halogen light source HL-2000. All the equipment was controlled on a desktop computer with FIAlab software installed (Lenovo, Intel Core i5).

2.4.5.1. Lab-on-valve

The flow cell was integrated in the Lab-on-valve structure (Figure 2.7), in Plexiglas, capable of settling optical fibres that were mounted to perform a spectrophotometric detection. The optical path length could be changed from 1.5 to 10 mm (Figure 2.7, A and B). Two different lengths of light path were used, 10 mm (in chapter 4) and 3 mm in (chapter 6).

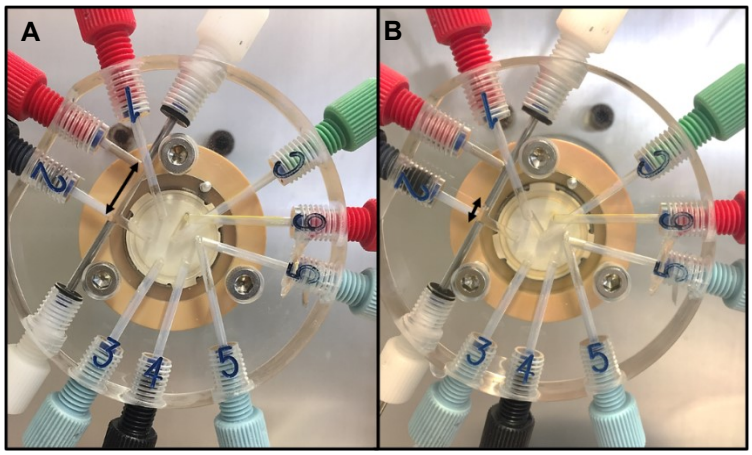

Figure - 2.7 Photograph of the Lab-on-valve flow cell with two different lengths of optical path: **(A)** 10 mm; **(B)** 3 mm.

2.4.5.2. Micro sequential injection

The micro sequential injection system, in chapter 5, comprised a FIA-Z-Cell 100 mm – Plexiglas FIA-Z Cell (Figure 2.8) with adjustable optical path (10 cm light path and 250 mL inner volume).

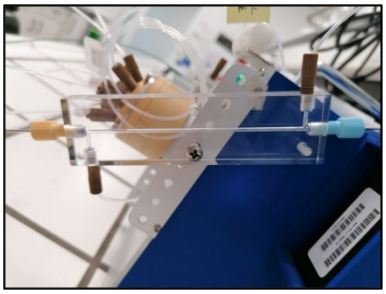

Figure - 2.8. Photograph of the FIA-Z-Cell 100 mm used in chapter 5.

2.5. Study and Characterisation of the Method

The parameters for each method were studied to reach the targeted working range, the best possible sensitivity, and the lowest intercept (these last two parameters would allow a good limit of detection).

The optimization studies were carried out using a univariate method: each parameter was optimised by varying one parameter, and keeping the others fixed. Another objective was to decrease reagent and sample consumption and maximize the determination rate.

The working range was established by injecting a series of working standard solutions with different concentrations. The corresponding signal for the determined working range, in each developed method, was registered, either in fluorescence intensity (chapter 3) or absorbance (chapters 4, 5 and 6). The relationship between signal and concentration was linear in all the developed methodologies.

Therefore, the developed flow-based methods were characterized in terms of limit of detection and quantification, dynamic working range, determination rate, reagents consumption and applicability of the method to samples.

The determination rate and reagents consumption were calculated for one cycle and comprised a three-replica analysis of a sample.

2.6. Accuracy Assessment

For comparison and validation purposes, the results obtained with the developed methods were compared with those obtained by reference methods. Alternatively, when it was not possible to perform a reference method, the results were compared with a selected comparison method. Otherwise, certified reference samples were analysed with the developed methods and the obtained analyte concentration compared with the certified values.

Chapter 3

Chip-based spectrofluorimetric determination of iodine in a multi-syringe flow platform with and without in-line digestion – application to salt and algae samples

Chip-based spectrofluorimetric determination of iodine in a multi-syringe flow platform with and without in-line digestion – application to salt and algae samples

In this chapter, a flow-based spectrofluorimetric method for iodine determination was developed. The system consisted of a miniaturized chip-based flow manifold for solutions handling and with integrated spectrofluorimetric detection. As liquid driver, a multi-syringe module was used. Iodide was quantified from its catalytic effect on the redox reaction between Ce(IV) and As(III), based on the Sandell-Kolthoff reaction. The method was applied for the determination of iodine in salt, pharmaceutical, supplement pills and seaweed samples without off-line pre-treatment. An in-line oxidation process, aided by UV radiation, was implemented to analyse some samples (supplement pills and seaweed samples) to eliminate interferences and release iodine from organo-iodine compounds. This feature, combined with the fluorometric reaction, makes this method simpler, faster and more sensitive than the classic approach of the Sandell-Kolthoff reaction. The method allowed to determine iodine within a range of 0.20 – 4.0 µmol/L, with or without the in-line UV digestion, with a limit of detection of 0.028 µmol/L and 0.025 µmol/L, respectively.

Keywords: Iodine, Spectrofluorimetry, Chip-based manifold, Multi-syringe flow system, In-line UV digestion, Photooxidation, Sandell-Kolthoff reaction.

3.1 Introduction

Iodine is abundant in the oceans, as iodide, being present in the aquatic environment of the earth, but rare in most parts of the terrestrial environment, which leads to iodine deficiency in plants, animals grown on these soils and consequently, in populations in such areas (1,2).

The iodine intake is critical for nervous system function throughout life, but particularly during fetus development, as it is required for thyroid hormone synthesis (3). Even in less severe iodine deficiency, a normal thyroid gland can adapt and keep thyroid hormone production within the normal range. Prolonging thyroid hyperactivity associated with such adaptation leads to thyroid growth (2).

In Europe, two-thirds of the countries reported inadequate iodine intakes, being iodine deficiency a major public health concern, as it seems to be re-emerging (4)(5). In Portugal, results point to an inadequate iodine intake in pregnant women (6), being recommended an iodine supplementation during pregnancy with 150-200 µg/day (7).

In the human diet, iodine main sources are marine foodstuffs – fish, shellfish, algae, and sea salt (8). Salt iodization programmes had been implemented in more than 120 countries around the world (9,10). It is a highly cost-effective strategy to prevent iodine deficiency (10). Even though over the past four decades occurred a major global expansion of salt iodization, much of Europe has remained iodine deficient (11).

A significant number of consumers in the world sustains natural products over artificial ones. An alternative to iodized salt is the use of naturally iodized salt (marine salt) and seaweed as an iodine source (12). In Portugal, marine salt, by itself, contains a naturally high amount of iodine. Even though the presence of a high quantity of iodine in marine salt, it is still required a fortification to be used as an effective alternative to fight iodine insufficiency (8).

In many Asian countries, eatable seaweed products have been consumed as they are low in calories and full of nutrients (13). The use of iodine-rich seaweed for consumption is a method largely used by Japan, being the only population in the world in which excessive intake of iodine (2). Iodine is accumulated from seawater into seaweeds making them a good dietary source of iodine. Disorders resulted from iodine deficiency can be eliminated with adequate consumption of seaweed (13).

To assess iodine intake, different methods can be used to quantify iodine affordably and accurately in soil, plants, various foods and physiological samples (14). Iodine measurement is carried out mostly by a kinetic spectrophotometric method, the Sandell–Kolthoff reaction. The reaction is based on the reduction of yellow Ce(IV) by As(III) to colourless Ce(III), being very slow. This reaction is catalysed by trace amounts of iodide. These procedures can be executed manually or could be automated (14,15). To a smaller extent, the reaction, is also catalysed by iodate, in the

presence of arsenite, which is readily converted to iodide in an acidic medium. Various organic substances can potentially interfere in the Sandell-Kolthoff reaction, by chelating Ce(IV) or Ce(III) or directly affecting the reaction rate. The organo-iodine compounds will not react without a previous decomposition. Therefore, if the total content of iodide is aimed, complete sample mineralization is required to convert the iodine-organic forms to what can be considered iodine free from organic matter (14).

Several pre-treatment methods can be applied for the decomposition of the organo-iodine compounds. The pre-ashing temperature procedure can be used but may result in a significant loss of the analyte. Nevertheless, this is the method of choice for sample preparation for iodine determination by the US Food and Drug Administration. The digestion step usually uses perchloric acid, which requires special hoods and precautions. Acid digestion procedures do not have this problem. However, iodide in acid solution is easily oxidized by air, but studies show that iodine loss is consistent and is typically below 20% (14). Ammonium persulphate was proposed as an alternative to replace chloric acid as the oxidising reagent (16). The ammonium persulphate reagent is a non-explosive and less hazardous chemical, preventing the need for the use of a specialized hood. Applying this oxidising agent to eliminate interfering substances in urine became the method of choice in many laboratories, as the results of this method and the chloric acid one, correlated very closely (15,17).

The potentiometric method is a reference method for iodide determination (15,18). Another method of choice is the titration method, for being an accurate, ease of operating and low-cost method, that can be used for iodide determination in iodised salt sample (8,19). There are several other analytical methods for iodine quantification, including semi-quantitative methods, microplate method, automated methods, and technologically advanced methods, including the inductively coupled plasma mass spectrometry (ICP-MS) method (15). The latter allows an excellent sensitivity and, in some cases, allows to directly analyse the sample after dilution. Though, only a part of the iodine present is ionized (~25%) and so it is necessary to have an internal standard to account for matrix effects. The matrix effects need to be corrected as, for example, the salt content of a sample, as the extent of ionization in the plasma is susceptible to the ionizable material present (14). More sophisticated and automated technology can be used, for example, paired-ion reversed-phase high-performance liquid chromatography (HPLC), but is associated with a higher cost of the instrumentation (15).

Concerning flow-based systems, several methods for iodine determination were described in Table 3.1.

Table - 3.1 Some analytical characteristics of flow methods for the determination of iodine in different sample matrices; LOD – limit of detection.

Flow system	Method Characteristics	Detection	Matrix	Application range	LOD	Reference
SFA	Sandell-Kolthoff reaction	Spectrophotometry	urine	50 - 400 µg/L	-	(20)
FIA	Chemiluminescence reaction	Spectrophotometry	urine	0 - 5000 µg/L 10 - 40 mg/L	10 µg/L	(21)
FIA	Chemiluminescence reaction	Spectrophotometry	salt	126.9 - 1522.8 µg/L	12.7 µg/L	(22)
FIA	-	Potentiometry	urine and salt	0.317 - 126.9 (iodide) mg/L 0.444 - 253.8 (iodide+iodate) mg/L	176 (iodide) µg/L 225 (iodide+iodate) µg/L	(23)
FIA	Sandell-Kolthoff reaction	Spectrophotometry	urine	12.7 - 380.7 µg/L	12.7 µg/L	(24)
FIA	Sandell-Kolthoff reaction	Spectrophotometry	urine samples	4.95 - 40.0 µg/L 40.0 - 1001 µg/L	4.95 µg/L	(25)
FIA	Chemiluminescence reaction	Spectrophotometry	salt and pharmaceutical	1.3 - 63.5 µg/L	0.13 µg/L	(26)
Continuous and stopped FIA	Sandell-Kolthoff reaction	Spectrophotometry	urine samples	20 - 200 µg/L continuous 50 - 200 µg/L stopped	2.3 µg/L continuous 3 µg/L stopped	(27)
FIA	Liquid-liquid extraction	Spectrophotometry	biodiesel	13 to 135g I_2/ 100g	5 g I_2/ 100g	(28)
FIA	Polyvinyl alcohol reagent	Spectrophotometry	seawater and salt	1 - 12.7 µg/mL	60 ng/mL	(29)
FIA	-	Spectrophotometry	seawater and salt	0.51 - 4.06 µg/mL	40 ng/mL	(30)
FIA	Oxidation with tartaric acid	Potentiometry	-	-	25.4 µg/L	(31)
FIA	Gas diffusion unit	Potentiometry	-	up till 1269 µg/L	25.4 µg/L	(32)
FIA	Colorimetric reagent	Spectrophotometry	water recovery system samples	0.01 - 4 mg/L	52 µg/L	(33)
FIA	Sandell-Kolthoff reaction	Spectrophotometry	bottled drinking water	50 - 1000 µg/L	9.30 µg/L	(34)
FIA	-	Amperometry	iodized table salt	0 - 25 mg/L	0.5 mg/L	(35)
FIA	Sandell-Kolthoff reaction	Spectrophotometry	seawater and pharmaceutical preparation	4.3 - 70 µg/L	0.47 µg/L	(36)
FIA	Catalytic reaction	Spectrophotometry	milk	0 - 100 µg/L	0.99 µg/L	(37)

FIA	Iron(II)-tris bathophenanthroline iodide ion pair complex	Potentiometry	pharmaceutical preparations	1.3 - 1200 mg/L	0.5 mg/L	(38)
FIA	Iodine– starch reaction (gas diffusion unit)	Spectrophotometry	pharmaceutical	6000 - 10000 mg/L	1 mg/L	(39)
FIA	Sandell-Kolthoff reaction	Spectrophotometry	egg	-	0.58 µg/ g egg sample	(40)
FIA	Hanus reagent	Amperometry	vegetable oils	5 - 12 mg/L	6.3 mg/L	(35)
FIA	Parallel flow	Spectrophotometry	olive oil	90 - 125 g/L	38 g/L	(41)
FIA	Chemiluminescence reaction with gas-diffudion unit	Spectrophotometry	pharmaceutical	0.1 - 1.0 mg/L	0.1 mg/L	(42)
FIA	Sandell-Kolthoff reaction	Spectrophotometry	thyroid gland	5 – 200 µg/L	1.6 µg/L	(43)
FIA	blue $I_3(-)$ - starch complex	Spectrophotometry	iodized salt	0.63 - 5.1 mg/L	2 mg /kg	(44)
FIA	gas-diffusion cell	Spectrophotometry	marine pore water	0 - 400 mg/L	0.2 mg/L	(45)
FIA	Catalytic reaction	Spectrophotometry	sea water	0.75 - 150 µg/L	-	(46)
FIA	Iodate-acid reaction	Spectrophotometry	charcoals	0 - 317 mg/L	7.6 mg/L	(47)
FIA	Chemiluminescence reaction	Spectrophotometry	-	0.05 - 10 µg/L	0.05 µg/L	(48)
FIA	Catalytic reaction	Spectrophotometry	water	0.1 - 2 µg/L	0.1 µg/L	(49)
FIA	-	Potentiometry	pharmaceutical preparations	0.1269 - 12690 mg/L (iodide) 1.269 - 126.9 mg/L (iodine)	0.6345 mg/L (iodide) 1.269 mg/L (iodine)	(50)
FIA	Chemiluminescence reaction	Spectrophotometry	multivitamin tablets	1.0 - 10.0 mg/L	0.5 mg/L	(51)
FIA	Catalytic reaction	Spectrophotometry	stream sediments	0.060 - 0.150 mg/L	0.4 mg/L	(52)
FIA	-	Potentiometry	iodized table salts	3.2 - 95.2 mg/L	0.3 mg/L	(53)
FIA	-	Amperometry	water, serum, salt	0.0635 - 12,7 mg/L	0.63 µg/L	(54)
FIA	Chemiluminescence reaction	Spectrophotometry	salt	0.13 - 1.5 mg/L	12.7 µg/L	(22)
MSFIA	Spectrofluorimetric method - reaction with Alizarin Navy Blue Spectrophotometric method - reaction with iodide in acidic media	Spectrophotometry and Spectrofluorimetry	artificial fresh water	periodate 1.3 - 28 mg/L iodate 1.3 - 25 mg/L	periodate 0.44 mg/L iodate 0.13 mg/L	(55)

MSFIA	Sandell-Kolthoff reaction	Spectrofluorimetry	seawater	1 - 100 µg/L	0.3 µg/L	(56)
MFFIA	Sandell-Kolthoff reaction	Spectrofluorimetry	drinking water	50 - 400 µg/L	7.7 µg/L	(57)
SIA	Catalytic reaction	Spectrophotometry	tablets	0.1 - 6.0 µg/L	0.05 µg/L	(58)
SIA	-	Potentiometry	bathing waters and seaweed extracts	634.5 - 63450 µg/L	17.8 µg/L (iodide) 2.54 µg/L (iodate)	(59)

SFA - Segmented flow analysis

FIA - Flow injection analysis

MSFIA – Multi-syringe flow injection system

MFFIA – Microfluidic flow injection system

SIA –Sequential injection analysis

Among these, a portable, robust and simple method for in-field analysis of iodide in sea waters samples was proposed by Frizzarin *et al* work (56). It was composed of a miniaturized analyser, including a poly(methyl methacrylate) chip with integrated spectrofluorimetric detection. The solutions were propelled by a multi-syringe module. Iodide was determined through its catalytic effect on the reaction between Ce(IV) and As(III). The spectrofluorimetric detection method makes it a more sensitive method than spectrophotometric detection. The chip manifold allows to do the direct detection and solutions mixture in one device. The use of a multi-syringe module allows to reduce the manipulation and the quantity of reagents used, enabling the automation of the Sandell-Kolthoff classic reaction.

In this work (Chapter 3), an adaptation of the above-mentioned method is proposed for the determination of iodine in pharmaceutical and salt samples. Additionally, aiming to assess the total iodine content in algae-based supplements, an oxidation process is proposed. By incorporating an in-line digestion process with UV radiation, it is possible to analyse samples with high expected levels of organo-iodine compounds. By combining an in-line digestion process with fluorometric detection, a simpler, faster and more sensitive than the classic approach of the Sandell-Kolthoff reaction, was developed.

3.2 Experimental

3.2.1. Reagents and solutions

All the solutions were prepared with analytical grade chemicals and Milli-Q water, MQW (resistivity > 18 MΩ cm, Millipore, Bedford, MA, USA).

A 7.9 mmol/L (1.0 g/L) iodide solution was prepared from the 0.10 mol/L iodide stock solution (sodium iodide) acquired from Hanna instruments (HI 4011-01, Hanna Instruments, USA). The working solutions were daily prepared, within a range of 0.20– 4.0 µmol/L of iodide.

A cerium solution containing 1.85 mmol/L Ce(IV) and an arsenious solution containing 100 mmol/L As(III) and 0.43 mol/L NaCl, both (Ce(IV) and As(III)) solutions were prepared in 1 mol/L H_2SO_4 from appropriate amounts of ammonium cerium(IV) sulphate dihydrate (Sigma-Aldrich, Germany), sodium (meta)arsenite (Sigma-Aldrich, Germany) and sodium chloride (Merck, Germany) and a sulphuric acid stock solution, respectively.

The sulphuric acid solution, 1 mol/L, was prepared by dilution of the concentrated acid (d = 1.84, 95-97%, Fluka, Germany) in MQW.

An oxidant solution, 0.3% of potassium peroxodisulfate, was prepared by dissolving 0.30 g of potassium peroxodisulfate (Merck, Germany) in 100 mL of 1 mol/L of H_2SO_4.

3.2.2. Chip based and multi-syringe flow system manifold and procedure

3.2.2.1 Iodine determination

A chip (6.5 mm long, 4.4 mm wide and 1.4 mm height) was constructed in poly(methyl methacrylate), PMMA, with a 3D printer (Form1 +) by using the Rhinoceros software. The structure scheme was made as described in Frizzarin *et al* work (56). The chip includes a helicoidal microflow-channel (1.2 mm, 520 mm long) and connections, for the reagents and carrier solutions, inserted in the chip in a confluence mode. The spectrofluorimetric detection was integrated in the structure of the chip (2 mm optical path flow cell with ca. 8 µL internal volume). The two optical

fibers (600 µm core) were inserted in the chip, perpendicularly positioned, to irradiate the solution in the flow path from a 25-W deuterium source (Ocean Optics DH-2000-BAL). The emitted radiation is transmitted to a CCD multichannel spectrometer (Ocean Optics HR4000). The Autoanalysis software was employed for the system control and SpectraSuite software for data acquisition. The fluorescence emission registration was set to 365 nm, subtracting the registered baseline signal, at 285 nm. The integration time was set to 300 ms for all spectrofluorimetric measurements. The PTFE tubes (0.8 mm i.d.) were used for the multi-syringe-chip connections and holding coils.

A multi-syringe system was based on 3 glass syringes (5 mL each) (Figure 3.1) with solenoid valves (V) placed on the head section of the syringes, allowing solutions handling. Another solenoid valve (V1) was added to performed sample injection.

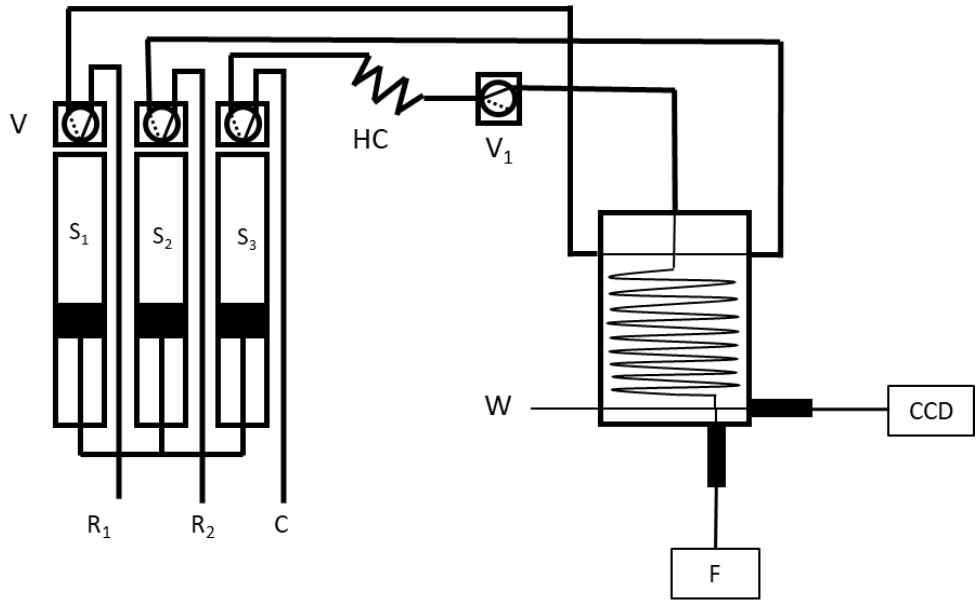

Figure - 3.1 Flow diagram of the chip multi-syringe flow injection analysis for iodine determination: S_1–S_3, syringe pumps; V, two-way solenoid valves; R_1, 1.85mmol/L Ce(IV); R_2, 100 mmol/L As(III), both R_i in 1 mol/L H_2SO_4; C, carrier (water); HC, 200 cm holding coil (V_1 to Chip – 20 cm); F, irradiation from a UV-VIS-NIR light source Micropack DH 2000-BAL; CCD, charged coupled device detector connected with optical fibers (600-µm core) for fluorescence measurement (Ocean Optics HR4000); W, waste.

The system manifold used for the determination of iodine is described in Figure 3.1. The system routine was operated according to the protocol described in Table 3.2.

Table - 3.2 Protocol for the spectrofluorimetric determination of iodine, using a multi-syringe chip-based flow system (MS-Chip method).

	Step	Active devices	Action	Flow rate	Description
Preparation steps	1	S_1, S_2, S_3	Aspirate 5.00 mL	10 mL/min	Fill the syringes with regents and carrier
	2	-	Dispense 2.15 mL	5 mL/min	-
	3	S_3, V_1	Aspirate 0.150 mL	10 mL/min	Sample aspiration
	4	S_3	Dispense 3.00 mL	5 mL/min	Clean the analytical path
	5	-	Aspirate 1.50 mL	10 mL/min	Fill the syringes with regents and carrier
Loop for iodine determination	6	S_3, V_1	Aspirate 0.35 mL	10 mL/min	Sample aspiration
	7	S_3,	Dispense 0.05 mL	5 mL/min	Sample injection
	8	S_1, S_2, S_3	Dispense 0.30 mL	5 mL/min	Reagents and sample injection
	9	S_3	Dispense 0.90 mL	0.4 mL/min	Transport through the chip manifold
	10	S_3	Dispense 0.60 mL	5 mL/min	Clean the analytical path
	11	-	Aspirate 1.50 mL	10 mL/min	Refill the syringes with regents and carrier

Firstly, the syringes were filled with the reagents and carrier (water) solution (step 1). Next, 2.15 mL was dispensed to allow the aspiration of the necessary sample volume (sample aspiration - step 2). The sample solution was aspirated (syringe S_3 and solenoid valve V_1) to the holding coil (HC) (step 3) to fill the tube connected to the solenoid valve. For cleaning the system (step 4), the carrier was propelled through the holding coil and chip. Before initiating the loop for the iodine determination, all the syringes were refilled with reagent and carrier solutions, (step 5). The sample solution was aspirated (syringe S_3 and solenoid valve V_1) to the holding coil (step 6) and a small sample volume (0.05 mL) was firstly propelled to the chip-manifold (step 7). The reagents and sample solutions were simultaneous introduced and mixed in the chip manifold (step 8) and propelled with the carrier solution in a lower flow rate (step 9). The analytical path was cleaned (step 10) and the syringes refilled with reagents and carrier solutions for the next determination (step 11), repeating a total of 3 times the determination loop for each sample.

3.2.2.2 Total iodine determination with in-line UV digestion

To attain in-line digestion, the analytical manifold was reconfigured to accommodate an additional syringe with an oxidant reagent (potassium peroxodisulfate 0.3% solution), resulting in another layout (Figure 3.2). In this method for total iodine determination, the mixture of the sample with the oxidant reagent was accomplished with the addition of a confluence after the solenoid valve (V1). A heated UV digester (Global FIA for zone fluidics instruments and components) set at 75˚ C was placed after the confluence, to promote the digestion. A debubbler device was added to prevent air bubbles entering the chip.

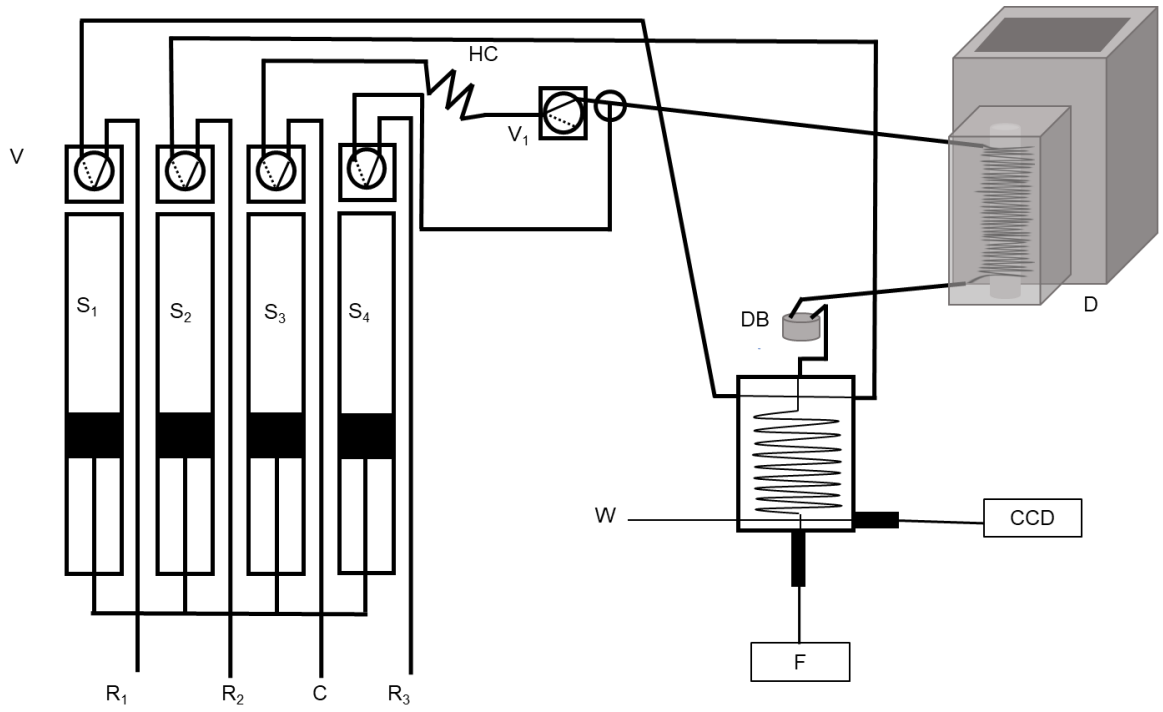

Figure - 3.2 Flow diagram of the chip multi-syringe flow injection analysis for total iodine determination: S_1–S_4, syringe pumps; V, two-way solenoid valves; R_1, 1.85 mmol/L Ce(IV); R_2, 100 mmol/L As(III); R_3, 0.30% Potassium persulphate, all R_i in 1 mol/L H_2SO_4; C, carrier (water); HC, 200 cm holding coil (V1 to confluence – 2 cm); D, Heated UV Digester (Global FIA) with 1000 mL holding coil; DB, debubbler (confluence to chip 1640 cm); F, irradiation from a UV-VIS-NIR light source Micropack DH 2000-BAL; CCD, ; CCD, charged coupled device detector for fluorescence measurement (Ocean Optics HR4000) connected through an optical fiber (600-µm core); W, waste.

The system routine was operated according to the protocol described in Table 3.3.

Table - 3.3 Protocol for the spectrofluorimetric determination of total iodine, using a multi-syringe chip-based flow system with in-line UV digestion (MS-Chip in-line UV digestion method).

	Step	Active devices	Action	Flow rate	Description
Preparation steps	1	S_1, S_2, S_3, S_4	Aspirate 5.00 mL	10 mL/min	Fill the syringes with regents and carrier
	2	-	Dispense 2.35 mL	5 mL/min	-
	3	S_3, V_1	Aspirate 0.150 mL	10 mL/min	Sample aspiration
	4	S_3	Dispense 3.00 mL	5 mL/min	Clean the analytical path
	5	-	Aspirate 3.32 mL	10 mL/min	Fill the syringes with regents and carrier
Loop for total iodine determination	6	S_3, V_1	Aspirate 0.150 mL	10 mL/min	Sample aspiration
	7	S_3, S_4	Dispense 0.150 mL	5 mL/min	Sample injection
	8	S_3	Dispense 1.02 mL		Sample and oxidant reagent injection through the UV digestor
	9	S_1, S_2, S_3	Dispense 0.300 mL		Reagents and sample injection
	10	S_3	Dispense 0.900 mL	0.4 mL/min	Transport through the chip manifold
	11	S_3	Dispense 1.10 mL	5 mL/min	Clean the analytical path
	12	-	Aspirate 3.32 mL	10 mL/min	Refill the syringes with regents and carrier

As previously described in Table 3.2, all the preparation steps for the filling of the reagents and sample (steps 1,2,3,4 and 5) were the same. The determination steps of the iodine loop are the same as previously described in Table 3.2, except for the steps 6, 7 and 8. These consisted of

sample aspiration (syringe S_3 and solenoid valve V_1) to the holding coil (step 6) and mixture with the oxidant reagent for the digestion step (step 7). To promote organo-iodine compounds digestion and elimination of interferents (photooxidation) sample and reagent were injected through the UV light unit (step 8).

The reagents and digested sample solutions were propelled and mixed in the Chip manifold (step 9) in a lower flow rate (step 10). Detection was carried out in a 2 mm flow cell placed ate the end of the chip. Next, the analytical path was cleaned (step 11) and the syringes refilled with reagents and carrier solutions for the next determination (step 12).

3.2.3. Sample collection and preparation

The two approaches developed, with and without in-line sample digestion, targeted the analysis of two types of samples, iodine supplements (dried algae and seaweed), and pharmaceutical and food salt, respectively.

3.2.3.1 Salt samples

A total of 13 marine salt samples from different sources were selected. For the iodine quantification of the salt samples, 8 g of marine salt was dissolved in 25 mL of MQW and then diluted 1/40. To determine the iodine concentration in the salt samples, calibration curves were performed within the range of 0.20– 4.0 µmol/L of iodide.

3.2.3.2 Iodine supplement samples

Two pharmaceutical samples, two iodine supplement pills samples (dried algae) and one dried seaweed sample, were analysed. The suspension of the pharmaceutical and supplement pills samples was made as described in Table 3.4.

Table - 3.4 Preparation steps of the samples to be analysed in the MS-Chip flow system method.

	Sample ID	Amount of sample (dissolved in 100 mL)	Dilution factor
Pharmaceutical sample	#Pharm 1	1/10 of one pill	-
	#Pharm 2		
	#Pharm 3		
	#Pharm 4	1 pill	10x
	#Pharm 5		
Supplement pills sample	#Algae 1	1 pill	10x
	#Algae 2	1/10 of one pill	-
	#Algae 3		

The preparation of the #Pharm 4, #Pharm 5 and #Algae 1 samples consisted in directly dissolving one sample pill in 100 mL MQW and then diluted to 1/10.

The iodine pharmaceutical and supplement algae pills, #Pharm 1, 2 and 3, and #Algae 2 and 3 samples were prepared by weighting 1/10 of one pill mass and dissolving in 100 mL of MQW.

One algae sample (#Algae 4), consisting in 1 g of dried seaweed, was soaked in 100 mL of MQW and heated to 37˚C for 30 min.

The iodine concentration for the pharmaceutical samples was calculated by performing calibration curves within the range of 0.20– 4.0 µmol/L of iodine, using the MS-Chip method.

To accomplish the iodine determination in algae samples (algae supplements pills and seaweed), calibration curves were performed within the range of 0.20– 4.0 µmol/L of iodine, using the MS-Chip in-line UV digestion method.

3.2.4 Accuracy assessment

3.2.4.1 Determination of iodine

To validate the method, several salt samples were analysed using a potentiometric method. For iodide determination, an anion selective electrode (iodide electrode (HI 4111, Hanna Instruments, USA) was used and, for iodate determination, an iodometric titration method was chosen (8). The validation methods were performed by the group of the Laboratory of Hydrobiology, Institute of

Biomedical Sciences Abel Salazar (ICBAS), within an ongoing work collaboration. The use of the selective iodide electrode and the titration method, as reference methods, allowed to assess the value for the inorganic iodine (iodide plus iodate value) content in the salt samples and compared with the MS-Chip developed method.

Two pharmaceutical samples were analysed with the developed MS-Chip method for iodide determination and the result compared with the expected values: Yodafar 200 and Yodafar 300 (Bialport, Portugal), with 200 and 300 µg/L of iodide, respectively.

3.2.4.2 Determination of total iodine using an in-line UV digestion

Several algae supplement pills were analysed using the developed total iodine determination method (MS-Chip in-line UV digestion method) and the results compared with the supplement label value. The validation was made through recovery percentage with algae supplement and a seaweed sample.

3.3. Results and discussion

The developed methodologies aimed to quantify iodine in salt and algae supplement samples. Therefore, two procedures were developed in a chip-based approach: one method allowed the determination of the iodine content without pre-treatment, suitable for the salt and pharmaceutical samples; the other method included an in-line digestion step combining an UV digestor and oxidant reagent, being suitable for the algae supplement samples.
Several parameters were set according to a previous work (56), namely the reagent concentration, sample volume and flow rates. To minimize the influence of the schlieren effect (60), the registered base line signal at 285 nm was subtracted to the analytical signal registered at 365 nm.

3.3.1. Study of fluorometric determination of iodine

To achieve a method with a wider range of concentration for iodide determination, some parameters and conditions from the Frizzarin et al, 2015, work (56) were revisited and studied.
Maintaining the reagents and sample volume conditions reported, the influence on the Ce(IV) reagent concentration was studied in range of 1 mmol/L – 5 mol/L of Ce(IV). The Ce(IV) concentration 1.85 mmol/L was chosen, as it was the concentration that showed the highest sensitivity and linearity (Figure. 3.3).

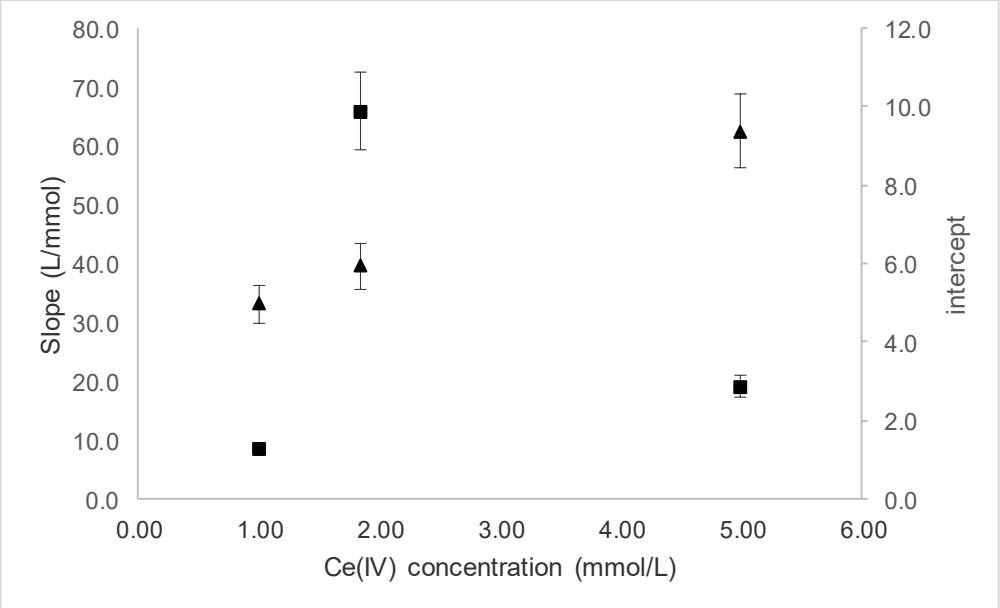

Figure - 3.3 Study of the influence of the Ce(IV) reagent solution concentration on the analytical curve slope (■) and intercept (▲).

The concentration of the As(III) reagent solution was increased from 60 mmol/L to 100 mmol/L of As(III) and 0.43 mol/L of NaCl was added to this reagent solution. This alteration was based on the results described in Machado, et al, 2017 (17), where the conditions of the Sandell-Kolthoff reaction method were improved. This alteration resulted in an improvement of 19% in the sensitivity.

The influence of the sulphuric acid concentration was studied for the reagent solutions preparation. A range of 137 mmol/L – 2 mol/L of H_2SO_4 was tested for both reagents (Ce(IV) and As(III)). The sulphuric acid concentration chosen was 1 mol/L of H_2SO_4, as it was the concentration that showed the highest sensitivity (Figure. 3.4) and a higher coefficient of determination.

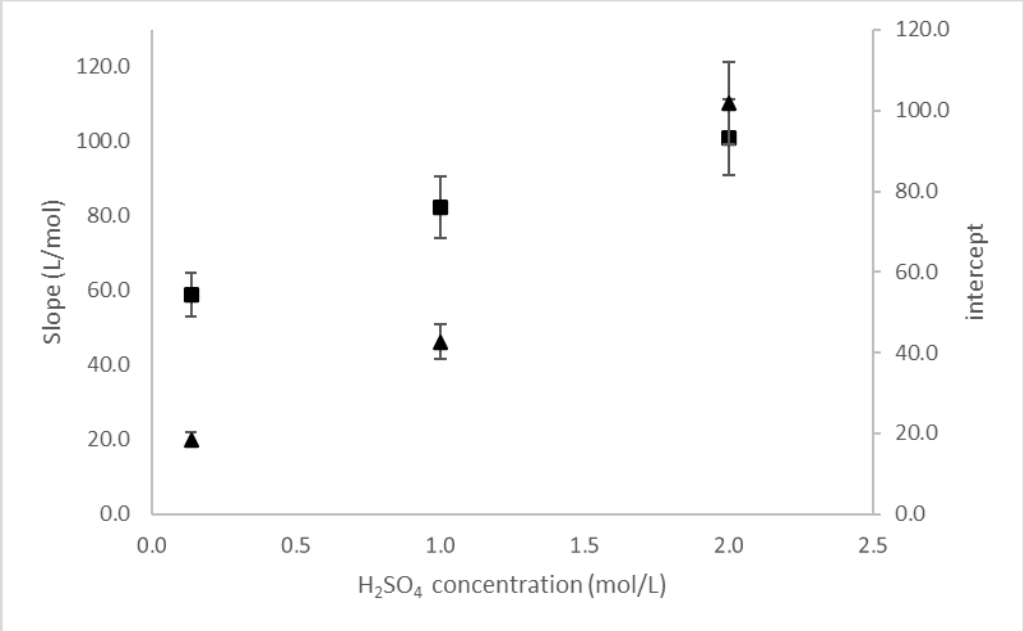

Figure - 3.4 Study of the influence of H_2SO_4 concentration in the 1.85 mmol/L of Ce(IV) reagent solution on the analytical curve slope (■) and intercept (▲)..

It has also been reported that the presence of chloride added to the arsenic reagent helps the conversion of iodate to iodide in less than 1 minute (27). In order to study if the reagent conditions in the developed method, described previously, allowed the conversion of iodate in iodide, the analysis of an iodate and iodide standard was performed.

A standard with 0.99 µmol/L of iodate and 0.99 µmol/L of iodide, to a final concentration of 1.98 µmol/L of inorganic iodine, was injected and the result compared to the one standard of 1.98 µmol/L of iodide. There was no significant difference (-2%) between the combined iodide and iodate standard, and the iodide standard of 1.98 µmol/L. This indicated that the iodate present in the standard solution is converted to iodide and the total inorganic iodine can be quantified with the described MS-Chip system.

3.3.2. Study of the fluorometric determination of total iodine

To allow a mixture of an oxidant reagent in the way to the digestor, a fourth syringe and a confluence were added to the developed system (Figure 3.2). A fourth syringe was filled with 1 mol/L of H_2SO_4 to study the dilution effect of the confluence addition in the total iodine determination system. These changes reduced the sensitivity to half, as it was expected. The amount of standard or sample injected was set to half (150 µL) and mixed with 150 µL of the oxidant reagent, contained in the fourth syringe. In the end, the same volume of 300 µL was propelled to the Chip to be mixed with the Sandell-Kolthoff reaction reagents (Ce(IV) and As(III)).
For the determination of the total iodine, an oxidant reagent, 0.15% of a potassium persulfate, was used (61), based on a procedure developed by Santos et al, 2013.

3.3.2.1 Study of the temperature influence

To study the conversion of the diverse iodine forms to iodide, three temperatures, 25, 45 and 75˚C, were tested. Iodoacetic acid standards were used as a model to study the efficiency of the conversion of organo-iodine compounds to iodide (62,63). Calibration curves with iodoacetic acid and iodide standards were compared. Higher temperatures were not studied because of the air bubbles formation. Nevertheless, a debubbler device was attached before the chip, to eliminate the maximum number of possible formed bubbles.

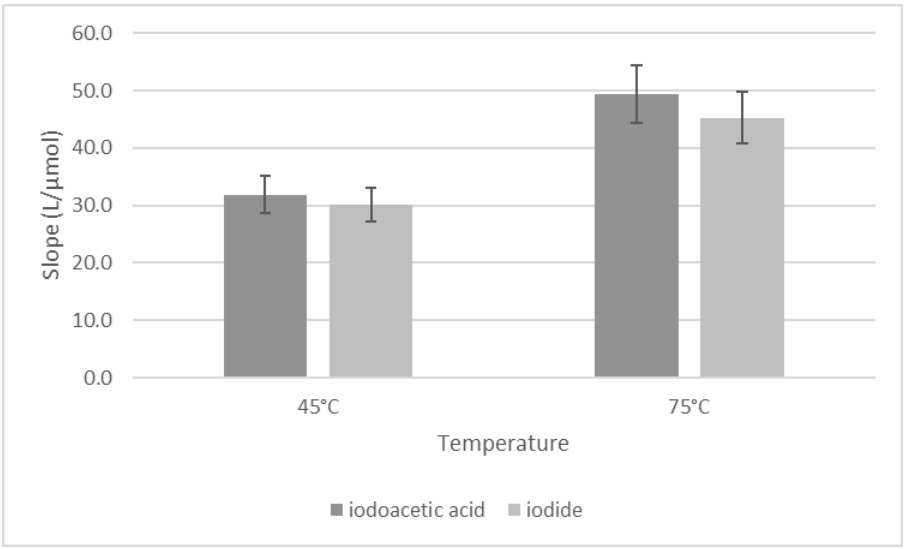

Figure - 3.5 Effect of the temperature on the conversion of the diverse iodine forms to iodide in the MS-Chip in-line UV digestion system

At 25 C, the conversion (about 30%) was not sufficient, even using a higher concentration (0.30%) of potassium persulfate.
Therefore, the reactor temperature was increased to 45ºC. In these conditions, there was an efficient conversion of the diverse iodine forms to total iodide, as there was no statistical difference between the calibration curve with iodoacetic acid and iodide standards (Figure 3.5).
Anyway, a study with a temperature to 75ºC was carried out, and an improvement of 45% in the sensitivity (Figure 3.5) was observed. Aiming to improve the determination sensitivity, the temperature of 75˚C was chosen.

3.3.3 Study of the flow rate influence using the MS- Chip in-line UV digestion system

In order to increase the contact time between reagents and sample and the reaction extension, the flow rate of the developed method was studied.

The initial flow-rate of 10 mL/min for both, aspiration and propulsion, was compared, using calibration curves with iodide standards, to a 5 mL/min flow rate. There was no significant difference between results with the two flow-rates (Figure 3.6).
Aiming to decrease the time per determination, a flow rate of 5 mL/min for propulsion and a 10 mL/min for the aspiration, was tested (Figure 3.6).

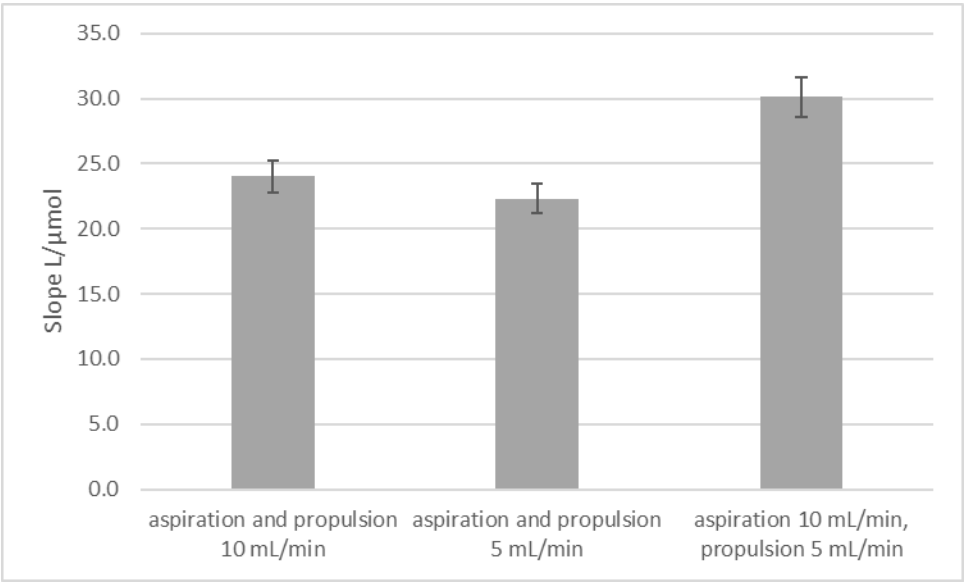

Figure - 3.6 Study of the influence of the flow rate with the MS-Chip in-line UV digestion system

There was an increase of sensitivity of 35% using the combined flow rate (aspiration 10 mL/min and propulsion 5 mL/min), if compared with the flow rate of 5 mL/min. In comparison with the flow rate of 10 mL/min, the use of a combined flow rate of 10/5 mL/min demonstrated and increase of 25% in sensitivity.

In conclusion, using the aspiration flow rate of 10 mL/min and the propulsion rate of 5 mL/min was the best combination, as it allowed to decrease the time per determination and to increase the reaction extension (Figure 3.6).

3.3.4 Interference assessment

3.3.4.1 Interferents of the Sandell-Kolthoff reaction

As thiocyanate and ascorbic acid are known interferents in the Sandell-Kolthoff reaction (14,24,27,64), an interference study for these species was conducted.

3.3.4.1.1 Study of the oxidant concentration

For these interferents species study, the conditions previously established, temperature of 75°C and 0.15% of the oxidant reagent concentration, were used. In these conditions, the tested thiocyanate concentrations did not interfere in the determination (signal variation <9%).

For the elimination of the ascorbic acid interference, three concentrations of the oxidant reagent (0.15, 0.22 and 0.3% of potassium persulfate) were tested. The interference of the ascorbic acid was eliminated (signal variation <4%) when a concentration of the oxidant reagent (potassium persulfate) of 0.3% was used (Table 3.5).

These tested ions, the tested concentration and the respective percentages are presented in Table 3.5.

Table - 3.5 Assessment of the Sandell-Kolthoff reaction interferents with the developed MS-Chip in-line UV digestion method, using an iodide standard of 100.0 µg/L and 0.3% of potassium persulfate as oxidant reagent.

Interferent	Concentration mg/L	% Interference
SCN^-	5	3
	22	9
$C_6H_8O_6$	6.6	6
	13.2	4
	26.5	13

The interference percentage was calculated as relative deviation between the signals obtained, with (AI&Int) and without (AI) the potential interfering ion: % Interference = [(AI&Int− AI) ÷ AI].

As a conclusion of this study, an option was made to set the persulfate concentration to 0.3% for further studies.
As this change could potentially influence the sensitivity of the determination, a study was conducted by tracing calibration curves with different potassium persulfate concentrations (Figure 3.7).

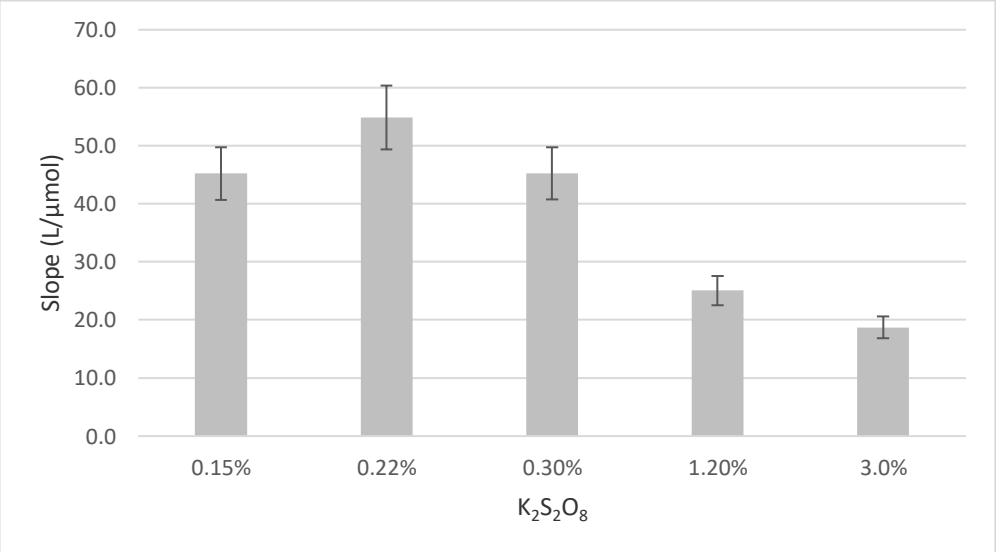

Figure - 3.7 Study of the influence different oxidant reagent concentrations in the determination.

There was no statistical difference (9%) when the potassium persulfate concentration was increased from 0.15% to 0.3% (Figure 3.7). The increase of the oxidant concentration to 1.2 and 3.0% led to a decrease in the sensitivity (-45 and -56 % respectively).

To confirm that, in these modified conditions, the conversion efficiency was still maintained, a study was carried out using three different concentrations (0.15, 0.22 and 0.3%) of potassium persulfate; calibration curves with standards with iodoacetic acid and iodide were traced ((Figure 3.8).

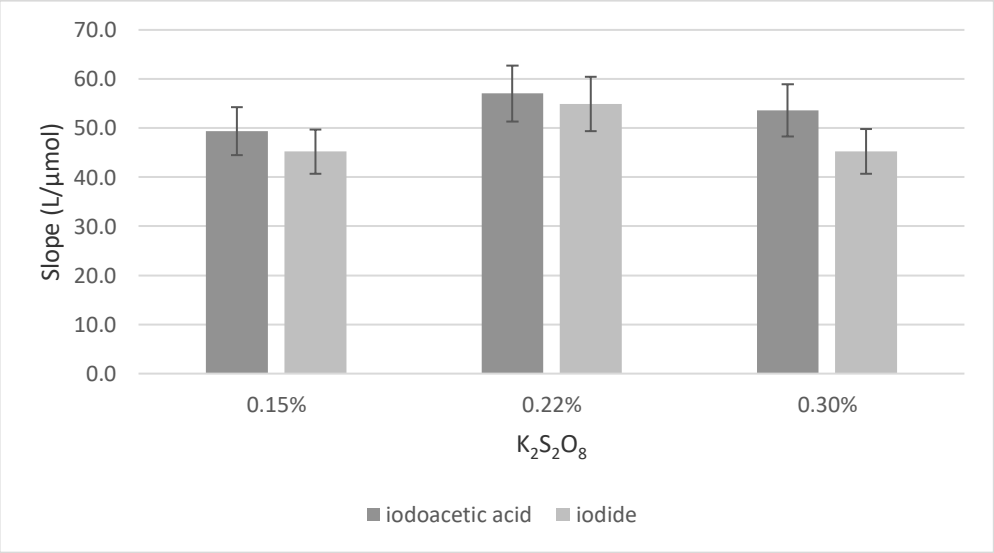

Figure - 3.8 Study of the conversion of the iodine forms in iodide using different oxidant reagent concentrations in the digestion reaction.

It was observed that the conversion efficiency was not still statistically different from 100%. A 0.3% of potassium persulfate solution was set as the oxidant reagent concentration in the developed method.

3.3.4.2 Other potential interfering ions

To evaluate the interference of other anions in the determination of total iodine, an interference study was carried out for several anions usually present in algae (65–68). The tested ions and the respective interference percentages are presented in Table 3.6.

Table - 3.6 Assessment of the influence of potential interfering ions present in algae with the developed MS-Chip in-line UV digestion method, using an iodide standard of 200.0 µg/L.

Potential interferent	Reference concentration in algae mg/Kg	Expected concentration in tested sample mg/L	Tested concentration mg/L	Interference in I^- determination %
NO_3^-	4500[a]	45	10	-6
			50	-4
			150	-10
			500	-20
NO_2^-	40.9[a]	0.41	0.04	-2
			40	-7
			50	-11
PO_4^{3-}	5400	54	0.5	-3
			500	1
			1000	2
			1600	-1
			2500	-1
			5000	-3
			8000	-8
			10000	-2
			15000	-11
CN^{-*}	0.3	0.003	2.2	3
			9.9	9
$C_6H_8O_6^*$	118.8	1.2	6.6	6
			13.2	4
			26.5	13

*using an iodide standard of 100 µg/L

[a] - reference concentration in plants

The results demonstrated that the amount for each possible interferent did not interfere with the iodine determination using the MS-Chip in-line UV digestion method.

3.3.5. Figures of merit

The characteristics of the two developed methods for iodine determination were summarized in Table 3.7.

Table - 3.7 Features of the two developed MS-Chip methods for iodine quantification in salt and algae samples.

	Dynamic range, (µmol/L)	Typical calibration curve[a] A = S x µmol/L I + b	LOD (µmol/L)	LOQ (µmol/L)	One Determination (h)	Analysis rate (h^{-1})[b]	Effluent production (mL)[b]	Reagent consumption (µmol)[c]
MS-Chip	0.20 - 4.0	A= 91.17±1.24 x [I] + 65.87±9.326 R^2= 0.998±0.002	0.025	0.199	0.049	1.18	71	(Ce(IV)) 0.555 (As(III)) 30.0 ($K_2S_2O_8$) 1.65[d]
MS-Chip with in-line UV	0.23 - 4.0	A= 42.18±3.524 x [I] + 177.7±15.86 R^2= 0.996±0.001	0.028	0.231	0.058	1.40	110	

[a] - five calibration curves

[b] - calibration curve with eight standards

[c] – one determination

[d] - oxidation reagent

The limits of detection and quantification, LOD and LOQ, were calculated according to IUPAC recommendations (69,70): three (LOD) and ten (LOQ) times the standard deviation of 10 consecutive injections of MQW, was used.

To perform one analytical curve with eight concentration values in triplicates, 24 analytical cycles were needed. As for an individual sample in triplicate only 3 analytical cycles (without time variation) were needed. An analytical cycle was the sum of the time needed for each step.

The consumption values of effluent production, per calibration curve of eight standards, and reagents consumption per determination was also calculated.

3.3.6. Application to iodine containing samples - accuracy assessment

3.3.6.1 Salt samples

Accuracy assessment was obtained by analysing a total of 13 marine salt samples with the developed MS-Chip method and with a comparison method (potentiometric detection and an iodometric titration method); the results are presented in Figure 3.9.

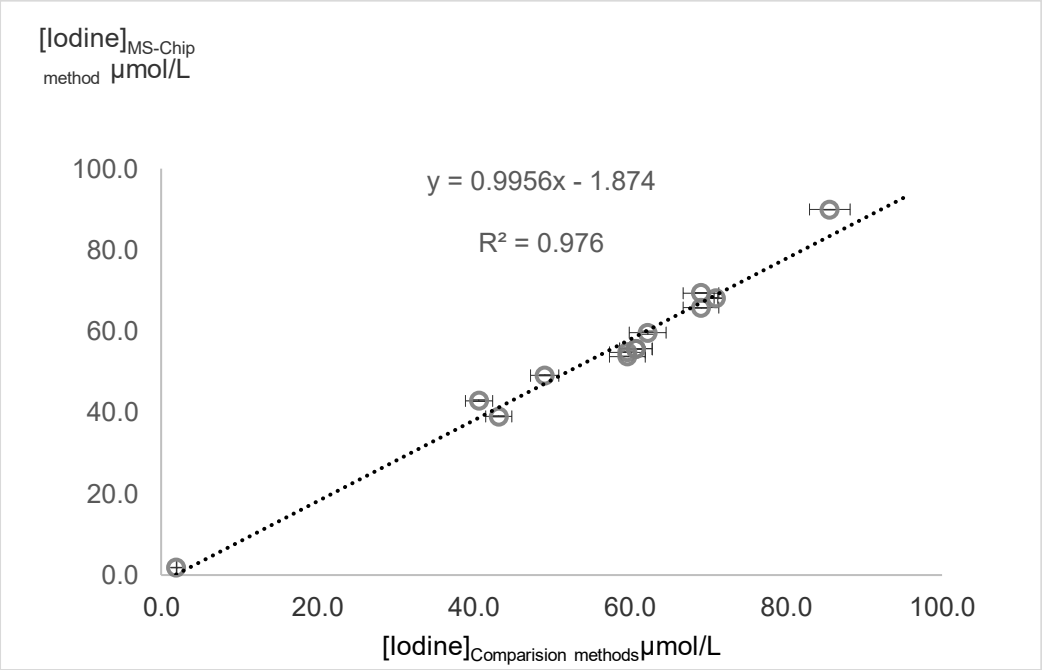

Figure - 3.9 Comparison of the results obtained with the proposed MS-Chip method and with the comparison methods (potentiometric detection method (iodide selective electrode) and an iodometric titration method (for iodate quantification)), for the analysis of marine salt samples.

A linear relationship between MS-Chip method (µmol/L) and Comparison iodine (iodate and iodide) methods (µmol/L) was established for inorganic iodine. The results were plotted (Figure 3.9) and the equation found was: $[Iodine]_{MS\text{-}Chip\ method}$ 0.9956 (±0.0473) x $[Iodine]_{Comparison\ methods}$ – 1.8737 (±2.8239), where the values in parenthesis are 95% confidence limits (71). These figures show that the estimated slope and intercept do not differ statistically from values 1 and 0, respectively. Therefore, there is no evidence for systematic differences between the two sets of results.

3.3.6.2 Supplement iodine samples

Five pharmaceutical samples and one algae supplement sample were analysed with the developed MS-Chip and MS-Chip in-line UV digestion methods as described in the Table 3.8. The iodine concentration for the reference samples with the developed methods were compared to the expected reference values. The correspondent relative deviation for each sample was calculated.

Table - 3.8 Results obtained with the proposed flow system (MS-Chip and MS-Chip in-line UV digestion methods) for six reference samples; five pharmaceutical samples and one algae supplement sample: RD, relative deviation between the two set of results; SD standard deviation of the developed method.

Sample ID	Expected value[I-] (µmol/L)	MS-Chip Method [I] (µmol/L)	SD	RD%
#Pharm 1	0.81	0.83	0.02	1.5%
#Pharm 2	1.76	1.78	0.01	1.5%
#Pharm 3	2.52	2.61	0.20	3.6%
#Pharm 4	1.58	1.60	0.01	1.3%
#Pharm 5	2.36	2.40	0.03	1.5%
#Algae 1	1.58	1.66*	0.20	5.2%

*MS-Chip in-line UV digestion method [I] (µmol/L)

No significant differences (relative deviation, RD <5%) were observed for the calculated relative deviation (RD) for each analysed sample. The average of the relative deviation was of 2%. A statistical test (t-test) was used to evaluate if the mean expected/determination value did significantly differ from 100%. For a 95% significance level, the calculated t-value was 0.493 with a correspondent critical value of 3.495; the calculated t-value is lower than the critical value, thus indicating that the results are not statistically different.

3.3.7 Recovery studies

To further validate the method, standard additions were performed, and recovery percentages calculated to validate de MS-Chip in-line UV digestion method. To three different algae samples, 0.79 µmol/L and/or 1.58 µmol/L of iodide were added, and the samples analysed by the developed method.

The information about the different samples, the initial concentration, the added value of iodide, the concentration found and the recovery percentages, were calculated according to the IUPAC (72). The results were summarized in Table 3.9.

Table - 3.9 Recovery percentages calculated from spiked supplement algae and seaweed samples assessed with the MS-Chip in-line UV digestor developed method; SD, standard deviation; RSD, relative standard deviation.

Sample ID	Initial µmol/L	SD	RSD%	Added µmol/L	Found µmol/L	SD	RSD%	Recovery (%)
#Algae 2	1.74	0.01	0.6%	1.58	3.33	0.03	0.9%	100%
#Algae 3	2.13	0.05	2.3%	0.79	2.97	0.17	5.7%	106%
				1.58	3.96	0.15	3.8%	116%
#Algae 4	0.27	0.02	7.4%	0.79	0.97	0.12	12%	89%

The average of the recovery percentages was 103% with a standard deviation of 11%. A statistical test (t-test) was used to evaluate if the mean recovery value did significantly differ from 100%. For a 95% significance level the calculated t-value was 0.181 with a correspondent critical value of 4.177, indicating that no multiplicative interferences were found.

3.4. Conclusions

The use of a multi-syringe flow system, with the possibility of an in-line UV digestion additional step for the determination of total iodine, demonstrated to be advantageous compared to the classic approach of the Sandell-Kolthoff reaction (17). In the developed method, no pre-treatment steps were required, reagents and sample volume consumption was reduced and automation was accomplished.

The in-line digestion approach, here described, presents an efficient conversion of organo-iodide compounds to iodide, avoiding any off-line treatments, which is a significant advantage over classical methods or other previously described flow methods (27,34,56,57,73).

The achieved range of iodine determination (0.20 – 4.0 µmol/L of iodine) allows to analyse samples within the reference range values of iodine intake (levels of insufficient intake within <0.16 to 0.78 µmol/L, adequate levels of 0.79 to 1.57 µmol/L, above requirement levels 1.58 to 2.36 µmol/L and excessive levels ≥2.36 µmol/L of iodine (74)).

Additionally, the developed method can be effectively applied to iodine determination in salt, supplements (algae), seaweed and pharmaceutical samples, which are examples of intake forms of iodine in the population.

References

1. Hess SY. The impact of common micronutrient deficiencies on iodine and thyroid metabolism: the evidence from human studies. Best Pract Res Clin Endocrinol Metab. 2010;24(1):117–132.

2. Laurberg P, Cerqueira C, Ovesen L, Rasmussen LB, Perrild H, Andersen S, et al. Iodine intake in Portuguese pregnant women: results of a countrywide study. Eur J Endocrinol. 2010;163(1):13–27.

3. Costeira MJ, Oliveira P, Santos NC, Ares S, Saenz-Rico B, De Escobar GM, et al. Psychomotor development of children from an iodine-deficient region. J Pediatr. 2011;159(3):447–453.

4. Henjum S, Lilleengen AM, Aakre I, Dudareva A, Gjengedal ELF, Meltzer HM, et al. Suboptimal iodine concentration in breastmilk and inadequate iodine intake among lactating women in Norway. Nutrients. 2017;9(7):643.

5. Garnweidner-Holme L, Aakre I, Lilleengen AM, Brantsæter AL, Henjum S. Knowledge about iodine in pregnant and lactating women in the Oslo area, Norway. Nutrients. 2017;9(5).

6. Limbert E, Prazeres S, São Pedro M, Madureira D, Miranda A, Ribeiro M, et al. Iodine intake in Portuguese pregnant women: results of a countrywide study. Eur J Endocrinol. 2010;163(4):631–635.

7. Lopes MS, Castro JJ de, Marcelino M, Oliveira MJ, Carrilho F, Limbert E. Iodine and Thyroid: What a Clinic Should Know. Acta Med Port. 2012;25(3):174–178.

8. Lobato CB, Machado A, Mesquita RBR, Lima L, Bordalo AA. Can non-fortified marine salt cover human needs for iodine? Int J Food Sci Nutr. 2019;70(3):349–354.

9. Andersson M, Karumbunathan V, Zimmermann MB. Global iodine status in 2011 and trends over the past decade. J Nutr. 2012;142(4):744–750.

10. Hess SY, Ouédraogo CT, Young RR, Bamba IF, Stinca S, Zimmermann MB, et al. Urinary iodine concentration identifies pregnant women as iodine deficient yet school-aged children as iodine sufficient in rural Niger. Public Health Nutr. 2017;20(7):1154–1161.

11. Zimmermann MB, Andersson M. Prévalence du déficit iodé en Europe en 2010. Ann Endocrinol (Paris). 2011;72(2):164–166.

12. Aquaron R, Delange F, Marchal P, Lognoné V, Ninane L. Bioavailability of seaweed iodine

in human beings. Cell Mol Biol (Noisy-le-grand). 2002;48(5):563–569.

13. Yeh TS, Hung NH, Lin TC. Analysis of iodine content in seaweed by GC-ECD and estimation of iodine intake. J Food Drug Anal. 2014;22(2):189–196.

14. Shelor CP, Dasgupta PK. Review of analytical methods for the quantification of iodine in complex matrices. Vol. 702, Analytica Chimica Acta. 2011. p. 16–36.

15. Jooste PL, Strydom E. Methods for determination of iodine in urine and salt. Best Pract Res Clin Endocrinol Metab. 2010;24(1):77–88.

16. Pino S, Fang SL, Braverman LE. Ammonium persulfate: A safe alternative oxidizing reagent for measuring urinary iodine. Clin Chem. 1996;42(2):239–243.

17. Machado A, Lima L, Mesquita RBR, Bordalo AA. Improvement of the Sandell-Kolthoff reaction method (ammonium persulfate digestion) for the determination of iodine in urine samples. Clin Chem Lab Med. 2017;55(9):E206–E208.

18. American Public Health Association; American Water Works Association; Water Environment Association. Standard methods for the examination of water and wastewater. 23th ed. American Public Health Association; 2017.

19. Zimmermann MB, Jooste PL, Pandav CS. Iodine-deficiency disorders. Lancet. 2008 Oct 4;372(9645):1251–1262.

20. Garry PJ, Lashley DW, Owen GM. Automated Measurement of Urinary Iodine. Clin Chem. 1973;19(9):950–953.

21. Burguera JL, Brunetto MR, Contreras Y, Burguera M, Gallignani M, Carrero P. Head-space flow injection for the on-line determination of iodide in urine samples with chemiluminescence detection. Talanta. 1996;43(6):839–850.

22. Yaqoob M, Atiq-Ur-Rehman, Waseem A, Nabi A. Determination of iodide using flow injection with acidic potassium permanganate chemiluminescence detection. Luminescence 2006; 21(4):221–225.

23. Machado A, Mesquita RBR, Oliveira S, Bordalo AA. Development of a robust, fast screening method for the potentiometric determination of iodide in urine and salt samples. Talanta. 2017;167:688–694.

24. Tsuda K, Namba H, Nomura T, Yokoyama N, Yamashita S, Izumi M, et al. Automated Measurement of Urinary Iodine with Use of Ultraviolet-Irradiation. Clin Chem. 1995;41(4):581–585.

25. Yaping Z, Dongxing Y, Jixiang C, Tianshiu L, Huiqin C. Spectrophotometric determination of urinary iodine by flow-injection analysis with on-line catalytic digestion. Clin Chem.

1996;42(12):2021–2027.

26. Waseem A, Yaqoob M, Nabi A. Flow-injection method for the determination of iodide/iodine using Ru(bpy)33+-NADH chemiluminescence detection. Luminescence. 2008 Oct;23(5):316–320.

27. Nacapricha D, Muangkaew S, Ratanawimarnwong N, Shiowatana J, Grudpan K. Continuous and stopped flow injection for catalytic determination of total iodine in urine. Analyst. 2001;126(1):121–126.

28. Pereira AC, Rocha FRP. Liquid-liquid microextraction in a multicommuted flow system for direct spectrophotometric determination of iodine value in biodiesel. Anal Chim Acta. 2014 Jun 4;829:28–32.

29. Kuznetsov V V., Ermolenko Y V., Seffar L. Flow-injection determination of elemental iodine by polyvinyl alcohol. J Anal Chem. 2004 Jul;59(7):688–693.

30. Kuznetsov V V., Ermolenko Y V., Seffar L. Amylose and amylopectin as reagents for the flow-injection determination of elemental iodine. J Anal Chem 2007;62(5):479–485.

31. Trojánek A, Papoff P. Pneumatoamperometric flow-injection determination of iodide. Anal Chim Acta. 1991 Jun 14;247(1):73–77.

32. Motomizu S, Yoden T. Porous membrane permeation of halogens and its application to the determination of halide ions and residual chlorine by flow-injection analysis. Anal Chim Acta. 1992 May 25;261(1–2):461–469.

33. Williamson JP, Emmert GL. A flow injection analysis system for monitoring silver (I) ion and iodine residuals in recycled water from recovery systems used for spaceflight. Anal Chim Acta. 2013 Aug 20;792:72–78.

34. Choengchan N, Lukkanakul K, Ratanawimarnwong N, Waiyawat W, Wilairat P, Nacapricha D. Use of pseudo-first order kinetics in flow injection for determination of trace inorganic iodine. Anal Chim Acta. 2003 Dec 4;499(1–2):115–122.

35. Jakmunee J, Grudpan K. Flow injection amperometry for the determination of iodate in iodized table salt. Anal Chim Acta. 2001 Jul 3;438(1–2):299–304.

36. Abouhiat FZ, Henriquez C, Horstkotte B, El Yousfi F, Cerda V. A miniaturized analyzer for the catalytic determination of iodide in seawater and pharmaceutical samples. Talanta. 2013;108:92–102.

37. Nogueira ARA, Mockiuti F, Souza GB, Primavesi O. Flow Injection Spectrophotometric Catalytic Determination of Iodine in Milk. Anal Sci. 1998;14(3):559–564.

38. Hassan SSM, Marzouk SAM. Sequential flow-injection potentiometric determination of

iodide and iodine in povidone iodine pharmaceuticals. Electroanalysis. 1993;5(9–10):855–861.

39. Nacapricha D, Uraisin K, Ratanawimarnwong N, Grudpan K. Simple and selective method for determination of iodide in pharmaceutical products by flow injection analysis using the iodine-starch reaction. Anal Bioanal Chem. 2004;378(3):816–821.

40. Srivorakul T, Varanusupakul P, Alahmad W. Development of a Sample Treatment Method for a Flow Injection Determination of Iodine in Eggs: A Comparison Study. Anal Sci. 2020 Apr 10;36(4):491–495.

41. Thomaidis NS, Georgiou CA. Direct parallel flow injection multichannel spectrophotometric determination of olive oil iodine value. Anal Chim Acta. 2000 Jan 24;405(1–2):239–245.

42. Ratanawimarnwong N, Amornthammarong N, Choengchan N, Chaisuwan P, Amatatongchai M, Wilairat P, et al. Determination of iodide by detection of iodine using gas-diffusion flow injection and chemiluminescence. Talanta. 2005 Feb 15;65(3):756–761.

43. Zabala J, Carrión N, Murillo M, Quintana M, Chirinos J, Seijas N, et al. Determination of normal human intrathyroidal iodine in Caracas population. J Trace Elem Med Biol. 2009 Jan 1;23(1):9–14.

44. Choengchan N, Uraisin K, Choden K, Veerasai W, Grudpan K, Nacapricha D. Simple flow injection system for colorimetric determination of iodate in iodized salt. Talanta. 2002 Dec 6;58(6):1195–1201.

45. Håkedal JT, Egeberg PK. Determination of Iodide in Brines by Membrane Permeation Flow Injection Analysis†. Analyst. 1997;122(11):1235–1237.

46. Oguma K, Kitada K, Kuroda R. Microchemical determination of Iodate and iodide in sea waters by flow injection analysis. Microchim Acta 1993 1101. 1993;110(1):71–77.

47. Monks CD, Nacapricha D, Taylor CG. Determination of iodide ion in impregnated charcoals by flow injection. Analyst. 1993;118(6):623–626.

48. Fujiwara T, Mohammadzai IU, Kojima M, Kumamaru T. An improved method for the flow-injection determination of iodine using the luminol chemiluminescence reaction in a reversed micellar medium of cetyltrimethylammonium chloride in 1-hexanol-cyclohexane. Anal Sci. 2006;22(1):67–71.

49. Yonehara N, Kozono S, Sakamoto H. Flow Injection-Spectrophotometric Determination of Trace Amounts of Iodide by Its Catalytic Effect on the 4, 4′-Bis(dimethylamino)-diphenylmethane- Chioramine T Reaction. Anal Sci. 1991 Apr 10;7(2):229–234.

50. Davey DE, Mulcahy DE, O'Connell GR. Potentiometric flow-injection determination of iodide

and iodine. Talanta. 1990;37(3):313–316.

51. Nacapricha D, Sangkarn P, Karuwan C, Mantim T, Waiyawat W, Wilairat P, et al. Pervaporation-flow injection with chemiluminescence detection for determination of iodide in multivitamin tablets. Talanta. 2007 Apr 30;72(2):626–633.

52. Liu G, Li J, Zhao X. Ion Exchange-Flow Injection Spectrophotometric Simultaneous Determination of Traces of Bromide and Iodide in some Chinese Standard Samples. Geostand Newsl. 1995;19(2):215–220.

53. Nellaiappan S, Kumar AS. Selective flow injection analysis of iodate in iodized table salts by riboflavin immobilized multiwalled carbon nanotubes chemically modified electrode. Electrochim Acta. 2013 Oct 30;109:59–66.

54. Nikolic SD, Mutic JJ, Lolic AD, Manojlovic DD. Sensitive flow-injection amperometric detection of iodide using Mn3+ and As3+. Anal Sci. 2005;21(5):525–529.

55. Ensafi AA, Dehaghi GB. Flow-injection simultaneous determination of iodate and periodate by spectrophotometric and spectrofluorometric detection. Anal Sci. 2000;16(1):61–64.

56. Frizzarin RM, Aguado E, Portugal LA, Moreno D, Estela JM, Rocha FRP, et al. A portable multi-syringe flow system for spectrofluorimetric determination of iodide in seawater. Talanta. 2015;144:1155–1162.

57. Inpota P, Strzelak K, Koncki R, Sripumkhai W, Jeamsaksiri W, Ratanawimarnwong N, et al. Microfluidic Analysis with Front-Face Fluorometric Detection for the Determination of Total Inorganic Iodine in Drinking Water. Anal Sci. 2018;34(2):161–167.

58. Tesfaldet ZO, Van Staden JF, Stefan RI. Sequential injection spectrophotometric determination of trace amounts of iodide by its catalytic effect on the 4,4′-methylenebis(N,N-dimethylaniline)-chloramine-T reaction. Talanta. 2004;64(5 SPEC. ISS.):1213–1219.

59. Santos IC, Mesquita RBR, Bordalo AA, Rangel A. Iodine speciation in coastal and inland bathing waters and seaweeds extracts using a sequential injection standard addition flow-batch method. Talanta. 2015;133:7–14.

60. Zagatto EAGG, Arruda MAZZ, Jacintho AO, Mattos IL. Compensation of the Schlieren effect in flow-injection analysis by using dual-wavelength spectrophotometry. Anal Chim Acta. 1990;234(C):153–160.

61. Santos IC, Mesquita RBR, Machado A, Bordalo AA, Rangel AOSS. Sequential injection methodology for carbon speciation in bathing waters. Anal Chim Acta. 2013;778:38–47.

62. Gong T, Zhang X. Determination of iodide, iodate and organo-iodine in waters with a new total organic iodine measurement approach. Water Res. 2013;47(17):6660–6669.

63. Pan Y, Zhang X. Total organic iodine measurement: A new approach with UPLC/ESI-MS for off-line iodide separation/detection. Water Res. 2013;47(1):163–172.

64. Ford HC, Johnson LA. Ascorbic acid interferes with an automated urinary iodide determination based on the ceric-arsenious acid reaction. Clin Chem. 1991;37(5):759–759.

65. Amorim K, Lage-Yusty MA, López-Hernández J. Changes in bioactive compounds content and antioxidant activity of seaweed after cooking processing. 2012;10(4):321–324.

66. Umar S, Iqbal M. Nitrate accumulation in plants, factors affecting the process, and human health implications. A review. Agron Sustain Dev. 2007;27(1):45–57.

67. Mikkelsen R. A Closer Look at Phosphorus Uptake by Plants. 2013.

68. Kurashova I, Halevy I, Kamyshny A. Kinetics of Decomposition of Thiocyanate in Natural Aquatic Systems. Environ Sci Technol. 2018;52(3):1234–1243.

69. Currie LA. Nomenclature in Evaluation of Analytical Methods Including Detection and Quantification Capabilities (IUPAC Recommendations 1995). Int Union Pure Appl Chem. 1995;67:1699–1723.

70. International Union of Pure and Applied Chemistry. Nomenclature, symbols, units and their usage in spectrochemical analysis-ii. data interpretation. Pure Appl Chem. 1976 Jan 1;45(2):99–103.

71. Miller JN, Miller JC. Statistics and Chemometrics for Analytical Chemistry. Sixth edit. Pearson Education Limited; 2010.

72. Burns D, Danzer K, Townshend A. Use of the Terms “Recovery” and “Apparent Recovery” in Analytical Procedures. Int Union Pure Appl Chem. 2002;74(11):2201–2205.

73. Abouhiat FZ, Henríquez C, Horstkotte B, El Yousfi F, Cerdà V. A miniaturized analyzer for the catalytic determination of iodide in seawater and pharmaceutical samples. Talanta. 2013 Apr 15;108:92–102.

74. World Health Organization. Urinary iodine concentrations for determining iodine status in populations. Vitamin and Mineral Nutrition Information System. WHO/NMH/NHD/EPG/13.1. 2013.

Chapter 4

Measurement of iron(III) in waters by microsequential injection solid phase spectrometry using an hexadentate 3-hydroxy-4-pyridinone chelator as reagent

Measurement of iron(III) in waters by microsequential injection solid phase spectrometry using an hexadentate 3-hydroxy-4-pyridinone chelator as reagent

In this chapter, the hexadentate 3,4–hydroxypyridinone ligand was used as reagent for the spectrophotometric quantification of iron(III) in fresh and sea waters, using a micro sequential injection lab-on-valve (μSI-LOV) system in a solid phase spectrometry (SPS) mode. To implement SPS, thus eliminating the sample matrix, a packed column in the flow cell was used; the chosen sorbent was Nitrilotriacetic Acid Superflow resin (NTA). The possibility of performing an analytical curve resorting to just one standard was also demonstrated. The consumption of the hexadentate ligand was about 30 μg per determination and the effluent production lower than 2.5 mL. The dynamic concentration range was 0.45 – 9.0 μmol/L, with a limit of detection of 0.13 μmol/L and limit of quantification 0.43 μmol/L. The proposed μSILOV-SPS methodology was successfully applied to river, ground, estuarine, tap, and sea waters.

Keywords: hexadentate 3,4-hydroxypyridinone ligand; iron(III) quantification; solid phase spectrometry; fresh and saline water samples.

The work described in this chapter was published: Joana L. A. Miranda, Raquel B. R. Mesquita, Ana Nunes, Maria Rangel, António O. S. S. Rangel, Talanta, volume 191, 2019, pages 409-414.

4.1. Introduction

Iron is introduced in the ocean by dust deposition and the concentration of iron in seawater is expected to be in the order of nanomol/L thus being difficult to quantify (1); additionally, sea water is a high complex matrix due to abundance of other analytes such as magnesium, calcium and chloride. Due to its relevancy, as part of oceanic biogeochemistry and biological activity, there is the need to exploit new analytical techniques with low detection limits (2). One of the challenges of targeting iron quantification in sea waters is the potential interferences from the matrix, namely high salinity. Atomic absorption spectrometry (AAS) or inductively coupled plasma mass spectrometry (ICP-MS) display good selectivity and sensitivity but they have low tolerance for high salt content. Furthermore, these techniques do not allow in-situ analysis, and require expensive instrumentation and consumables. Alternatively, molecular spectrophotometric techniques can be used for iron quantification in environmental samples, potentially allowing in situ determination and analyte speciation. Another advantage of molecular spectrophotometric detection is its potential for easy coupling with flow analysis techniques (3). Several features result from this combination like achieving lower reagent consumption and effluent production, multi-parametric determinations, and automation. Flow techniques comprises relatively inexpensive components, including low-cost miniaturized detectors, thus allowing the efficient implementation of methods for water analysis (4). However, the colour-forming reactions used in molecular spectrophotometry may involve toxic chromogenic reagents. In this context, use of iron chelators based on 3-hydroxy-4-pyridinone was recently described (5–8) aiming at a greener approach for iron determination. In most of the reported work, bidentate ligands were used (5–7) but one exploited the use of a hexadentate 3-hydroxy-4-pyridinone chelator (CP256) and proved to be the best choice (higher sensitivity) (8). This chelator, CP256, a tripodal hydroxypyridinone was a specially designed hexadentate ligand with high affinity for complexing iron(III) (log β = 34.4) (9) and with a 1:1 stoichiometry. The experience in working with these ligands proved the significant advantage in using micro sequential injection lab-on-valve technique (μSI-LOV) (6) over conventional sequential injection analysis (5). The use of μSI-LOV enables a step further in miniaturization with consequent minimization of reagent and sample consumption. Moreover, the μSI-LOV technique permits to accommodate a sorbent material at the flow cell and potentially to perform the measurement directly at the solid material (10) (solid phase spectrometry). This feature was also previously exploited with the bidentate ligands, using NTA Superflow resin for iron(III) retention (6). The choice of this resin was based on its necessary transparency (10) and selective retention of iron (III) at a pH $\approx$ 2 (1,11,12). 4 In this work, a μSI-LOV method with solid phase spectrophotometry (SPS) for the iron(III) quantification with a specially designed hexadentate 3-hydroxy-4-pyridinone chelator (CP256) is proposed. The idea is to retain iron(III) in the NTA resin placed in the flow cell and to discard the water matrix towards waste. Then, if the CP256 ligand is perfused through the solid material, the colored complex can be measured directly at the cell, and elute the iron(III) from the resin. In this

way, the solid material can be used for several measurement cycles. In order to minimize the number of solutions prepared and the amount consumed in the analytical process, a single standard strategy to obtain the analytical curve was also implemented. This consists in using a single standard solution, and loading different amounts of iron(III) into the column, by varying the volume of standard sent to the sorbent material.

4.2. Experimental

4.2.1. Reagents and solutions

All the solutions were prepared with analytical grade chemicals and Milli-Q water (MQW) resistivity > 18.2 MΩ cm (Millipore, USA).

The hexadentate 3,4-hydroxypyridinone ligand (CP256) solution was obtained by dissolving approximately 10 mg of the synthesised ligand in 20.0 mL of MQW, corresponding to a concentration of 0.5 g/L (521 µmol/L). The ligand had been previously synthesized and characterized (9) and the denotation of CP256 was adopted from that work.

The 0.60 mol/L carbonate buffer, pH 10.6, was prepared by dissolving 2.52 g of sodium hydrogen carbonate (Merck, Germany) in 50.0 mL of water and the pH adjusted to 10.6 with 2.5 mol/L sodium hydroxide.

The 0.5 mol/L nitric acid was prepared from dilution of the concentrated acid (d = 1.4; 65%, Merck).

The 180 µmol/L iron(III) stock solution was obtained by dilution of the commercial standard of 18.0 mmol/L (1001 mg/L Fluka - Sigma-Aldrich, Switzerland). This solution was used to prepare an 18.0 µmol/L iron(III) intermediate solution to weekly prepare the Fe^{3+} working standards in the 0.45 - 9.0 µmol/L range, with 0.013 mol/L nitric acid.

The chelating resin was Nitrilotriacetic Acid (NTA) Superflow resin (Qiagen, Netherlands), highly cross-linked 6% agarose, 60 – 160 µm of bead diameter, 50% suspension in 30% ethanol. To load the resin into the flow cell, a 1:3 (v/v) dilution was made to ensure a <10% ethanol concentration. The NTA resin was packed daily and washed with nitric acid (pH ≈ 2) after each cycle. A working day could include about 4 analytical curves, corresponding to about 60 cycles.

4.2.2. Sequential injection manifold and procedure

The micro sequential injection lab-on-valve solid phase spectrometry (µSI-LOV-SPS) method developed is outlined in Figure 4.1. It consisted of a FIAlab – 3500 (FIAlab Instruments, USA) comprising a bi-directional syringe pump of 2.5 mL and a lab-on-valve head mounted on the top of a six-port selection valve. The detection system comprised a USB 2000 Ocean Optics (USA) CCD spectrophotometer, fiber optics cables (FIA-P200-SR, 400 mm) and a Mikropack DH2000-BAL deuterium halogen light source. For flow programming and data acquisition, FIAlab for Windows 5.0 software on a personal computer (HP Compaq) was used. The bead column was attained by

packing the NTA resin between the two optical fibers with a 10 mm optical path (Figure 4.1 B). To prevent resin losses, a PTFE stopper (aligned with the central channel) and a PEEK tube, with inner diameter of 0.06 mm (1560, Nat 1/16x.0025x5ft, Upchurch Scientific, USA), were used.

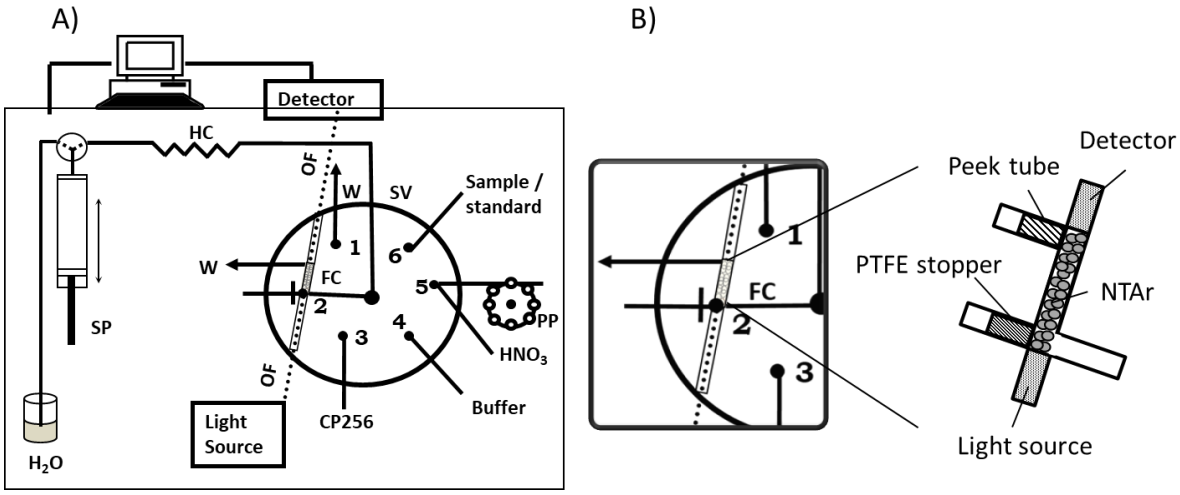

Figure. 4.1 The micro sequential injection lab-on-valve solid phase spectrometry (μSI-LOV-SPS) manifold: A) SV, 6 port selection valve; SP, 2.5 mL syringe pump; HC, 150 cm holding coil; FC, flow cell with NTA resin with 10 mm optical path; OF, optical fibers; W, waste; CP256, 0.5 g/L hexadentate 3,4- hydroxypyridinone solution; Buffer, 0.6 mol/L carbonate buffer, pH 10.6; HNO_3, 0.5 mol/L; B) flow cell detail, scheme of NTA resin packed between the two optical fibers.

For the connection of the different components of the flow system, tubes of polytetrafluoroethylene (PTFE) with 0.8 mm inner diameter were used, including a 1.5 m holding coil. Operating procedures of the developed flow system for iron(III) determination with the respective volumes used is shown in Table 4.1.

Table - 4.1 Operation procedure of the developed μSI-LOV-SPS method for iron(III) determination using a single standard.

Step	Valve position	Flow rate (μL/s)	Volume (μL)	Description
A	-	200	970 - 1300*	Filling the syringe with carrier
B	6	100	40 - 700*	Aspiration of standard
C	2	10	60 - 1050*	Propelling to detector through the NTA resin
D	3	80	60	Aspiration of hexadentate ligand
E	4	10	5	Aspiration of buffer
F	-	-	-	Reference scan
G	2	10	515	Propelling to detector, absorbance measurement, and iron(III) removal from NTA resin
H	5	100	250	Aspiration of nitric acid
I	2	10	750	Propelling through the NTA resin for washing /conditioning

* values used for samples

The syringe pump was filled with carrier prior to the aspiration of standard solutions (step A and B), then standard was propelled towards the flow cell through the NTA column (step C) for iron(III) retention. For attaining an analytical curve, different volumes of the same standard were used, resulting in different retained amounts. The volume propelled was 1.5 times larger than the volume of the standard solution to ensure a complete washing of the column. Afterwards, the CP256 ligand and buffer solutions were sequentially aspirated (steps D and E) and a reference scan was made (step F) before propelling the solutions through the NTA resin, to ensure similar detection conditions. The reference scan enabled to minimize the effect of the beads movement when propelling sample/standards solutions. Then, the ligand and buffer were sent through the column (step G) for the coloured complex formation, allowing both the absorbance measurement, and iron(III) removal from the NTA resin. After the measurement, nitric acid was aspirated and propelled through the NTA resin to prepare it for the next cycle by appropriate reconditioning (steps H and I).

4.2.3. Sample collection and preparation

The natural waters, including river, ground, estuarine, tap, and sea waters used, were collected in polyethylene plastic bottles of 0.5 L capacity and acidified (pH < 2) at the collection according to the reference standard procedure (13).

4.2.4. Accuracy assessment

Three certified water samples were analysed with the developed μSI-LOV method and the result compared with the certified values: NRC-CNR SLRS-4 (river water) from National 7 Research Council, Canada, SPS-SW2 (sea surface water) from National Institute of Standards and Technology (USA) and NIST 1640 (spring water) from National Institute of Standards and Technology. Additionally, a ground water and a tap water were analysed by atomic absorption spectrometry (APHA 3111B) (13), and the results also compared to those obtained with the developed μSI-LOV method.

4.3. Results and discussion

The developed work aimed to quantify iron(III) in various types of natural waters, including sea waters, using solid phase extraction of iron(III) prior to the determination to eliminate potential matrix interferences. The idea was to use solid phase spectrometry, made possible by the optical transparency of the NTA resin (14), together with the capacity of the hexadentate ligand (CP256) to remove iron(III) from the NTA by forming a coloured complex (maximum absorption at 460 nm) (8). Several parameters were set according to previous studies, namely the use of carbonate buffer, pH 10.6, solution (0.6 mol/L) to ensure the appropriate reaction pH (pH ≈ 7) (8) and the minimal reproducible amount of 5 μL for buffer volume (8,15). In a previous work, an attempt was made to use both the ligand with the buffer in a single solution. However, the reagent solution prepared this way was not stable; an increase of the solution colour was observed, meaning that it had to be prepared daily (6). To minimize the influence of the schlieren effect (16), the analytical signal corresponded to subtracting the absorbance measured at 800 nm from the one at 460 nm.

4.3.1. Solid phase spectrometry study

4.3.1.1. Resin column – NTA resin

As mentioned above, NTA superflow resin was packed in the flow cell to attain matrix elimination prior to colour-forming reaction. The first study was to assess the efficiency of retaining iron(III) in NTA resin at pH ≈ 2. For this study, two analytical curves were set by using standards in the range 0.90 – 9.0 μmol/L, with and without the use of NTA, using the same volumes of ligand solution (60 μL) and standard solution (700 μL) and the same optical pathlength (1 cm).

The analytical curve with NTA (A_{NTA} = 0.0446 ± 0.0039x [Fe^{3+}] + 0.029 ± 0.014) represented over a 15-fold increase in sensitivity when compared to the analytical curve obtained without the NTA (A = 0.00285 ± 0.00007 x [Fe^{3+}] + 0.0004 ± 0.0003). Furthermore, with NTA, it was possible to increase the dynamic concentration range, starting from 0.45 μmol/L.

The results indicate that the iron(III) was efficiently retained in NTA at pH ≈ 2 and that the hexadentate ligand CP256 effectively eventually removed it.

4.3.1.2 Column breakthrough

The column breakthrough corresponds to the maximum amount of iron(III) that can be retained in the column of sorbent material. This was assessed by using an iron(III) standard of 9 µmol/L and successively increasing different volumes of this solution, therefore loading different mass values into the packed NTA resin. The absorbance values increased significantly (>14%) up to 6.27 nmol (0.35 µg) of iron(III) and then started to stabilize (<7% increase); so, that amount was considered as the maximum amount retained in the 10 mm NTA resin column (ESI Figure 4.1). As this value corresponded to the highest value of the analytical curve, some problems could arise in working close to the column breakthrough. To minimize potential problems, a washing step after propelling the sample and prior to the colour-forming reaction was studied; the washing volume was set to 1.5 times the sample volume.

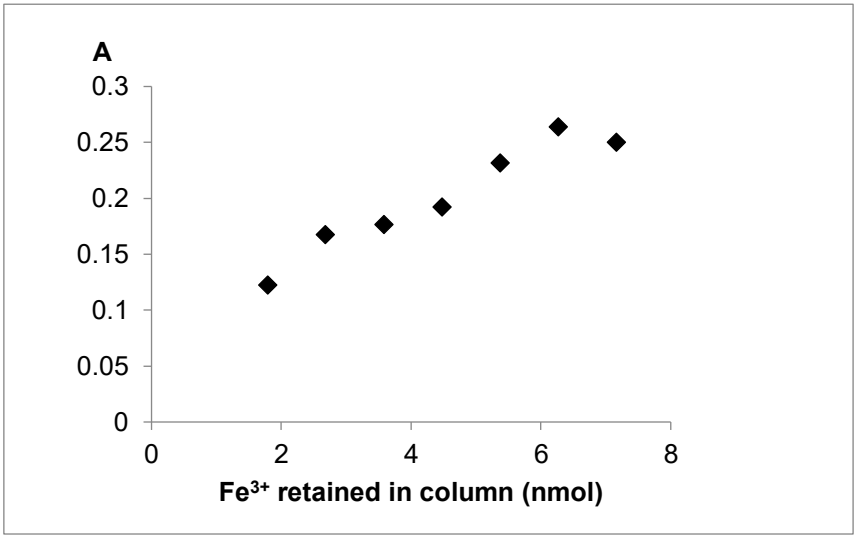

ESI Figure - 4.1 Evaluation of the maximum amount of iron(III) retained in the NTA resin (breakthrough of the beads column).

4.3.2. Study of physical-chemical parameters for the complex formation

4.3.2.1 Sample volume

The sample volume was set to 700 µL as higher volumes would result in working above the maximum NTA column breakthrough.

4.3.2.2. Hexadentate ligand solution (CP256)

The concentration of CP256 ligand, 0.5 g/L, was adopted from the previous work (8), so the following study was to assess the influence of the volume of ligand. From the tested range of 40 - 70 µL, a volume of 60 µL was chosen as it corresponded to the highest sensitivity (calibration curve slope) as it is shown in Figure 4.2.

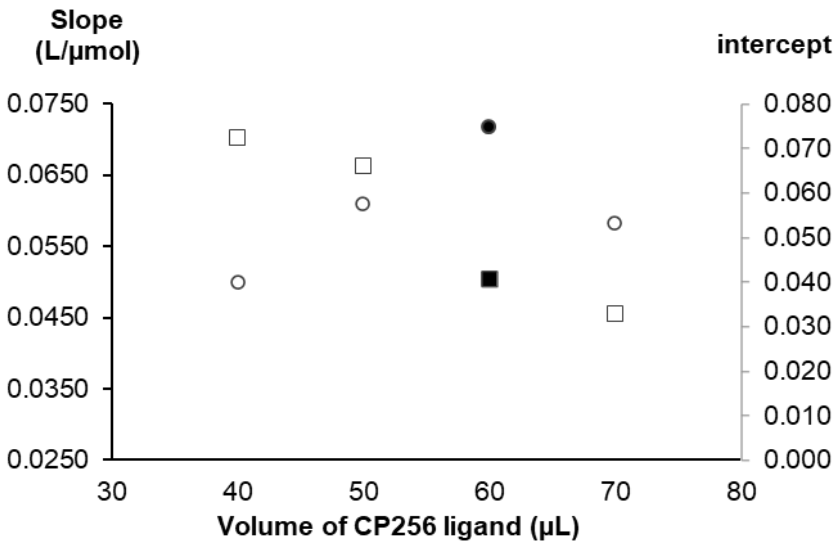

Figure - 4.2 Study of the influence of CP256 ligand solution volume on the calibration curve slope (○) and intercept (□); the points in black represent the chosen volume.

4.3.3 Calibration with one standard

Exploiting the feature of retaining the analyte and discarding the matrix, a one standard approach was tested. The idea was to use only a single standard and passing different volumes through the NTA, resulting in different amounts retained and eluted with the same reagent volume, thus resulting in an analytical curve. If successful, this strategy would have the advantage of preparing only a single standard solution, producing less waste volume, and improve the analytical curve rate. The 9 µmol/L iron(III) standard was used to achieve a calibration range from 0.45 to 9.0 µmol/L, like the analytical curve with multiple standards, and the two analytical curves were compared (Table 4.2). For the multiple standards analytical curve, 700 µL of each standard solution (step B in Table 4.1) was aspirated and propelled through the NTA resin.

Table - 4.2 Comparison between the analytical curves obtained from a single standard and multiple standards within 0.45 – 9.0 µmol/L dynamic range.

Procedure	Analytical curve[a] A = S x µmol/L Fe + b	Time for an analytical curve (h)	Effluent volume (mL)
Single Standard	A= 0.0483±0.0011x [Fe^{3+}] + 0.003 ± 0.001 R^2=0.999 ±0.000	0.95	25
Multiple Standards	A= 0.0467±0.0039x [Fe^{3+}] + 0.023±0.014 R^2=0.9998 ±0.0008	1.6	35

[a] n=4

There was no difference between the two approaches in the method sensitivity (slope relative deviation ≈ 3%). However, as expected, there was a significant improvement in time saving, over 30 min, and in effluent volume produced, 30% decrease. So, the analytical curve made with only a single standard, and loading different volumes, was the approach chosen. The LOD and LOQ were calculated for each approach from the analytical curve intercept (17), and the results showed no significant differences (the relative deviations < 8%).

4.3.4. Interference assessment

4.3.4.1. Salinity

Considering the aim of applying the developed method to seawater samples, potential salinity interference in the determination was a key parameter to assess. Iron standards were prepared in both MQW water and in synthetic seawater (18) and the established calibration curves compared. The estimated slopes of the calibration curves were evaluated at 95% confidence intervals, and there was no statistical difference (relative deviation <3%).

4.3.4.2. Other ions

In order to evaluate the potential interference of other cations in the reaction or NTA retention, an interference study was carried out for several bivalent and trivalent cations. For this study, several standards were prepared displaying the same iron(III) concentration (2.7 µmol/L), and with different ratios of potential interfering metal ion (Me). The interference percentage was calculated as relative deviation between the signals obtained, with ($A_{Fe\&Me}$) and without (A_{Fe}) the potential interfering ion $[(A_{Fe\&Me} - A_{Fe}) \div A_{Fe}]$. The tested ions, the maximum ratio without interference, the minimal interfering ratio and the respective percentages are presented in Table 4.3.

Table - 4.3 Assessment of the influence of potential interfering ions (Me) with the developed μSI-LOV-SPS method, using an iron standard of 2.7 μmol/L; values with grey shadow represent the minimal ratio with significant interference.

Potential interfering ion (Me)	Ratio Iron : Me (1:x)	% interference
Al^{3+}	9	4%
	35	-1%
Ca^{2+}	14	-1%
	28	-13%
Co^{2+}	1	-5%
	2	-8%
Cu^{2+}	1	0.3%
	6	-13%
Mg^{2+}	77	-3%
	345	9%
Mn^{2+}	2	0%
	14	-15%
Ni^{2+}	32	2%
	48	19%
Zn^{2+}	4	2%
	11	10%
NO_3^-	75	2%
	300	-26%
Cd^{2+}	0.007	3%
	0.008	24%
Pb^{2+}	0.005	2%
	0.007	29%

In the case of cadmium and lead, the ratio 1:0.008, corresponding to a concentration of these cations over 100 times lower than the iron(III) concentration, results in a significant interference (>20%). However, that would correspond to concentration of Cd and Pd of about 27 ηmol/L, which is not expected in natural waters.

As for the ions with relative high content in seawaters, namely magnesium, up to a concentration 300 times higher than the iron(III) concentration produced no significant interference (≈ 9%), a key feature for seawater application.

4.5. Analytical characteristics

The characteristics of the developed μSI-LOV-SPS method for iron(III) determination based on the colorimetric reaction with CP256 ligand were summarized in Table 4.4.

Table - 4.4 Features of the developed μSI-LOV-SPS method for iron(III) quantification in water samples using CP256 ligand as a colour-forming reagent; AC, analytical curve.

Dynamic range (μmol/L)	Analytical curve[a] A = S x μmol/L Fe + b	LOD (μmol/L)	LOQ (μmol/L)	RSD %	Analysis time (h)		Effluent production (mL)	
					AC[b]	Sample[c]	AC[b]	Sample[c]
0.45 – 9.0	A= 0.0481±0.0026x [Fe^{3+}] + 0.005±0.002 R^2=0.999 ±0.000	0.13	0.43	3.2 (2.60±0.08)	0.9[b]	0.09[c]	25[b]	2.3[c]

[a] n=4

[b] Corresponds to one analytical curve with fifteen cycles

[c] Average of one analytical cycle/determination

The limits of detection and quantification, LOD and LOQ, were calculated according to IUPAC recommendations (17), i.e as the concentration calculated from a signal of either three (LOD) or ten (LOQ) times the mean of the intercept for four analytical curves.

The repeatability of the method was assessed by calculating the relative standard deviation (RSD) of a water sample. The analysis frequency was calculated for the entire analytical curve due to the single standard approach, and for an individual sample. To perform one analytical curve with five concentration values in triplicates 15 analytical cycles, with different times for each concentration, are needed. As for an individual sample in triplicate only 3 analytical cycles (without time variation) are needed. An analytical cycle is the sum of the time needed for each step plus the time necessary for the port selection in the selection valve. The same approach was used to calculate the effluent production, per analytical curve and per single determination.

The overall reagent consumption per cycle was 30 μg of CP256 ligand, 252 μg of $NaHCO_3$ and about 2 μg of HNO_3, which can be considered low consumption values. The high affinity of the CP256 ligand for iron(III) enabled it to act, not only as colour-forming reagent, but also as eluent. All the reagent solutions were stable for at least a month.

4.6. Accuracy assessment - application to natural waters

To validate the method, three certified surface water samples were analysed with developed μSI-LOV-SPS method: a river water, a spring water and a sea water. The obtained iron(III) concentration was compared to the certified values: the certified river water, NRC-CNR SLRS-4, with a certified iron(III) content of 103 ± 5 μg/L (1.84 ± 0.09 μmol/L), presented an iron(III) concentration of 1.85 ± 0.16 μmol/L corresponding to a relative deviation of 0%; the spring water, NIST 1640, resulted in a concentration of 0.573 ± 0.30 μmol/L using the developed μSI-LOV method to compare to a certified value of 36.5 ± 0.2 μg/L (0.654 ± 0.004 μmol/L) corresponding to a relative deviation of -12%; for the sea water, SPS-SW2, with certified iron content of 100 ± 1 μg/L (1.79 ± 0.02 μmol/L) the concentration obtained was 1.95 ± 0.16 μmol/L corresponding to a relative deviation of 9%.

Further accuracy assessment was obtained by analysing two natural samples with the developed μSI-LOV-SPS method and with the reference procedure, atomic absorption spectrometry (AAS) (13). The results were compared and the relative deviation calculated (Table 4.5).

Table - 4.5 Accuracy assessment: results obtained with the proposed flow system (μSI-LOV-SPS) and with atomic absorption spectrometry (AAS): RD, relative deviation between the two set of results; SD standard deviation.

Water sample	Sample ID	μSI-LOV-SPS (μmol/L±SD)	AAS (μmol/L±SD)	RD%
River	R #1	1.90±0.03	1.82±0.02	4.6%
	R #2	0.846±0.103	0.824±0.018	2.7%
Mineral	M #1	0.839±0.047	0.842±0.036	-0.3%
Tap	T #1	5.85±0.38	6.18±0.01	-5.3%
	T #3	5.71±0.37	5.12±0.09	-6.8%
Well	W #1	1.28±0.13	1.25±0.18	2.4%
	W #2	1.18±0.06	1.16±0.02	1.7%

The relative deviation (RD) was calculated and no significant differences were observed (RD<7%). In addition, standard additions were performed and recovery percentages calculated. To five different water samples, 1.8 μmol/L and 3.6 μmol/L of iron(III) were added and the samples analysed by the developed method. The information about the different samples, the initial

concentration, the added value, the concentration found and the recovery percentages, calculated according to the IUPAC (19), as initial concentration subtracted to found concentration and divided by the added concentration, were summarized in Table 4.6.

Table - 4.6 Recovery percentages; SD, standard deviation, RSD, relative standard deviation.

Water source	pH	Initial Fe(III) concentration			Added	Found			Recovery (%)
		µmol/L	SD	RSD%	µmol/L	µmol/L	SD	RSD%	
Mineral	6.32	0.411 (< LOQ)	0.089	31	1.80	2.38	0.14	13	109
					3.60	4.19	0.03	2	105
River	6.67	< LOD	-	-	1.80	2.01	0.06	4	112
					3.60	3.72	0.01	0	103
Estuary	8.02	0.555	0.049	14	1.80	2.02	0.11	8	81
					3.60	3.69	0.12	5	87
Sea	8.10	0.269 (< LOQ)	0.003	3	1.80	1.67	0.16	14	93
					3.60	3.85	0.13	5	107
Thermae	7.49	0.304 (< LOQ)	0.050	24	1.80	1.93	0.02	1	90
					3.60	3.63	0.05	2	92

The average of the recovery percentages was 98% with a standard deviation of 10%. A statistical test (t-test) was used to evaluate if the mean recovery value did significantly differ from 100%. For a 95% significance level the calculated t-value was 0.175 with a correspondent critical value of 2.685. The statistical results indicate the absence of multiplicative matrix interferences proving that the developed µSI-LOV methodology was applicable to different types of water samples.

4.7. Conclusions

The use of solid phase spectrophotometry (SPS) to exploit the efficiency of CP256 ligand as a colorimetric reagent for the determination of iron(III) coupled to the NTA iron(III) retention capacity proved to be an highly effective method. In fact, although both the CP256 ligand and the NTA resin had been previously used in a sequential injection approach (8), the improvement for a SPS mode in a micro sequential injection lab-on-valve platform (μSI-LOV SPS) added up important advantages, namely time saving, reduction in sample consumption and effluent production, and a most relevant four-fold decrease of detection limit.

The choice of μSI-LOV technique enabled to perform detection directly on the NTA resin after matrix elimination and in-line iron(III) pre-concentration, discarding extra steps of elution and washing as well as minimizing flow dispersion. The pre-concentration and matrix discarding has proved essential for attaining the required dynamic ranges for natural waters application (6,8,20,21).

Furthermore, the SPS approach, with the NTA resin placed at the detector and the colourforming reaction being carried out in the resin surface, permitted the use of single standard solution approach, reducing the number of standard solutions needed and decreasing even further analysis time and effluent production.

References

1. Spolaor A, Vallelonga P, Gabrieli J, Cozzi G, Boutron C, Barbante C. Determination of Fe 2+ and Fe 3+ species by FIA-CRC-ICP-MS in Antarctic ice samples. J Anal At Spectrom. 2012;27(2):310–317.

2. Achterberg EP, Holland TW, Bowie AR, Mantoura RFC, Worsfold PJ. Determination of iron in seawater. Vol. 442, Analytica Chimica Acta. Elsevier; 2001. p. 1–14.

3. Worsfold PJ, Lohan MC, Ussher SJ, Bowie AR. Determination of dissolved iron in seawater: A historical review. Vol. 166, Marine Chemistry. Elsevier; 2014. p. 25–35.

4. Mesquita RBR, Rangel AOSS. A review on sequential injection methods for water analysis. Anal Chim Acta. 2009;648(1):7–22.

5. Mesquita RBR, Suárez R, Cerdà V, Rangel M, Rangel AOSS. Exploiting the use of 3,4-HPO ligands as nontoxic reagents for the determination of iron in natural waters with a sequential injection approach. Talanta. 2013;108:38–45.

6. Suárez R, Mesquita RBR, Rangel M, Cerdà V, Rangel AOSS. Iron speciation by microsequential injection solid phase spectrometry using 3-hydroxy-1(H)-2-methyl-4-pyridinone as chromogenic reagent. Talanta. 2015;133:15–20.

7. Mesquita RBR, Moniz T, Miranda JLA, Gomes V, Silva AMN, Rodriguez-Borges JE, et al. Synthesis and characterization of a 3-hydroxy-4-pyridinone chelator functionalized with a polyethylene glycol (PEG) chain aimed at sequential injection determination of iron in natural waters. Polyhedron. 2015;101:171–178.

8. Miranda JLA, Mesquita RBR, Nunes A, Rangel M, Rangel AOSS. Iron speciation in natural waters by sequential injection analysis with a hexadentate 3-hydroxy-4-pyridinone chelator as chromogenic agent. Talanta. 2016;148:633–640.

9. Nunes A, Podinovskaia M, Leite A, Gameiro P, Zhou T, Ma Y, et al. Fluorescent 3-hydroxy-4-pyridinone hexadentate iron chelators: Intracellular distribution and the relevance to antimycobacterial properties. J Biol Inorg Chem. 2010;15(6):861–77.

10. Ruzicka J. Lab-on valve: Universal microflow analyzer based on sequential and bead injection. Analyst. 2000;125(6):1053–1060.

11. Lohan MC, Aguilar-Islas AM, Franks RP, Bruland KW. Determination of iron and copper in seawater at pH 1.7 with a new commercially available chelating resin, NTA Superflow. Anal Chim Acta. 2005;530(1):121–129.

12. de Jong J, Schoemann V, Lannuzel D, Tison JL, Mattielli N. High-accuracy determination of

iron in seawater by isotope dilution multiple collector inductively coupled plasma mass spectrometry (ID-MC-ICP-MS) using nitrilotriacetic acid chelating resin for pre-concentration and matrix separation. Anal Chim Acta. 2008;623(2):126–139.

13. Eaton; AD, Clesceri; LS, Greenberg; AE, Franson; MAH, Health AP. Standard Methods for the Examination of Water and Wastewater. In: American Public Health Association, editor. 20th ed. Washington, DC, USA; 1999. p. Part 3000 Metals.

14. Santos IC., Mesquita RBR., Rangel AOSS. Micro solid phase spectrophotometry in a sequential injection lab-on-valve platform for cadmium, zinc, and copper determination in freshwaters. Anal Chim Acta. 2015;891:171–178.

15. González A, Mesquita RBR, Avivar J, Moniz T, Rangel M, Cerdà V, et al. Microsequential injection lab-on-valve system for the spectrophotometric bi-parametric determination of iron and copper in natural waters. Talanta. 2017;167:703–708.

16. Zagatto EAGG, Arruda MAZZ, Jacintho AO, Mattos IL. Compensation of the Schlieren effect in flow-injection analysis by using dual-wavelength spectrophotometry. Anal Chim Acta. 1990;234(C):153–160.

17. Currie LA. Nomenclature in Evaluation of Analytical Methods Including Detection and Quantification Capabilities (IUPAC Recommendations 1995). Int Union Pure Appl Chem. 1995;67:1699–1723.

18. Kester DR, Duedall IW, Connors DN, Pytkowicz RM. Preparation of Artificial Seawater. Limnol Ocean. 1967;12(1):176–178.

19. Burns D, Danzer K, Townshend A. Use of the Terms “Recovery” and “Apparent Recovery” in Analytical Procedures. Int Union Pure Appl Chem. 2002;74(11):2201–2205.

20. Ohno S, Teshima N, Sakai T, Grudpan K, Polasek M. Sequential injection lab-on-valve simultaneous spectrophotometric determination of trace amounts of copper and iron. Talanta. 2006;68(3):527–534.

21. Horstkotte B, Chocholouš P, Solich P. Large volume preconcentration and determination of nanomolar concentrations of iron in seawater using a renewable cellulose 8-hydroquinoline sorbent microcolumn and universal approach of post-column eluate utilization in a Lab-on-Valve system. Talanta. 2016;150:213–223.

Chapter 5

New hydrophilic 3-hydroxy-4-pyridinone chelators with ether-derived substituents: synthesis and evaluation of analytical performance in the determination of iron in waters

New hydrophilic 3-hydroxy-4-pyridinone chelators with ether-derived substituents: synthesis and evaluation of analytical performance in the determination of iron in waters

Three new hydrophilic 3-hydroxy-4-pyridinone chelators containing ether-derived substituents were prepared by a more sustainable synthetic protocol that involves the use of microwave heating and commercially available amines, allowing the successful production of highly water soluble chelators with improved reaction yields and reaction times. Compared with parent 3-hydroxy-4-pyridinone ligands, the new compounds were obtained faster and in higher amounts, facilitating the scale up of the synthesis, which is crucial to produce these ligands and their respective iron(III) complexes for many biological, analytical and agricultural applications. Ligands were fully characterized by ^{1}H and ^{13}C Nuclear Magnetic Resonance, High Resolution Mass Spectrometry and Single Crystal X-Ray Diffraction and their performance in the analytical determination of iron(III) in water samples was evaluated by sequential injection methods. The results obtained are scientifically relevant, pointing out the potential of the new and straightforwardly synthesized ligands as analytical reagents for determination of iron(III).

Keywords: 3-hydroxy-4-pyridinone; iron chelator; water solubility; microwave assisted synthesis; X-ray diffraction; sequential injection

The work described in this chapter was published: Tânia Moniz, Luís Cunha-Silva, Raquel B. R. Mesquita, Joana L. A. Miranda, André M. N. Silva, Ana M. G. Silva, António O. S. S. Rangel, Baltazar de Castro and Maria Rangel, Polyhedron, volume 160, 2019, pages 145–156.

Important note: *My contribution in this publication was the evaluation of the analytical performance of the different 3-hydroxy-4-pyridinone chelators, as chromogenic reagents in the determination of iron in waters; sections 5.2.4 and 5.3.5.*

5.1. Introduction

Hydroxypyridinones are *N*-heterocyclic chelators containing two vicinal oxygen atoms belonging to carbonyl and hydroxyl groups, which confer high affinity towards M^{II}/M^{III} metal ions. Among other hydroxypyridinones, namely 1-hydroxy-2-pyridinone and 3-hydroxy-2-pyridinone, 3-hydroxy-4-pyridinones (3,4-HPOs) are the most studied type of ligands (1,2). In the last decades, the chemistry and applications of 3,4-HPO have been a central topic of research in the groups of R. C. Hider (3–8), M. A. Santos (1,9) and M. Rangel (10–17) thus providing a good number of ligands and complexes that found application in biomedical, analytical, environmental and agriculture applications.

3,4-HPOs are synthetically versatile allowing functionalization by introduction of different substituents in several positions of the heterocyclic ring, providing chelators with different denticity, physicochemical properties, namely the spectroscopic properties, charge and hydro-lipophilic balance (HLB), without changing their chelating capacity (18–21). Accordingly, 3,4-HPO have been conjugated with different moieties such as fluorophores (14,22,23), photosensitizers agents for photodynamic therapy (24,25), aminoacids (26) and glycosyl units (27) to be applied in many different fields.

Regarding analytical applications, 3,4-HPO ligands can be used as greener alternative reagents in colorimetric methods for determination of iron in natural waters. This is a topic of great interest since conventional reagents may display high toxicity (28). Additionally, in the environmental context, the total iron content is not as significant as the free ionic iron content, so methods like Inductively Coupled Plasma Mass Spectrometry (ICP-MS) and Atomic Absorption Spectroscopy (AAS) are not as useful as the spectrophotometric determinations. Monitoring the iron content in natural waters is important due to its impact in aesthetic aspects in water, namely color, and also to possible effects in structures deployed in the water bodies.

N-alkyl-3-hydroxy-4-pyridinones, described in this work as “first generation chelators for analytical purposes” (Figure 5.1), have been tested and successfully used for the spectrophotometric sequential injection determination of iron in waters (29,30), although we found that the analytical performance is hampered by ligand’s solubility in aqueous media. In line with this fact, a new 3,4-HPO ligand (**PEG-HPO** or **MRB12** (12)) functionalized with a hydrophilic ethylene glycol chain to improve its solubility in water was designed and designated as “second generation 3,4-HPO analytical applications” (Figure 5.1). Both the ligand and its iron(III) complex proved to be highly soluble in water providing a lower detection limit and higher sensitivity in flow-based methods for iron determination in water samples (11,12). As a disadvantage, we found that the synthesis of **MRB12** is costly and poorly efficient presenting numerous reaction steps and a low reaction yield.

In our point of view, the vast number of applications of 3,4-HPO chelators and in particular their promising analytical performance justifies an effort to improve their preparation by means of more efficient and sustainable synthetic routes. Herein, we report the synthesis of other water soluble "second generation 3,4-HPO ligands" containing ether groups (**MRB13**, **MRB15** and **MRB16**, Figure 5.1). The use of microwave-assisted organic chemistry instead of "traditional" reflux in oil-bath (12,15,23), allowed reduction of both the reaction times and the possible formation of secondary products. We considered that the use of simpler ether substituents in the nitrogen atom of the heterocyclic ring could reduce the number of reagents as also the number of synthetic steps and consequently improve the efficiency of the synthetic approach without compromising water solubility and the analytical performance.

The structural characterization of all ligands was achieved by ^{1}H and ^{13}C Nuclear Magnetic Resonance, High Resolution Mass Spectrometry and Single Crystal X-Ray Diffraction.

The 3,4-HPO ligands **MRB13**, **MRB14**, **MRB15** and **MRB16** were investigated regarding their potential use in the analytical determination of iron(III) by sequential injection methods (SI) and results were compared with those reported for **PEG-HPO** or **MRB12** ligand. The assessment of potential interferences of a set of metal ions in the determination of iron in water samples was also investigated for all the ligands.

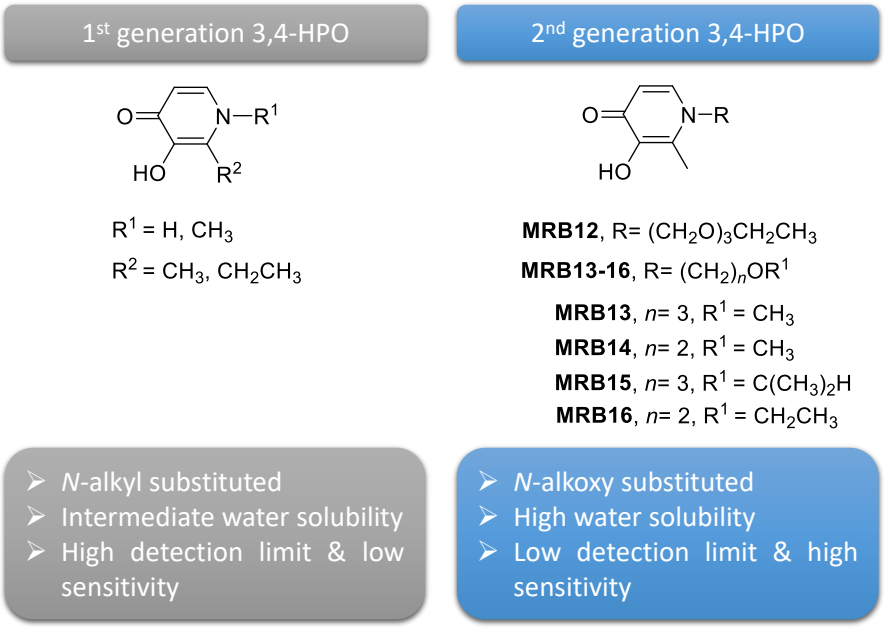

Figure - 5.1 Numbering and formulae of first and second generation 3,4-HPO used for analytical determination of iron in water samples.

5.2 Experimental

5.2.1 Materials and physical measurements

Chemicals were obtained from Sigma–Aldrich (grade puriss, p.a.) or Fluka (p.a.) and were used as received unless otherwise specified. The 3-benzyloxy-2-methyl-4-pyrone (Scheme 1, A) was synthesized in our laboratory following the procedures described in the literature (31).

Microwave-assisted reactions were carried out in a CEM Discovery Labmate circular single-mode cavity instrument (300 W max magnetron power output) from CEM Corporation, using standard Pyrex vessels (capacity 30 mL) under sealed vessel conditions. NMR spectra were recorded on a Bruker Avance III 400 spectrometer, operating at 400.15 MHz for ^{1}H and 100.62 MHz for ^{13}C atoms, equipped with pulse gradient units, capable of producing magnetic field pulsed gradients in the z-direction of 50.0 G/cm. Two-dimensional $^{1}H/^{1}H$ correlation spectra (COSY), gradient selected $^{1}H/^{13}C$ heteronuclear single quantum coherence (HSQC) and $^{1}H/^{13}C$ heteronuclear multiple bond coherence (HMBC) spectra were acquired using the standard Bruker software.

High resolution electrospray ionisation mass spectra (ESI-MS) were obtained in a Thermo Scientific LTQ-Orbitrap XL mass spectrometer, externally calibrated with a standard kit provided by the manufacturer. The spectrometer was operated in the positive ionization mode setting the capillary voltage to +3.0 kV, sheath gas flow to 6 and the temperature of the ion transfer capillary to 275 °C. Spectra were recorded for *m/z* values between 250 and 2000 in the Fourier Transform (FT) mode with resolution (FWHM) set at 60000. Samples were prepared in water, diluted in a 50%(v/v) water: methanol mixture immediately before analysis and directly infused into the electrospray ion source utilizing the syringe pump in the mass spectrometer at 10 µl min^{-1}. NMR and Mass spectrometry analyses were performed at Laboratório de Análise Estrutural, Centro de Materiais da Universidade do Porto (CEMUP) (Portugal).

5.2.2 Synthesis of protected 3,4-HPO ligands

5.2.2.1 Synthesis of 1-(3'-methoxypropyl)-2-methyl-3-benzyloxy-4-(1*H*)-pyridinone (MRB13p)

A mixture of amine **1** (3-methoxypropylamine) (2.086 g, 0.0234 mol) and protected pyrone (3-benzyloxy-2-methyl-4-pyrone) (0.505 g, 0.0023 mol) dissolved in dried ethanol (2 mL) was placed in a 30 mL reaction vial, which was then closed under argon atmosphere and placed in the cavity of a CEM microwave reactor. The reaction vial was irradiated to 80ºC during 4 hours, using 100 W

maximum power. The reaction solvent was evaporated and the crude oil resultant was dissolved in 30 mL of H_2O and the pH adjusted to 1 with HCl 10%. The starting materials were removed by liquid/liquid extraction with diethyl ether. The organic layer was rejected. The pH of aqueous phase was adjusted to 10 with a solution of NaOH 5% and the product was then extracted to the organic layer with dichloromethane. The organic phase was concentrated to afford compound **MRB13p** (0.620g, 92% yield) as dark brown oil.

400.15 MHz ^{1}H NMR ($CDCl_3$, ppm): δ 1.83 (m, 2H, H2'), 2.09 (s, 3H, 2-CH_3), 3.26 (t, *J* 5.6 Hz, 2H, H3'), 3.29 (s, 3H, -OCH_3), 3.88 (t, *J* 7.0 Hz, 2H, H1'), 5.19 (s, 2H, -C$\underline{H}_2C_6H_5$), 6.41 (d, *J* 7.5 Hz, 1H, H5), 7.24 (d, *J* 7.5 Hz, 1H, H6), 7.29-7.32 (m, 3H, $H_{meta+para}$-$CH_2C_6\underline{H}_5$), 7.38-7.40 (m, 2H, H_{ortho}-$CH_2C_6\underline{H}_5$). 100.62 MHz ^{13}C NMR ($CDCl_3$, ppm): δ 12.2 (2-CH_3), 30.3 (C2'), 50.4 (C1'), 58.6 (-OCH_3), 67.8 (C3'), 72.9 (-$\underline{C}H_2C_6H_5$), 117.0 (C5), 127.9 and 128.2 ($C_{meta+para}$-C_6H_5), 129.0 (C_{ortho}-C_6H_5), 137.5 (Cq, -C_6H_5), 138.6 (C6), 141.1 (C2), 145.9 (C3), 173.2 (C4).

5.2.2.2 Synthesis of 1-(2'-methoxyethyl)-2-methyl-3-benzyloxy-4-(*1H*)-pyridinone (MRB14p)

A mixture of amine **2** (2-methoxyethylamine) (0.691g, 0.00928 mol) and protected pyrone (3-benzyloxy-2-methyl-4-pyrone) (0.501g; 0.00232 mol) dissolved in dried ethanol (2 mL) was placed in a 30 mL reaction vial, which was then closed under argon atmosphere and placed in the cavity of a CEM microwave reactor. The reaction vial was irradiated to 90ºC during 4 hours, using 100 W maximum power. The reaction solvent was evaporated and the crude oil resultant was dissolved in 30 mL of H_2O and the pH adjusted to 1 with HCl 10%. The starting materials were removed by liquid/liquid extraction with diethyl ether. The organic layer was rejected. The pH of aqueous phase was adjusted to 10 with a solution of NaOH 5% and the product was then extracted to the organic layer with dichloromethane. The organic phase was concentrated to afford compound **MRB14p** (0.434g, 69% yield) as dark brown oil.

400.15 MHz ^{1}H NMR ($CDCl_3$, ppm): δ 2.10 (s, 3H, 2-CH_3), 3.24 (s, 3H, -OCH_3), 3.49 (t, *J* 5.0 Hz, 2H, H2'), 3.92 (t, *J* 5.0 Hz, 2H, H1'), 5.15 (s, 2H, -C$\underline{H}_2C_6H_5$), 6.37 (d, *J* 7.5 Hz, 1H, H5), 7.28–7.30 (m, 1H, H6 and 3H, $H_{meta+para}$-$CH_2C_6\underline{H}_5$), 7.38-7.40 (m, 2H, H_{ortho}-$CH_2C_6\underline{H}_5$). 100.62 MHz ^{13}C NMR ($CDCl_3$, ppm): δ 12.3 (2-CH_3), 52.8 (C1'), 58.8 (-OCH_3), 70.9 (C2'), 72.6 (-$\underline{C}H_2C_6H_5$), 116.4 (C5), 127.6 and 127.9 ($C_{meta+para}$-C_6H_5), 128.7 (C_{ortho}-$\underline{C}_6H_5$), 137.2 (Cq, -C_6H_5), 139.0 (C6), 141.3 (C2), 145.4 (C3), 173.0 (C4).

5.2.2.3 Synthesis of 1-(3'-isopropoxypropyl)-2-methyl-3-benzyloxy-4-(*1H*)-pyridinone (MRB15p)

A mixture of amine **3** (3-isopropoxypropylamine) (1.645g, 0.0141 mol) and protected pyrone (3-benzyloxy-2-methyl-4-pyrone) (0.507g, 0.0024 mol) dissolved in dried ethanol (2 mL) was placed in a 30 mL reaction vial, which was then closed under argon atmosphere and placed in the cavity of a CEM microwave reactor. The reaction vial was irradiated to 80ºC during 4 hours, using 100 W maximum power. The reaction solvent was evaporated and the crude oil resultant was dissolved in 30 mL of H_2O and the pH adjusted to 1 with HCl 10%. The starting materials were removed by liquid/liquid extraction with diethyl ether. The organic layer was rejected. The pH of aqueous phase was adjusted to 10 with a solution of NaOH 5% and the product was then extracted to the organic layer with dichloromethane. The organic phase was concentrated to afford compound **MRB15p** (0.565g, 89% yield) as dark brown oil.

400.15 MHz ^{1}H NMR ($CDCl_3$, ppm): δ 1.14 (d, *J* 6.3 Hz, 6H, 4'-$(CH_3)_2$), 1.83 (quint, *J* 6.2 Hz, 2H, H2'), 2.11 (s, 3H, 2-CH_3), 3.30 (t, *J* 5.4 Hz, 2H, H3'), 3.51 (m, *J* 6.3 Hz, 1H, 4'-CH), 3.89 (t, *J* 7.0 Hz, 2H, H1'), 5.24 (s, 2H, -C$\underline{H}_2C_6H_5$), 6.40 (d, *J* 7.6 Hz, 1H, H5), 7.22 (d, *J* 7.6 Hz, 1H, H6), 7.28–7.42 (m, 5H, $CH_2C_6\underline{H}_5$). 100.62 MHz ^{13}C NMR ($CDCl_3$, ppm): δ 12.3 (2-CH_3), 22.0 (4'-$(CH_3)_2$), 30.8 (C2'), 50.5 (C1'), 63.1 (C3'), 71.9 (C4'), 72.9 (-$\underline{C}H_2C_6H_5$), 117.2 (C5), 127.9 and 128.2 and 129.2 (-$\underline{C}_6H_5$), 137.7 (Cq, -$\underline{C}_6H_5$), 138.5 (C6), 140.7 (C2), 146.1 (C3), 173.4 (C4).

5.2.2.4 Synthesis of 1-(2'-ethoxyethyl)-2-methyl-3-benzyloxy-4-(*1H*)-pyridinone (MRB16p)

A mixture of amine **4** (2-ethoxyethylamine) (0.825g, 0.0092 mol) and protected pyrone (3-benzyloxy-2-methyl-4-pyrone) (0.500g, 0.00231 mol) dissolved in dried ethanol (2 mL) was placed in a 30 mL reaction vial, which was then closed under argon atmosphere and placed in the cavity of a CEM microwave reactor. The reaction vial was irradiated to 80ºC during 5 hours, using 100 W maximum power. The reaction solvent was evaporated and the crude oil resultant was dissolved in 30 mL of H_2O and the pH adjusted to 1 with HCl 10%. The starting materials were removed by liquid/liquid extraction with diethyl ether. The organic layer was rejected. The pH of aqueous phase was adjusted to 10 with a solution of NaOH 5% and the product was then extracted to the organic layer with dichloromethane. The organic phase was concentrated to afford compound **MRB16p** (0.576, 91% yield) as dark brown oil.

400.15 MHz ^{1}H NMR ($CDCl_3$, ppm): δ 1.11 (t, *J* 7.0 Hz, 3H, 3'-CH_3), 2.11 (s, 3H, 2-CH_3), 3.39 (q, *J* 7.0 Hz, 2H, H3'), 3.55 (t, *J* 5.0 Hz, 2H, H2'), 3.92 (t, *J* 5.0 Hz, 2H, H1'), 5.19 (s, 2H, -C$\underline{H}_2C_6H_5$), 6.39 (d, *J* 7.8 Hz, 1H, H5), 7.26 (d, *J* 7.8 Hz, 1H, H6), 7.30–7.42 (m, 5H, $CH_2C_6\underline{H}_5$). 100.62 MHz ^{13}C NMR ($CDCl_3$, ppm): δ 12.7 (2-CH_3), 15.0 (3'-CH_3), 53.3 (C1'), 67.0 (C3'), 69.1 (C2'), 73.0 (-$\underline{C}H_2C_6H_5$), 116.9 (C5), 127.9 and 128.2 and 129.0 (-C_6H_5), 137.6 (Cq, -C_6H_5), 139.1 (C6), 141.1 (C2), 145.8 (C3), 173.5 (C4).

5.2.2.5 Removal of benzyl protecting group of 3,4-HPO ligands

Each protected 3,4-HPO: **MRB13p** (0.620 g, 0.0022 mol), **MRB14p** (0.434 g, 0.0016 mol), **MRB15p** (0.565 g, 0.0018 mol) and **MRB16p** (0.576 g, 0.0020 mol) was dissolved in ethanol (20 mL) and HCl (20 µL) and placed into a hydrogenation vessel. The air was removed with N_2, a catalytic amount of 10% Pd/C (w/w) was added and the mixture was stirred at room temperature, with H_2 at 40 psi for 6 h. The reaction mixtures were filtered, washed with methanol and chloroform and the solvents were evaporated in vacuum to give a brown oil product. The resulting residues were dried under vacuum to give the hydrochloride salt of each 3,4-HPO: **MRB13** (0.477 g, 95% yield), **MRB14** (0.366 g, 100% yield), **MRB15** (0.457 g, 98% yield) and **MRB16** (0.430, 92% yield).

1-(3'-methoxypropyl)-2-methyl-3-hydroxy-4-*1H*-pyridinone hydrochloride (MRB13): MS: calculated for $C_{10}H_{16}NO_3^+$: 198.1125 (monoisotopic molecular weight M^+), found: HRMS: 198.1121. 400.15 MHz ^{1}H NMR (MeOD-d*4*, ppm): δ 2.11 (quint, *J* 6.7 Hz, 2H, H2'), 2.65 (s, 3H, 2-CH_3), 3.32 (s, 3H, -OCH_3), 3.43 (t, *J* 5.6 Hz, 2H, H3'), 4.48 (t, *J* 7.3 Hz, 2H, H1'), 7.12 (d, *J* 6.9 Hz, 1H, H5), 8.13 (d, *J* 6.9 Hz, 1H, H6). 100.62 MHz ^{13}C NMR (MeOD-d*4*, ppm): δ 12.7 (2-CH_3), 31.1 (C2'), 55.4 (C1'), 59.0 (-OCH_3), 69.5 (C3'), 111.8 (C5), 139.5 (C6), 143.7 (C2), 145.1 (C3), 159.8 (C4).

1-(2'-methoxyethyl)-2-methyl-3-hydroxy-4-(*1H*)-pyridinone hydrochloride (MRB14): MS: calculated for $C_9H_{14}NO_3^+$: 184. 0968 (monoisotopic molecular weight M^+), found: HRMS: 184.0969. 400.15 MHz ^{1}H NMR (MeOD-d*4*, ppm): δ 2.64 (s, 3H, 2-CH_3), 3.31 (s, 3H, -OCH_3), 3.78 (t, *J* 4.7 Hz, 2H, H2'), 4.59 (t, *J* 4.7 Hz, 2H, H1'), 7.16 (d, *J* 6.8 Hz, 1H, H5), 8.14 (d, *J* 6.8 Hz, 1H, H6). 100.62 MHz ^{13}C NMR (MeOD-d*4*, ppm): δ 13.2 (2-CH_3), 57.2 (C1'), 59.4 (-OCH_3), 71.6 (C2'), 111.4 (C5), 140.0 (C6), 143.9 (C2), 144.7 (C3), 159.7 (C4).

1-(3'-isopropoxypropyl)-2-methyl-3-hydroxy-4-(*1H*)-pyridinone hydrochloride (MRB15): MS: calculated for $C_{12}H_{20}NO_3^+$: 226.1438 (monoisotopic molecular weight M^+), found: HRMS: 226.1442. 400.15 MHz ^{1}H NMR (MeOD-d*4*, ppm): δ 1.12 (d, *J* 6.3 Hz, 6H, 4'-$(CH_3)_2$), 2.10 (quint, *J* 6.4 Hz, 2H, H2'), 2.66 (s, 3H, 2-CH_3), 3.49 (t, *J* 5.6 Hz, 2H, H3'), 3.57 (m, *J* 6.3 Hz, 1H, 4'-CH), 4.48 (t, *J* 7.0 Hz, 2H, H1'), 7.10 (d, *J* 7.0 Hz, 1H, H5), 8.13 (d, *J* 7.0 Hz, 1H, H6). 100.62 MHz ^{13}C NMR (MeOD-

d_4, ppm): δ 12.8 (2-CH_3), 22.3 (4'-$(CH_3)_2$), 31.5 (C2'), 55.6 (C1'), 65.0 (C3'), 73.1 (C4'), 111.6 (C5), 139.4 (C6), 143.6 (C2), 145.1 (C3), 159.6 (C4).

1-(2'-ethoxyethyl)-2-methyl-3-hydroxy-4-(*1H*)-pyridinone hydrochloride (MRB16): MS: calculated for $C_{10}H_{16}NO_3^+$: 198.1125 (monoisotopic molecular weight M^+), found: HRMS: 198.1125. 400.15 MHz ^{1}H NMR (MeOD-d_4, ppm): δ 1.10 (t, *J* 7.0 Hz, 3H, 3'-CH_3), 2.67 (s, 3H, 2-CH_3), 3.48 (q, *J* 7.0 Hz, 2H, H3'), 3.85 (t, *J* 5.0 Hz, 2H, H2'), 4.62 (t, *J* 5.0 Hz, 2H, H1'), 7.22 (d, *J* 7.0 Hz, 1H, H5), 8.19 (d, *J* 7.0 Hz, 1H, H6). 100.62 MHz ^{13}C NMR (MeOD-d_4, ppm): δ 13.3 (2-CH_3), 15.2 (3'-CH_3), 57.3 (C1'), 67.7 (C3'), 69.5 (C2'), 111.4 (C5), 140.0 (C6), 143.9 (C2), 144.5 (C3), 159.7 (C4).

5.2.3 Single-crystal X-ray diffraction

Suitable single crystals of the compounds **MRB13-MRB16** were manually harvested and a mounted on cryoloops using viscous FOMBLIN Y perfluoropolyether vacuum oil (LVAC 140/13, Sigma-Aldrich) (32). Diffraction data were collected at on a Bruker X8 Kappa APEX II Charge-Coupled Device (CCD) area-detector diffractometer controlled by the APEX2 software package (33) (Mo K_α graphite-monochromated radiation, λ = 0.71073 Å), and equipped with an Oxford Cryosystems Series 700 cryostream monitored remotely with the software interface Cryopad (acquisition temperature of 150.0(2) K) (34). Images were processed with the software SAINT+ (35), and the absorption effects were corrected by the multi-scan method implemented in SADABS (36). The structures were solved using SHELXT-2014(37,38), which allow the immediate location and identification of a considerable number of the heaviest atoms composing the asymmetric unit. The remaining absent and misplaced non-hydrogen atoms were located from difference Fourier maps from successive full-matrix least-squares refinement cycles on F^2 using SHELXL-v.2014 (37,39). All the non-hydrogen atoms were successfully refined using anisotropic displacement parameters.

Hydrogen atoms bonded to carbon were placed at their geometrical positions using the appropriate *HFIX* instructions (*137* for the terminal –CH_3, *23* for the –CH_2– and *43* for the aromatic groups) and included in subsequent refinement cycles in riding-motion approximation with isotropic thermal displacements parameters (U_{iso}) fixed at 1.2 or 1.5 × U_{eq} of the relative atom. Furthermore, the hydrogen atoms associated to hydroxyl groups and the crystallization water molecule (only in the **MRB16** structure) were markedly visible in the difference Fourier maps and included in subsequent refinement stages with the O–H distances restrained to 0.90 (2), and using a riding-motion approximation with an isotropic thermal displacement parameter fixed at 1.5 × U_{eq} of the oxygen atom.

Information concerning the crystallographic data collection and structure refinement details is summarized in Table 5.1, while the geometrical details about the strong hydrogen bonding interactions are shown in Table 5.4. Crystallographic data (excluding structure factors) for the structures reported in this work have been deposited to the Cambridge Crystallographic Data Centre (CCDC) as supplementary publication numbers: CCDC-1845145 (**MRB13**), CCDC-1845146 (**MRB14**), CCDC-1845147 (**MRB15**) and CCDC-1845148 (**MRB16**) Copies of the data can be obtained online: *https://www.ccdc.cam.ac.uk/structures/*.

Table - 5.1 Crystal and structure refinement data for compounds **MRB13-MRB16**.

	MRB13	**MRB14**	**MRB15**	**MRB16**
Formula	$C_{10}H_{16}ClNO_3$	$C_9H_{14}ClNO_3$	$C_{12}H_{20}ClNO_3$	$C_{10}H_{18}ClNO_4$
Mr	233.69	219.66	261.74	251.70
Crystal morphology	Colourless block	Colourless prism	Colourless block	Colourless prism
Crystal size /mm	0.12×0.04×0.03	0.19×0.15×0.11	0.14×0.09×0.06	0.20×0.03×0.02
Crystal system	Monoclinic	Orthorhombic	Monoclinic	Monoclinic
Space group	$P2_1/c$	$P2_12_12_1$	$P2_1/c$	$P2_1/c$
a /Å	7.768(2)	7.087(7)	11.9647(15)	7.5041(7)
b /Å	13.119(3)	11.804(11)	8.6675(11)	13.1185(12)
c /Å	11.731(3)	12.141(11)	13.3471(19)	12.6117(12)
α/°	90	90	90	90
β/°	108.919(10)	90	106.863(6)	93.190(4)
γ/°	90	90	90	90
Volume /Å^3	1131.0(5)	1015.6(2)	1324.6(3)	1239.6(2)
Z	4	4	4	4
$p_{Calc.}$ (g cm^{-3})	1.372	1.437	1.312	1.349
F(000)	496	464	560	536
μ(mm^{-1})	0.325	0.357	0.286	0.308
θ range (°)	3.672 to 25.677	3.750 to 27.474	3.947 to 26.370	3.60 to 25.025
Index ranges	−9 ≤ h ≤ 9 −15 ≤ k ≤ 15 −14 ≤ l ≤ 11	−8 ≤ h ≤ 9 −15 ≤ k ≤ 15 −15 ≤ l ≤ 15	−13 ≤ h ≤ 14 −10 ≤ k ≤ 10 −16 ≤ l ≤ 16	−8 ≤ h ≤ 8 −15 ≤ k ≤ 15 −14 ≤ l ≤ 14
Reflections collected	8788	8296	15993	29379
Independent reflections	2139 (R_{int} = 0.0903)	2317 (R_{int} = 0.0349)	2700 (R_{int} = 0.0606)	2165 (R_{int} = 0.0271)
Final *R* indices [I>2σ(I)]	R_1 = 0.0499; wR_2 = 0.1008	R_1 = 0.0277; wR_2 = 0.0669	R_1 = 0.0381; wR_2 = 0.0886	R_1 = 0.0242; wR_2 = 0.0630
Final *R* indices (all data)	R_1 = 0.0956; wR_2 = 0.1186	R_1 = 0.0305; wR_2 = 0.0690	R_1 = 0.0593; wR_2 = 0.0980	R_1 = 0.0266; wR_2 = 0.0645
Largest diff. peak and hole /e Å^3	0.262 and −0.318	0.202 and −0.184	0.305 and −0.202	0.216 and −0.157

5.2.4 Analytical procedure for iron(III) quantification

5.2.4.1 Reagents and solutions

Ligand stock solutions were obtained by dissolving circa 20 mg of each ligand in 2.0 mL of Milli-Q water (MQW), corresponding to an approximate concentration of about 42 mmol/L. Working ligand solutions were obtained by dilution of the stock solutions to final concentration of about 0.6 mmol/L.

A 0.25 mol/L hydrogen carbonate buffer solution was prepared by dissolving 1.05 g of sodium hydrogen carbonate (Merck, Germany) in 50 mL of water and adjusting the pH to 10.6 with 0.5 mol/L sodium hydroxide solution A solution of 0.5 M nitric acid was prepared from dilution of the concentrated acid (d = 1.4; 65%, Merck, Germany).

An iron(III) stock solution of 10 mg/L (180 µM) was obtained by dilution of the atomic absorption standard (1001 mg/L Fluka - Sigma-Aldrich, Switzerland). This solution was used to prepare the Fe^{3+} working standards in the dynamic range 0.1–1.0 mg/L (1.8 – 18 µmol/L) in 0.03 M nitric acid.

5.2.4.2 Analytical flow analysis procedure

The analytical procedure to test the different ligands as colorimetric reagent for iron(III) determination has been previously described(12). The micro sequential injection system comprised a MicroSIA of FIAlab (FIAlab Instruments, USA), consisting in a bi-directional syringe pump of 2.5 mL and an eight -port selection valve (Valco VICI Cheminert 170-0317L), connected to the central channel of with a PVC pumping tube.

The other system components were connected with PTFE (Omnifit) tubing, with 0.8 mm i.d.

Detection of the colorimetric reaction was attained with an Ocean Optics Flame – T – UV- Vis (FLMT01897) charged coupled device (CCD) detector, equipped with a pair of FIA-P600-Fiber cable 600 Micron diameter (SMA terminated on one end and PEEK sheath termination on the other end), an Ocean Optics halogen light source HL-2000 and a FIA-Z-Cell 100mm – Plexiglas FIA-Z Cell with adjustable optical path (10 cm light path and 250 µL inner volume). Data acquisition, made at 460 nm, 475 nm and 515 nm. All the equipment was controlled on a desktop computer with FIAlab software installed (Lenovo, Intel Core i5).

The protocol sequence used for iron(III) determination has also been previously detailed (12) and consisted in aspirating ligand solution (250 µL), followed by buffer solution (20 µL) and iron standard (500 µL), and then propelling the mixture towards the detector for signal registration.

5.3 Results and discussion

5.3.1 Design and synthesis of 3,4-HPOs

The general synthetic approach to prepare a 3-hydroxy-4-pyridinone ligand involves the reaction of a 3-hydroxy-4-pyrone with a primary amine (12,31,40). The hydroxyl group in the position 3 of the pyrone ring was previously protected with a benzyl group, according with methods previously described (31). Then, different -R substituents were introduced by the substitution of the oxygen by the nitrogen atom of the amine leading to 3,4-HPOs with different *N*-chains and variable physicochemical properties. The choice of the amine is determinant for the hydrophilic-lipophilic balance of the new 3,4-HPO ligand. Considering these criteria (discussed below), four alkoxyamines including 3-methoxypropylamine, 2-methoxyethylamine, 3-isopropoxypropylamine and 2-ethoxyethylamine, were selected to react with 3-benzyloxy-2-methyl-4-pyrone using microwave-assisted synthesis (Scheme 1, Table 5.2).

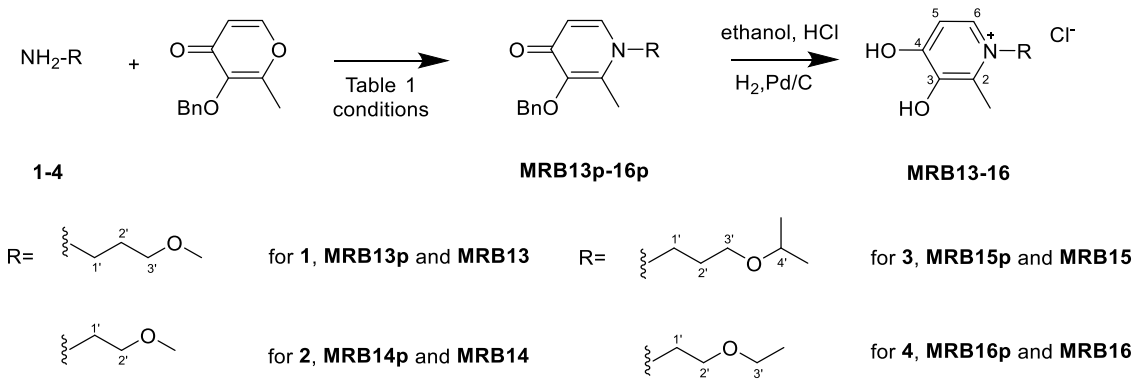

Scheme - 5.1 General approach to access *N*-alkoxy substituted 3-hydroxy-4-pyridinones.

Table - 5.2 Yields of *N*-alkoxy substituted 3-benzyloxy-4-pyridinones on microwave heating under closed vessel conditions[a]

***N*-alkoxy 3-benzyloxy-4-pyridinones**	**Conditions**	**Amine (excess)**	**Yield (%)**
MRB13p	80ºC, 4h	10 equiv.	92
MRB14p	90ºC, 4h	4 equiv.	69
MRB15p	80ºC, 4h	6 equiv.	89
MRB16p	80ºC, 5h	4 equiv.	91

[a] Reactions of primary amines with 3-benzyloxy-2-methyl-4-pyrone (0.5g, 2 mmol) were performed in dried ethanol (2 mL).

The synthesis of ligand **MRB14** was previously reported by Hider and co-workers (19,41) nonetheless in the present work the ligand was obtained by using microwave-assisted synthesis instead of the traditional heating method previously described. The compound **MRB14** was included in the set of molecules considered in the present work as it is structurally related and we are interested in the study of the influence of the chelator's structure for the performance of the ligands and their respective iron(III) complexes in the analytical and biological context, namely as plant fertilizers (17).

The protocol established for the synthesis of **MRB12** includes the preparation of the polyethylene glycol (PEG) functionalized amine thus implying two additional reaction steps, which constitutes a disadvantage. In the present work we chose to use commercially available amines (Scheme 1, **1**-**4**) to produce the new ligands. This alternative allowed the reduction of the numbers of reaction steps from 5 to 3 and significantly decreased the total time of reaction, when compared with the method described for the synthesis of **MRB12** (12). This choice of amines together with the use of microwave heating instead of "traditional" reflux in oil-bath aimed to contribute to a simpler and more sustainable synthetic protocol for ligand production, mainly by reducing reaction time and improve the reproducibility of the experiments.

The microwave heating process is based on the ability of a material to heat when exposed to an alternating electric field and depends on the dielectric properties of that material (expressed as the loss factor, tan δ) (42,43). In fact, the reactions under study were performed in ethanol, which presents a high tan δ value (tan δ = 0.941) (44), meaning that it is a strong microwave absorbing solvent and, in combination with reaction reagents, should provide an efficient absorption and rapid

heating profile. The microwave-assisted synthesis of the ligands afforded: (a) **MRB13p**, **MRB15p** and **MRB16p** in good reaction yields in 4 or 5 hours (69-92%) (Table 5.2) and (b) ligand **MRB14p** in a significantly shorten reaction time (4h) when compared with the "traditional" reflux protocol (18h) (19), a reduction of approximately 78%, despite maintaining the reaction yield.

In all reactions an excess of amine was used, starting from twofold excess, although we found that a fourfold excess is required to get ligands **MRB14p** and **MRB16p**. Ligand **MRB15p** required a higher amount of amine and the best results were obtained using six times more amine than the protected pyrone. Amine 1 seems to be the less reactive and a tenfold excess of amine was required to get the **MRB13p**.

Purification of the protected ligands was achieved by liquid-liquid extraction without need of extra purification by chromatography, in opposition with purification of **MRB12p**. This fact may justify the higher yields for **MRB13p-MRB16p** contrasting with 49% (**MRB12p**) (12).

In order to obtain the deprotected form of the 3,4-HPO ligand, the benzyl-protecting group was removed under a hydrogen atmosphere in the presence of Pd/C (10%) and HCl, yielding the **MRB13-MRB16** ligands hydrochloride salt in almost quantitative (92-100%) yield.

5.3.2 Selection of amine reagents and prediction of Log P values

Taking into account the objective of this work, the selection of amines was based on the Log P values, predicted using the ACD/Log P Software (45) (Table 5.3) and commercial availability.

Table - 5.3 Formulae of the 3,4-HPO chelators and the predicted Log P values.

Ligand name	**MRB12** (12)	**MRB13**	**MRB14**	**MRB15**	**MRB16**
Formulae	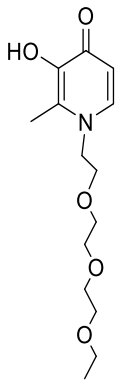	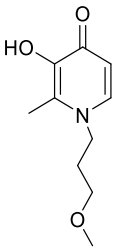	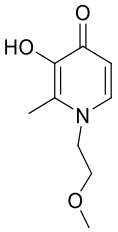	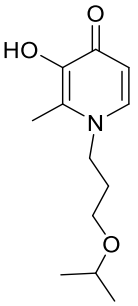	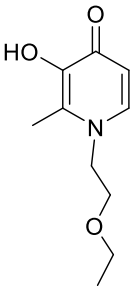
LogP (ACD lab)	-0.69	-0.38	-0.50	0.50	0.03

The reaction of the selected amines with the protected 2-methyl-3-hydroxy-4-pyrone originated the new set ligands listed in Table 5.3 that have log P values in the range -0.50 to 0.50.

Compounds **MRB13** and **MRB14** exhibit Log P values quite similar to that found for PEGylated 3,4-HPO (**MRB12**) (12). **MRB15** and **MRB16** Log P values are predicted to be slightly more lipophilic than **MRB12**, a property that may be advantageous for different applications.

5.3.3 NMR spectroscopy

The structures of the protected and deprotected ligands in solution were established by NMR analysis (^{1}H and ^{13}C, 1D and 2D experiments, including COSY, HSQC and HMBC spectra for unequivocal assignment of the most characteristic proton and carbon chemical shifts). The assignment of the resonance signals in ^{13}C NMR spectra of the protected and deprotected compounds was achieved by analysis of $^{1}H/^{13}C$ HSQC and $^{1}H/^{13}C$ HMBC spectra, which provide one and multiple bond ^{1}H-^{13}C connectivity, respectively. All the chemical shift values obtained are in a good agreement with those described in the literature for similar compounds (12,40). All spectra are available in supporting information (Figures S1-S22). As a representative example, the detailed discussion of the ^{1}H and ^{13}C spectra of compounds **MRB13p** and **MRB13** is described

below. For the other ligands synthetized, an extended description of the NMR spectra is available in supporting information.

^{1}H and ^{13}C spectra of **MRB13p** revealed multiplets in the aliphatic region (1.83, 3.26 and 3.88 ppm) which were assigned to protons of -CH_2 groups (H2', H3' and H1', respectively) of the *N*-substituent and their carbons, C2', C1' and C3', appear at 30.3, 50.4 and 67.8 ppm, respectively. Carbon C1' exhibited long range HMBC correlation with proton H6, allowing the assignment performed. The resonance signal of the methoxyl protons in the terminal group (-O$\underline{C}H_3$) appears at 3.29 ppm and the associated carbon (-O$\underline{C}H_3$) appears at 58.6 ppm and shows HSQC correlation. Upon the deprotection (**MRB13)**, significantly differences in the ^{1}H and ^{13}C spectra were detected as the shift of the protons closely to the pyridinone ring, namely 2-CH_3, H5 and H6 protons, in agreement with the results previously described (46). The most affected signal of the *N*-substituent was H1' proton which chemical shift varied from 3.88 to 4.48 ppm. In the ^{13}C spectrum, some variations were also verified, namely C1' carbon which signal shifted from 50.4 to 55.4 ppm. The resonance signal at 31.1 ppm was attributed to C2' carbon due to its HMBC correlation with H1'and H3' protons. C1' (55.4 ppm) has shown correlation with the signal H6, H3' and H2', allowing its attribution.

The observed differences in the chemical shifts of ^{1}H and ^{13}C nucleus in the spectra of the protected and deprotected forms of each compound are primarily justified by the different solvent used for the NMR studies of protected ($CDCl_3$) and deprotected forms (MeOD) which as deliberated by the different solubility of each form of the ligand. Moreover, the deprotection of the hydroxyl group in acidic reaction conditions leads to isolate the final ligands in the enolic form, thus justifying the variations of the chemical shifts of the protons and carbons signals (46).

5.3.4 Solid-state structures

Crystalline material of the four 3,4-HPO ligands (**MRB13 - MRB16**) revealing single-crystals suitable for X-ray diffraction analysis were obtained by controlled recrystallization from MeOH/$CHCl_3$ solvent mixtures. The solid-state crystalline structures were solved and determined in the monoclinic space group $P2_1/c$, with the exception of **MRB14** for which crystalized in the orthorhombic system (space group $P2_12_12_1$).

The crystal structure of ligand **MRB14** was firstly reported by Hider and co-workers (41). As it was possible to obtain crystalline material of **MRB14** revealing single-crystals suitable for X-ray diffraction analysis, we also included the description of the results obtained for this ligand. The information obtained constitutes additional structural characterization data and is also useful to compare with the results obtained for the newly described 3,4-HPOs (**MRB13**, **MRB15** and **MRB16**), in the same experimental conditions. The crystal structures support unequivocally the

synthesis of the desired organic molecules, all isolated in enolic forms as hydrochloride salts (Figure 5.2). The asymmetric units (asu's) of four crystal structures are identical, revealing only a respective cationic organic molecule (3,4-HPO ligand) and one chloride anion. The *asu* of **MRB16** comprises an additional crystallization water molecule. The bond distances of the common 3,4-HPO ring are identical between all the four molecules and also comparable to other previously reported (23,41,47,48). Interestingly, the C3−O2 bond distance is slightly longer in the **MRB15** and **MRB16** molecules [1.336(2) and 1.335(2) Å, respectively] than that in the **MRB13** [1.328(2) Å] and **MRB14** [1.324(3) Å] structures.

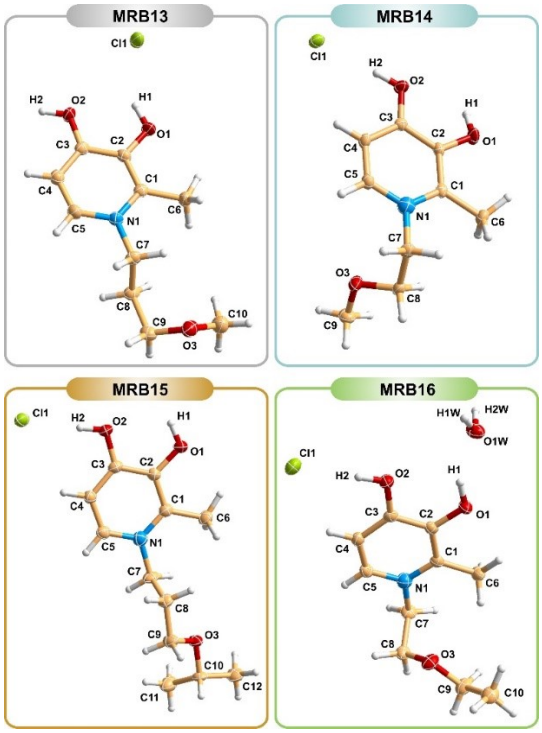

Figure - 5.2 Crystal structures of the 3,4-HPO molecules (**MRB13**, **MRB14**, **MRB15** and **MRB16**), showing the label scheme for all non-H-atoms which are represented as thermal ellipsoids drawn at the 50% probability level, while H-atoms are shown as small spheres with arbitrary radius.

The relative position of the chloride anions strongly influences the crystal packing arrangement in all the compounds, due to distinct O–H···Cl hydrogen bonds established with the respective organic molecules (Figure 3.5; see Table 5.3 for geometric details about the strong hydrogen bonding interactions found in all the structures). In the **MRB13** structure a pair of chloride anions bridges two neighbouring organic molecules positioned in anti-parallel mode, by O–H···Cl hydrogen bonds involving the hydroxyl groups in the pyridinone ring and originating discrete supramolecular species (Figure 5.3-**MRB13**).

In the structures of **MRB14** and **MRB15**, the O–H···Cl hydrogen bonds established between the hydroxyl groups of adjacent molecules and the chloride anions lead to the formation of one-dimensional supramolecular entities (Figure 5.3-**MRB14** and –**MRB15**). Both supramolecular chains show a zig-zag arrangement and extend along the *b*-axis of the respective unit cell.

The existence of crystallization water molecules in the structure of **MRB16** besides the chloride anions promotes an extensive hydrogen bonding network (strong O–H···O and O–H···Cl interactions) involving the contiguous organic molecules and leads to the formation of two-dimensional supramolecular structures (supramolecular layers) extended in the [100] direction of the unit cell (Figure 5.3-**MRB16**). In **MRB16**, contrasting with the remaining compounds where only the hydroxyl groups of the 3-hydroxy-4-pyridinone rings are engaged in the hydrogen bonds, the O-atoms of the ether groups in the chains are also involved.

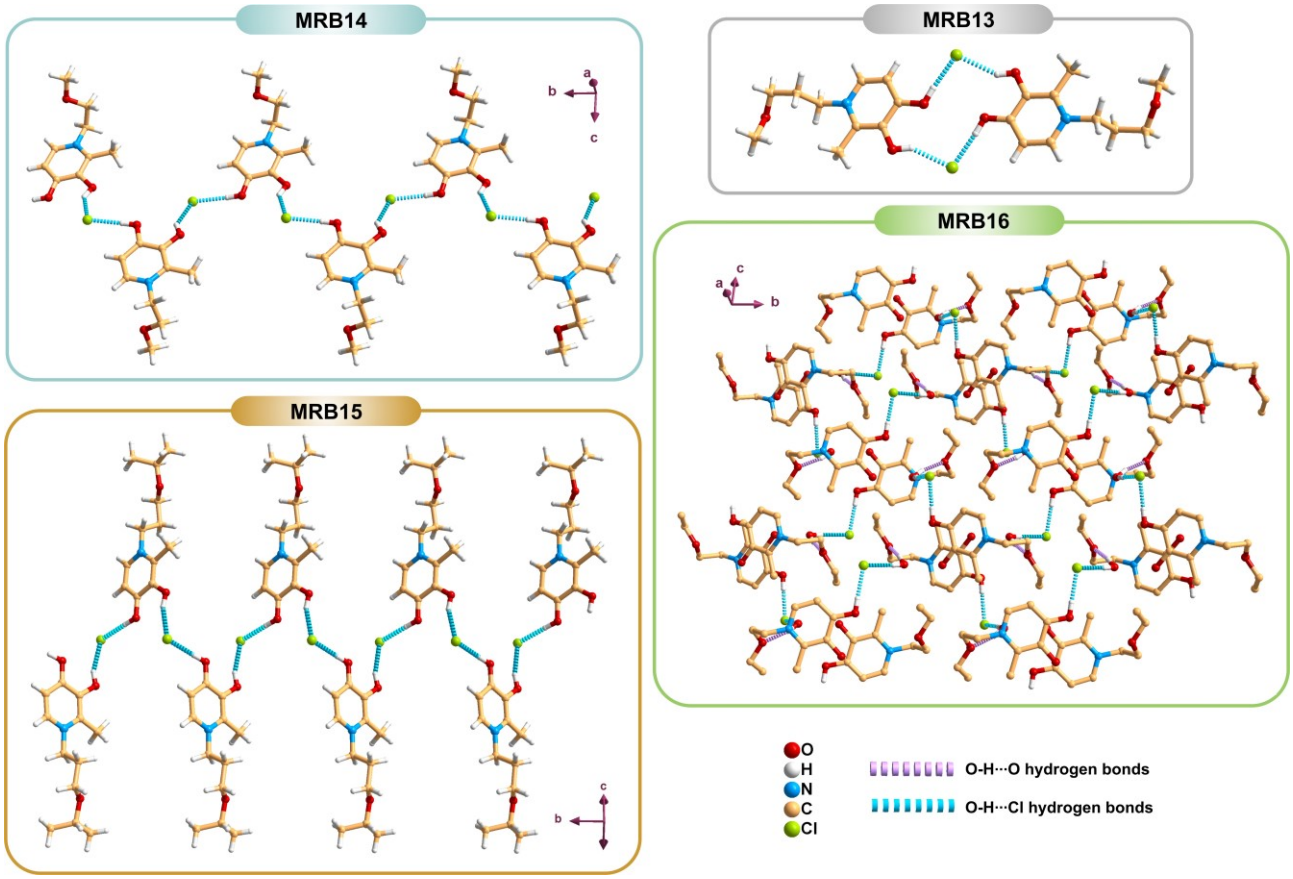

Figure - 5.3 O–H···Cl (blue dashed lines) and O–H···O (lavender dashed lines) hydrogen bond interaction originating discrete (**MRB13**), one-dimensional (**MRB14** and **MRB15**) and two-dimensional (**MRB16**) supramolecular structures.

Table - 5.4 Geometric information (distances in Å and angles in degrees) for the strong hydrogen bond interactions (D–H···A) of **MRB13**, **MRB14**, **MRB15** and **MRB16**.[a]

	D–H···A	***d*(H···A)**	***d*(D···A)**	**∠(DHA)**
MRB13	O1–H1···Cl1	2.221(18)	3.029(2)	149(3)
	O2–H2···Cl1^{i}	2.071(12)	2.954(2)	169(3)
MRB14	O1–H1···Cl1^{ii}	2.29(2)	3.037(3)	141(2)
	O2–H2···Cl1	2.092(13)	2.976(3)	177(3)
MRB15	O1–H1···Cl1^{iii}	2.234(13)	3.0576(14)	154(2)
	O2–H2···Cl1	2.032(10)	2.9336(13)	178(2)
MRB16	O1–H1···O1W	1.765(11)	2.5830(13)	152.5(16)
	O2–H2···Cl1	2.072(9)	2.9602(10)	177.1(15)
	O1W–H1W···O3^{iv}	1.906(9)	2.7812(13)	169.3(17)
	O1W–H2W···Cl1^{v}	2.280(9)	3.1722(11)	177.1(14)

[a] Symmetry transformation used to generate equivalent atoms: (i) *–x–2,–y+1,–z+1*; (ii) *–x+1, y–1/2, –z+1/2*; (iii) *–x+1, y–1/2, –z+3/2*; (iv) –x–1, –y+1, –z; (v) *x, –y+1/2, z–1/2*.

The extended packing of the supramolecular entities previously described (discrete in **MRB13**, one-dimensional in **MRB14** and **MRB15**, and two-dimensional structures in **MRB16**) is further reinforced by an extensive network of weak non-covalent interactions, particularly C−H···Cl, C−H···O and C−H···π interactions (not shown; Figure 5.4). As consequence of the overall hydrogen bonding network all the compounds reveal stable three-dimensional supramolecular structures with a crystal packing considerably dense.

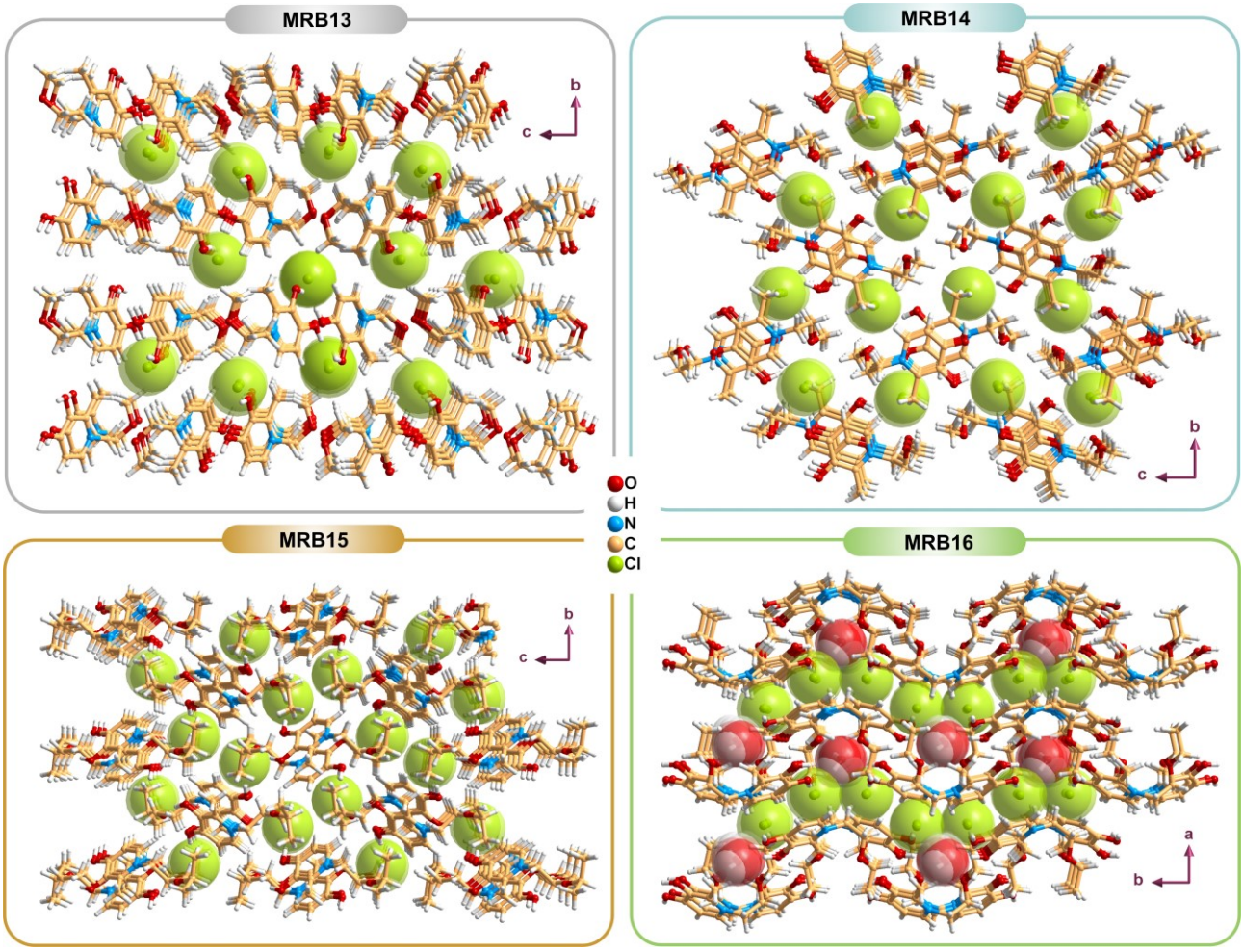

Figure - 5.4 Extended crystal packing viewed in the [1 0 0] (**MRB13**, **MRB14** and **MRB15**) and [0 0 1] (**MRB16**) direction of the respective unit cell, with the charge balancing chloride anions and crystallization water molecules (only in **MRB16**) drawn in space-filling model.

5.3.5 Analytical results

5.3.5.1 Features of the colorimetric determination of iron(III)

The performance of **MRB13**-**MRB16** as colorimetric reagents for iron(III) determination was evaluated using the previously described sequential injection method (12) and compared with preceding results obtained for the parent ligand **MRB12**.

Calibration curves were performed using iron(III) standards in the range 1.8 - 18 µmol/L (0.10-1.0 mg/L) and the analytical features displayed with the use of each ligand are summarized in Table 5.5. Data related with results obtained with **MRB12** was also included for comparison.

The sensitivity was set as the calibration curve slope and the limit of detection calculated as the concentration corresponding to 3 times the standard deviation of the blank signal. The precision was evaluated based on the relative standard deviation of the 9.0 µmol/L iron(III) standard.

Table - 5.5 Analytical features of the methods using different ligands for iron(III) determination considering the previously described SI method (12). LOD - Limit of detection; RSD - Relative standard deviation.

Ligand	**Ligand concentration of 0.6 mmol/L (g/L)**	**Sensitivity: calibration curve slope (L/mmol)**	**LOD (µmol/L)**	**Precision: RSD (%), [Fe^{3+}]=9.0 µmol/L**
MRB12 (12)	0.193	**s =** 12.8±0.4	1.27	1%
MRB13	0.140	**s =** 13.0±0.9	1.24	1%
MRB14	0.131	**s =** 13.6±0.7	1.40	1%
MRB15	0.157	**s =** 13.8±0.5	1.74	1%
MRB16	0.140	**s =** 13.7±0.8	1.79	2%

From analysis of the results summarized in Table 5.5, we verified that all ligands exhibited a good performance in the determination of iron(III). The results have shown no significant differences in the LOD and precision parameters between the ligands studied in the present work and with the previously tested **MRB12**. Also, no relevant differences were detected in the sensitivity of the method involving the different ligands comparing to the value determined for **MRB12** (relative deviation, RD <8%).

The results suggest that this new set of 3,4-HPO ligands functionalized with variable ether-derived chains possess a suitable water solubility to guarantee the high sensitivity and low detection limit when compared to the results obtained for the non-ether derived 3,4-HPO, Hmpp, and in a similar mode with that described for **MRB12** (12). Despite their variable Log P values (-0.69 <Log P < 0.50), all the these “ether derived 3,4-HPO ligands” exhibited similar performance in SI method analytical determination of iron(III).

5.3.5.2 Assessment of potential interferences in water monitoring

Additionally, as previously intended with **MRB12**, the potential application to natural waters requires an effective selectivity in comparison with other ions possibly present. In this context the assessment of potential interferences was carried out, based upon the expected values in natural waters, defined by UNFAO (United Nations Food and Agriculture Organization) (49). The percentage of interference (IP) was calculated comparing the analytical signal obtained for an iron(III) standard with a mixed standard of iron(III) and the potential interfering ion. Experiments were performed using concentrations of the potential interfering metal ion (M^{n+}) identical or greater than the UNFAO value. The standards were prepared with 0.50 mg/L (8.95 µmol/L) of iron(III) and with or without interfering ion. The tested interfering ions, with respective concentrations and the interference percentages are presented in Table 5.6.

The results shown in Table 5.6 are indicative that no significant interferences are expected from metal ions existent in natural waters. All the ligands tolerate the interference in quantities greater than the limits defined.

Table - 5.6 Assessment of the influence of potential interfering ions (M^{n+}), for the five ligands, using the developed μSIA method, using an iron standard of 0.50 mg/L (8.95 μmol/L); values with bold numbers represent the maximum ratio without significant interference (<10%).

Potential interfering ion (M^{n+})	UNFAO limits (mg/L)	[M^{n+}] (mg/L)	IP (%)				
			MRB12	MRB13	MRB14	MRB15	MRB16
Al^{3+}	5	**5** 10	**-5** -8	**-2** -14	**-** <10	**-8** -	**-3** -
Ca^{2+}	15	**15** 30	**-0.5** 11	**0.3** 16	**-** <10	**2** 12	**0.9** -21
Co^{2+}	0.1	**0.1** 0.3	**2** 11	**-0.5** 20	**-** 3	**5** 12	**6** -21
Mg^{2+}	5	**20** 40	**2** 24	**1** 21	**0.1** 24	**5** 16	**-** -1
Mn^{2+}	0.2	**20** 30	**5** 15	**4** 15	**7** 23	**1** 13	**-** 2
Ni^{2+}	0.2	**2** 5	**5** 13	**-** <10	**-** <10	**-** 7	**-4** 10
Zn^{2+}	2	**10** 30	**1** 12	**-5** 13	**1** 15	**-3** 15	**-** <10
Cu^{2+}	1.3	**5** 10	**5** 13	**2** 12	**-** <10	**4** 16	**-** <10
Cd^{2+}	-	**0.1** 0.5	**4** 17	**1** 14	**-** 5	**-** 2	**-** <10
Pb^{2+}	-	**0.1** 0.5	**3** 14	**-** -0.2	**-** 4	**0.5** 10	**-** 5
Cr^{3+}	-	**0.05** 0.1	**7** 13	**-** -2	**-** 2	**-** <10	**-** <10

5.4 Conclusions

We report the synthesis and structural characterization of three novel 3,4-HPO chelators with different ether derived substituents in the nitrogen atom of the heterocyclic ring. The three compounds, together with one previously described and revisited in this study, provide a range of Log P values between -0.69 < Log P < 0.50. Chelators were successfully obtained in high reaction yields by microwave-assisted methods and using commercially available amines as precursors. All the ligands were obtained in an easier, quicker, and more efficient and sustainable way in comparison with the methods described for the synthesis of a highly water soluble 3,4-HPO chelator, **MRB12** (12). The reduction of overall reaction times, the reproducibility of the experiments and the lower number of steps, constitutes a great advantage considering the need of these ligands as well as their respective metal ion complexes, to be used in many analytical, biological and agricultural applications.

In order to evaluate the potential of the new compounds as analytical reagents in iron(III) determination by sequential injection methods, we tested **MRB13-MRB16** ligands in the same conditions used for **MRB12**. Results showed that all the ligands described are promising molecules for this assay since they exhibit similar results, highlighting the fact that the structural differences introduced do not compromise their performance in iron(III) determination in aqueous samples. Also, results regarding the relevance of several metal ions as potential interferences reinforce the potential application of the ligands in natural water monitoring.

In summary, the new procedure is advantageous to obtain highly water soluble compounds that suitable for analytical applications like metal ion determination (11,12,30), biological purposes, such as the treatment of several diseases like Iron Overload (50–52), Diabetes (53–55) and in agriculture to address Plant Iron Deficiency Chlorosis (17,56–58).

Supporting Information

NMR structural characterization details for ligands MRB13-16 are provided in Supporting Information. CCDC-1845145 (MRB13), CCDC-1845146 (MRB14), CCDC-1845147 (MRB15) and CCDC-1845148 (MRB16) and crystallographic data in CIF format are also supplied as Supporting Information

References

1. Santos MA, Marques SM, Chaves S. Hydroxypyridinones as “privileged” chelating structures for the design of medicinal drugs. Coord Chem Rev. 2012;256(1–2):240–259.

2. Grazina R, Gano L, Šebestík J, Amelia Santos M. New tripodal hydroxypyridinone based chelating agents for Fe(III), Al(III) and Ga(III): Synthesis, physico-chemical properties and bioevaluation. J Inorg Biochem. 2009;103(2):262–273.

3. Zhou T, Ma Y, Kong X, Hider RC. Design of iron chelators with therapeutic application. Dalt Trans. 2012;41(21):6371–6389.

4. Cusnir R, Imberti C, Hider RC, Blower PJ, Ma MT. Hydroxypyridinone chelators: From iron scavenging to radiopharmaceuticals for PET imaging with gallium-68. Int J Mol Sci. 2017;18(1):1–23.

5. Liu ZD, Hider RC. Design of iron chelators with therapeutic application. Coord Chem Rev. 2002;232(1–2):151–171.

6. Liu ZD, Hider RC. Design of Clinically Useful Iron(III)-Selective Chelators. Med Res Rev. 2001;22(1):26–64.

7. Zhou T, Winkelmann G, Dai ZY, Hider RC. Design of clinically useful macromolecular iron chelators. J Pharm Pharmacol. 2011;63(7):893–903.

8. Hider RC, Roy S, Ma YM, Le Kong X, Preston J. The potential application of iron chelators for the treatment of neurodegenerative diseases. Metallomics. 2011;3(3):239–49.

9. Chaves S, Piemontese L, Hiremathad A, Santos MA. Hydroxypyridinone Derivatives: A Fascinating Class of Chelators with Therapeutic Applications - An Update. Curr Med Chem. 2017;25(1):97–112.

10. Chisté RC, Ribeiro D, Freitas M, Leite A, Moniz T, Rangel M, et al. Uncovering novel 3-hydroxy-4-pyridinone metal ion complexes with potential anti-inflammatory properties. J Inorg Biochem. 2016;155:9–16.

11. González A, Mesquita RBR, Avivar J, Moniz T, Rangel M, Cerdà V, et al. Microsequential injection lab-on-valve system for the spectrophotometric bi-parametric determination of iron and copper in natural waters. Talanta. 2017;167:703–708.

12. Mesquita RBR, Moniz T, Miranda JLA, Gomes V, Silva AMN, Rodriguez-Borges JE, et al. Synthesis and characterization of a 3-hydroxy-4-pyridinone chelator functionalized with a polyethylene glycol (PEG) chain aimed at sequential injection determination of iron in natural waters. Polyhedron. 2015;101:171–178.

13. Moniz T, Amorim MJ, Ferreira R, Nunes A, Silva A, Queirós C, et al. Investigation of the insulin-like properties of zinc(II) complexes of 3-hydroxy-4-pyridinones: Identification of a compound with glucose lowering effect in STZ-induced type I diabetic animals. J Inorg Biochem. 2011;105(12):1675–1682.

14. Moniz T, Nunes A, Silva AMG, Queirós C, Ivanova G, Gomes MS, et al. Rhodamine labeling of 3-hydroxy-4-pyridinone iron chelators is an important contribution to target Mycobacterium avium infection. J Inorg Biochem. 2013;121:156–166.

15. Moniz T, Queirós C, Ferreira R, Leite A, Gameiro P, Silva AMG, et al. Design of a water soluble 1,8-naphthalimide/3-hydroxy-4-pyridinone conjugate: Investigation of its spectroscopic properties at variable pH and in the presence of Fe3+, Cu2+ and Zn2+. Dye Pigment. 2013;98(2):201–211.

16. Moniz T, Silva D, Silva T, Gomes MS, Rangel M. Antimycobacterial activity of rhodamine 3,4-HPO iron chelators against Mycobacterium avium: Analysis of the contribution of functional groups and of chelator's combination with ethambutol. Medchemcomm. 2015;6(12):2194–2203.

17. Santos CS, Carvalho SMP, Leite A, Moniz T, Roriz M, Rangel AOSS, et al. Effect of tris(3-hydroxy-4-pyridinonate) iron(III) complexes on iron uptake and storage in soybean (Glycine max L.). Plant Physiol Biochem. 2016;106:91–100.

18. Burgess J, De Castro S, Oliveira C, Rangel M, Schlindwein W. Synthesis and characterization of 3-hydroxy-4pyridinone-oxovanadium(IV) complexes. Polyhedron. 1997;16(5):789–794.

19. Dobbin PS, Hider RC, Hall AD, Taylor PD, Sarpong P, Porter JB, et al. Synthesis, physicochemical properties, and biological evaluation of N-substituted 2-alkyl-3-hydroxy-4(1H)-pyridinones: orally active iron chelators with clinical potential. J Med Chem. 2002;36(17):2448–2458.

20. Scarrow RC, Riley PE, Abu-Dari K, White DL, Raymond KN. Ferric ion sequestering agents. 13. Synthesis, structures, and thermodynamics of complexation of cobalt(III) and iron(III) tris complexes of several chelating hydroxypyridinones. Inorg Chem. 1985;24(6):954–967.

21. Santos MA, Gil M, Gano L, Chaves S. Bifunctional 3-hydroxy-4-pyridinone derivatives as potential pharmaceuticals: synthesis, complexation with Fe(III), Al(III) and Ga(III) and in vivo evaluation with 67Ga. JBIC J Biol Inorg Chem 2005 105. 2005;10(5):564–580.

22. Fakih S, Podinovskaia M, Kong X, Collins HL, Schaible UE, Hider RC. Targeting the lysosome: Fluorescent iron(III) chelators to selectively monitor endosomal/ lysosomal labile iron pools. J Med Chem. 2008;51(15):4539–4552.

23. Silva AMG, Leite A, Andrade M, Gameiro P, Brandão P, Felix V, et al. Microwave-assisted synthesis of 3-hydroxy-4-pyridinone/naphthalene conjugates. Structural characterization and selection of a fluorescent ion sensor. Tetrahedron. 2010;66(44):8544–8550.

24. Battah S, Hider RC, MacRobert AJ, Dobbin PS, Zhou T. Hydroxypyridinone and 5-Aminolaevulinic Acid Conjugates for Photodynamic Therapy. J Med Chem. 2017;60(8):3498–3510.

25. Zhu CF, Battah S, Kong X, Reeder BJ, Hider RC, Zhou T. Design, synthesis and biological evaluation of 5-aminolaevulinic acid/3-hydroxypyridinone conjugates as potential photodynamic therapeutical agents. Bioorganic Med Chem Lett. 2015;25(3):558–561.

26. Li D-F, Hu P-P, Liu M-S, Kong X-L, Zhang J-C, Hider RC, et al. Design and Synthesis of Hydroxypyridinone-l-phenylalanine Conjugates as Potential Tyrosinase Inhibitors. J Agric Food Chem. 2013;61(27):6597–6603.

27. Liu G, Bruenger FW, Miller SC, Arif AM. Molecular structure and biological and pharmacological properties of 3- hydroxy-2-methyl-1-(β-D-ribofuranosyl or pyranosyl)-4-pyridinone: Potential iron overload drugs for oral administration. Bioorganic Med Chem Lett. 1998;8(21):3077–3080.

28. Marczenko Z, Balcerzak M. Separation, preconcentration, and spectrophotometry in inorganic analysis. First Edit. Elsevier. Netherlands; 2000.

29. Suárez R, Mesquita RBR, Rangel M, Cerdà V, Rangel AOSS. Iron speciation by microsequential injection solid phase spectrometry using 3-hydroxy-1(H)-2-methyl-4-pyridinone as chromogenic reagent. Talanta. 2015;133:15–20.

30. Mesquita RBR, Suárez R, Cerdà V, Rangel M, Rangel AOSS. Exploiting the use of 3,4-HPO ligands as nontoxic reagents for the determination of iron in natural waters with a sequential injection approach. Talanta. 2013;108:38–45.

31. Zhang Z, Rettig SJ, Orvig C. Lipophilic Coordination Compounds: Aluminum, Gallium, and Indium Complexes of 1-Aryl-3-hydroxy-2-methyl-4-pyridinones. Inorg Chem. 1991;30(3):509–515.

32. Kottke T, Stalke D. Crystal handling at low temperatures. J Appl Crystallogr.

1993;26(4):615–619.

33. APEX2. Data Collection Software Version 2012.4, Bruker AXS. Delft, The Netherlands; 2012.

34. Cryopad. Remote monitoring and control, Version 1.451. Oxford, United Kingdom: Oxford Cryosystems; 2006.

35. SAINT+. Data Integration Engine v. 8.27b© 1997-2012. Madison, Wisconsin, USA: Bruker AXS;

36. Sheldrick GM. SADABS 2012/1, Bruker AXS Area Detector Scaling and Absorption Correction Program. Madison, Wisconsin, USA: Bruker AXS; 2012.

37. Sheldrick GM. A short history of SHELX. Vol. 64. Acta Crystallographica; 2008. p. 112–122.

38. Sheldrick GM. SHELXL v. 2014/3, Program for Crystal Structure Refinement. University of Gottingen; 2014.

39. Sheldrick GM. SHELXT-2014, Programs for Crystal Structure Solution. University of Gottingen; 2014.

40. Queiros C, Amorim MJ, Leite A, Ferreira M, Gameiro P, Castro B de, et al. Nickel(II) and Cobalt(II) 3-Hydroxy-4-pyridinone Complexes: Synthesis, Characterization and Speciation Studies in Aqueous Solution. Eur J Inorg Chem. 2011;2011(1):131–140.

41. Xiao G, Van Der Helm D, Goerlitz FH, Hider RC, Dobbin PS. Structures of 3-hydroxy-1-(2-methoxyethyl)-2-methyl-4-pyridinone, its hydrochloride and 1-ethyl-3-hydroxy-2-methyl-4-pyridinone hydrochloride hydrate. Acta Crystallogr Sect C. 1993;49(9):1646–1649.

42. Huang W, Richert R. The Physics of Heating by Time-Dependent Fields: Microwaves and Water Revisited. J Phys Chem B. 2008;112(32):9909–9913.

43. Robinson J, Kingman S, Irvine D, Licence P, Smith A, Dimitrakis G, et al. Understanding microwave heating effects in single mode type cavities—theory and experiment. Phys Chem Chem Phys. 2010;12(18):4750–4758.

44. Kappe CO. Controlled microwave heating in modern organic synthesis. Angew Chemie - Int Ed. 2004;43(46):6250–6284.

45. Advanced Chemistry Developmet. Structure Drawing Software for Academic and Personal Use | ACD/LogP ChemSketch. Available from: https://www.acdlabs.com/resources/freeware/chemsketch/

46. Moniz T, Coimbra JTS, Brás NF, Cunha-Silva L, Ramos MJ, Fernandes PA, et al. Synthesis

and structural characterization, by spectroscopic and computational methods, of two fluorescent 3-hydroxy-4-pyridinone chelators bearing sulphorhodamine B and naphthalene. RSC Adv. 2016;6(5):4200–4211.

47. Burgess J, Fawcett J, Parsons SA. 3-Hydroxy-1-(3-imidazolylpropyl)-2-methyl-4-pyridinone dihydrochloride dihydrate. Acta Crystallogr Sect E. 2001;57(11):o1016–o1018.

48. Hall SR, Roy R, McLaughlin DT, Sullivan KJ, Barclay LRC, Vogels CM, et al. The Synthesis and Molecular Structure of 1-(3,4-Dihydroxyphenethyl)-3-hydroxy-2-methylpyridin-4(1H)-one Hydrochloride Methanol Solvate. Crystals. 2013;3(2):333–338.

49. Eaton; AD, Clesceri; LS, Greenberg; AE, Franson; MAH, Health AP. Standard Methods for the Examination of Water and Wastewater. In: American Public Health Association, editor. 20th ed. Washington, DC, USA; 1999. p. Part 3000 Metals.

50. Crisponi G, Remelli M. Iron chelating agents for the treatment of iron overload. Coord Chem Rev. 2008;252(10–11):1225–1240.

51. Kalinowski DS, Richardson DR. The Evolution of Iron Chelators for the Treatment of Iron Overload Disease and Cancer. Pharmacol Rev. 2005;57(4):547–583.

52. Kontoghiorghes GJ, Neocleous K, Kolnagou A. Benefits and risks of deferiprone in iron overload in thalassaemia and other conditions: Comparison of epidemiological and therapeutic aspects with deferoxamine. Drug Saf. 2003;26(8):553–584.

53. Jakusch T, Kiss T. In vitro study of the antidiabetic behavior of vanadium compounds. Coord Chem Rev. 2017 Nov 15;351:118–126.

54. Sakurai H, Kojima Y, Yoshikawa Y, Kawabe K, Yasui H. Antidiabetic vanadium(IV) and zinc(II) complexes. Coord Chem Rev. 2002;226(1–2):187–198.

55. Sakurai H, Yoshikawa Y, Yasui H. Current state for the development of metallopharmaceutics and anti-diabetic metal complexes. Chem Soc Rev. 2008;37(11):2383–2392.

56. Abadía J, Vázquez S, Rellán-Álvarez R, El-Jendoubi H, Abadía A, Álvarez-Fernández A, et al. Towards a knowledge-based correction of iron chlorosis. Plant Physiol Biochem. 2011;49(5):471–482.

57. Shenker M, Chen Y. Increasing Iron Availability to Crops: Fertilizers, Organo-Fertilizers, and Biological Approaches. Soil Sci Plant Nutr. 2005;51(1):1–17.

58. Lucena JJ. Fe chelates for remediation of Fe chlorosis in strategy I plants. J Plant Nutr. 2003;26(10–11):1969–1984.

Supplementary Information

New hydrophilic 3-hydroxy-4-pyridinone chelators with ether-derived substituents: synthesis and evaluation of analytical performance in the determination of iron in waters

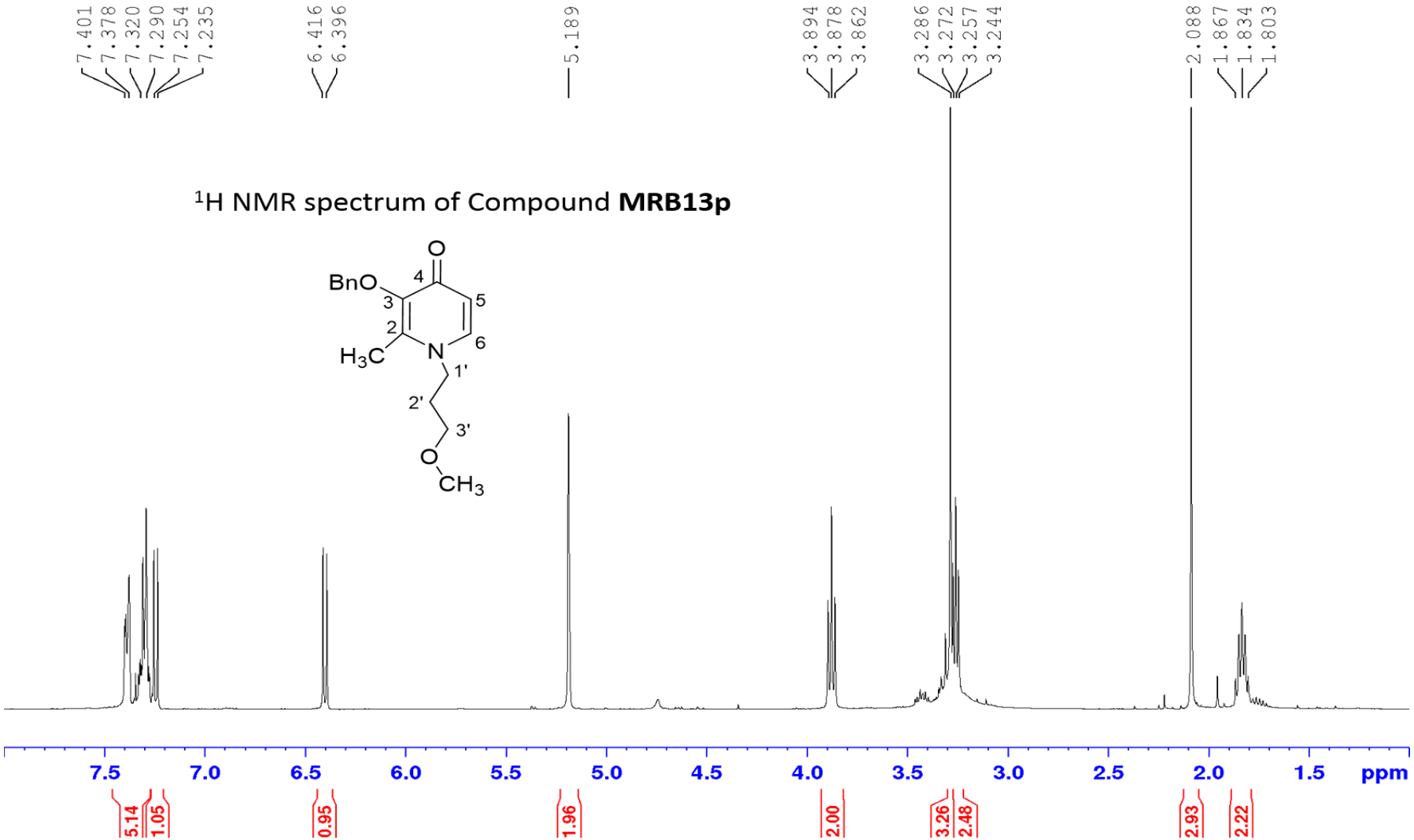

Figure - S1 400.15 MHz ^{1}H spectrum of compound **MRB13p**.

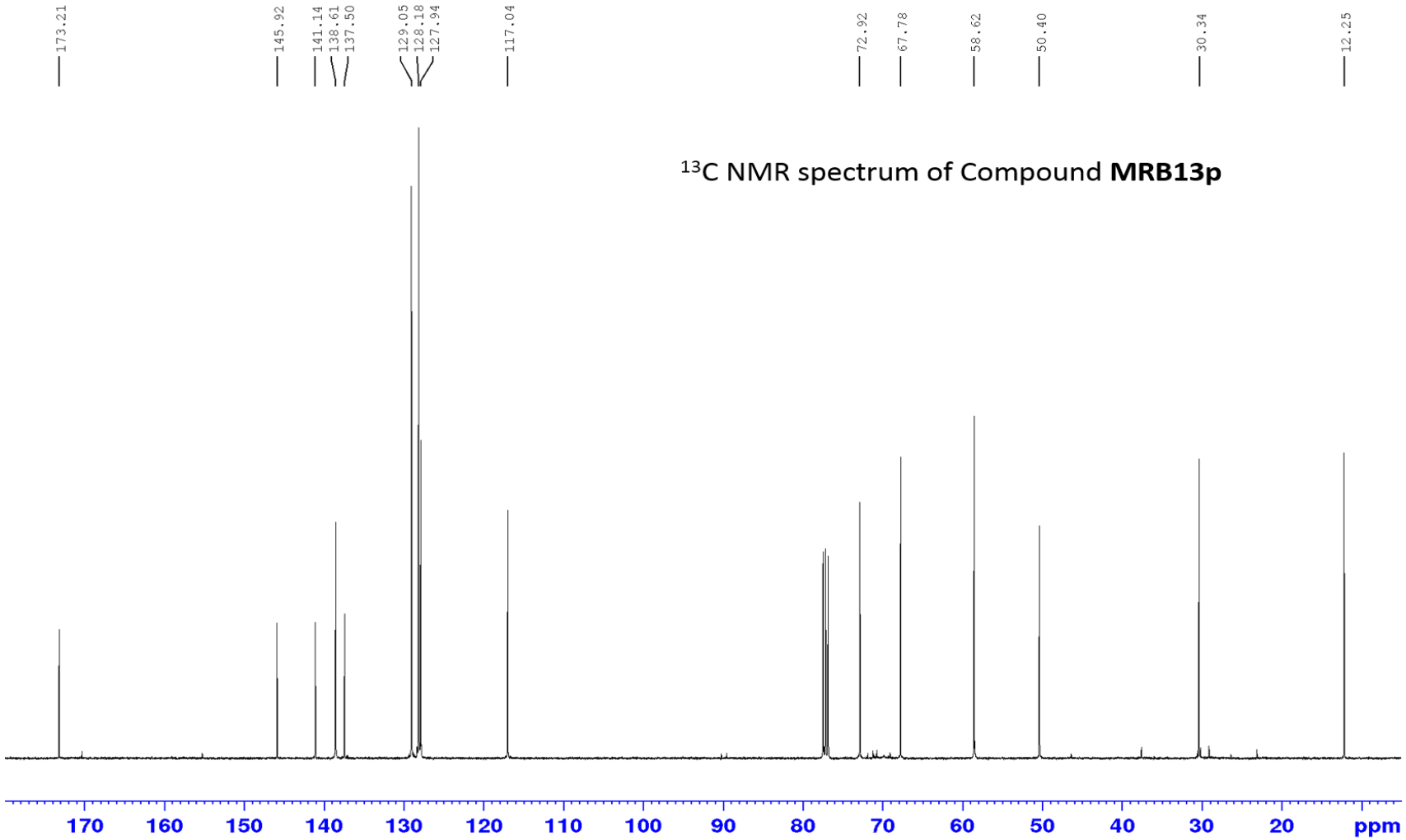

Figure - S2 100.62 MHz ^{13}C spectrum of compound **MRB13p.**

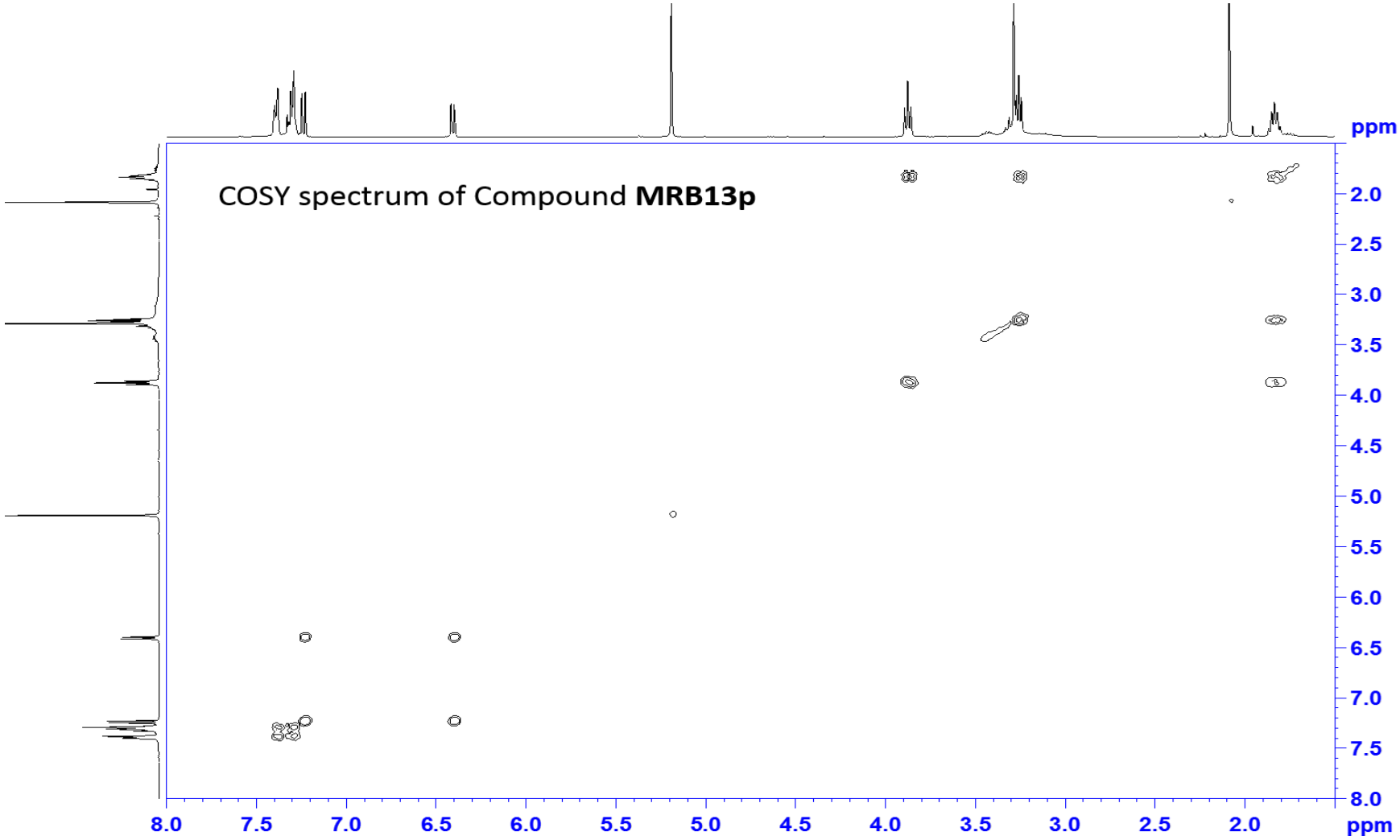

Figure - S3 $^{1}H/^{1}H$ COSY spectrum of compound **MRB13p**.

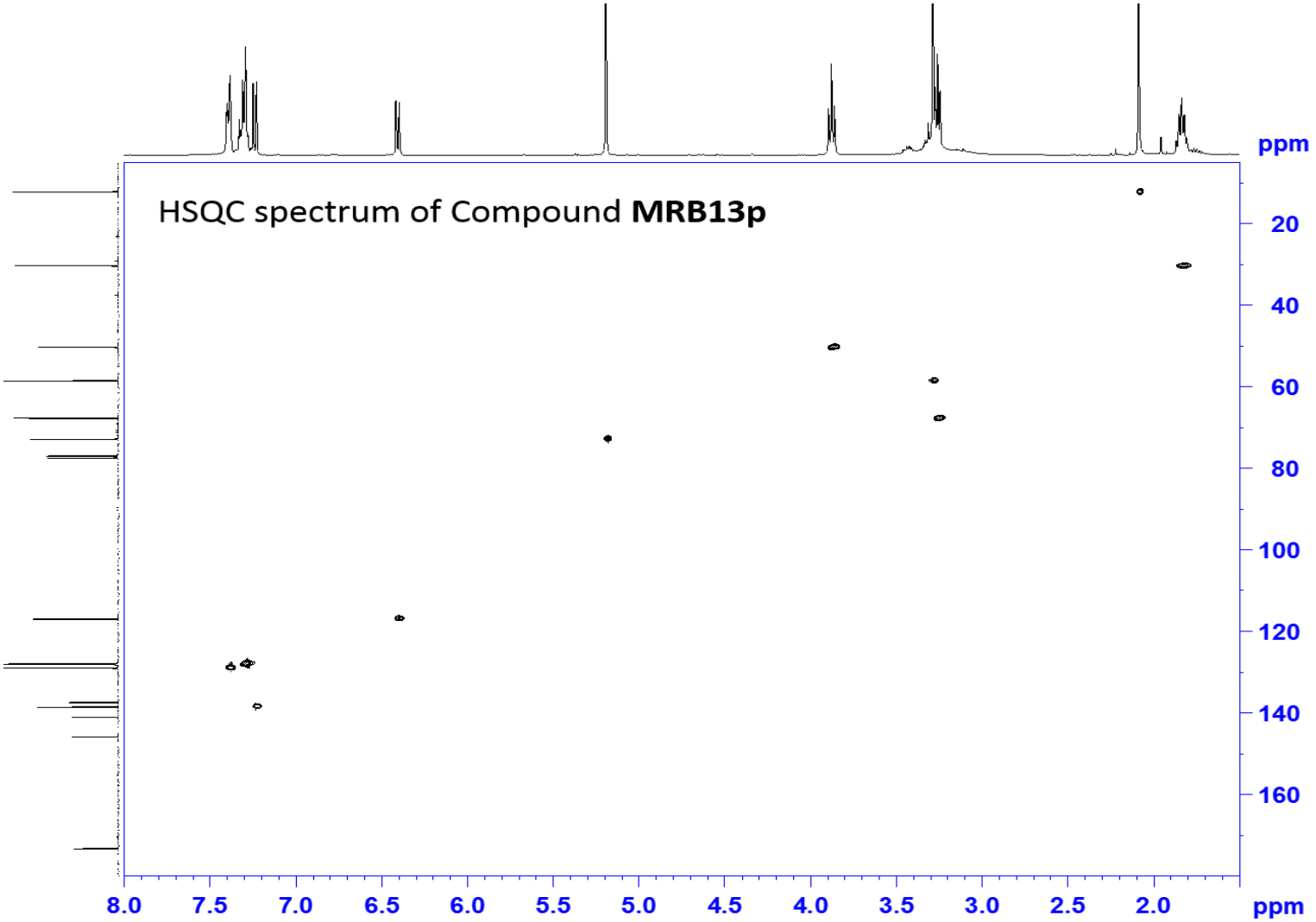

Figure - S4 $^{1}H/^{13}C$ HSQC spectrum of compound **MRB13p**.

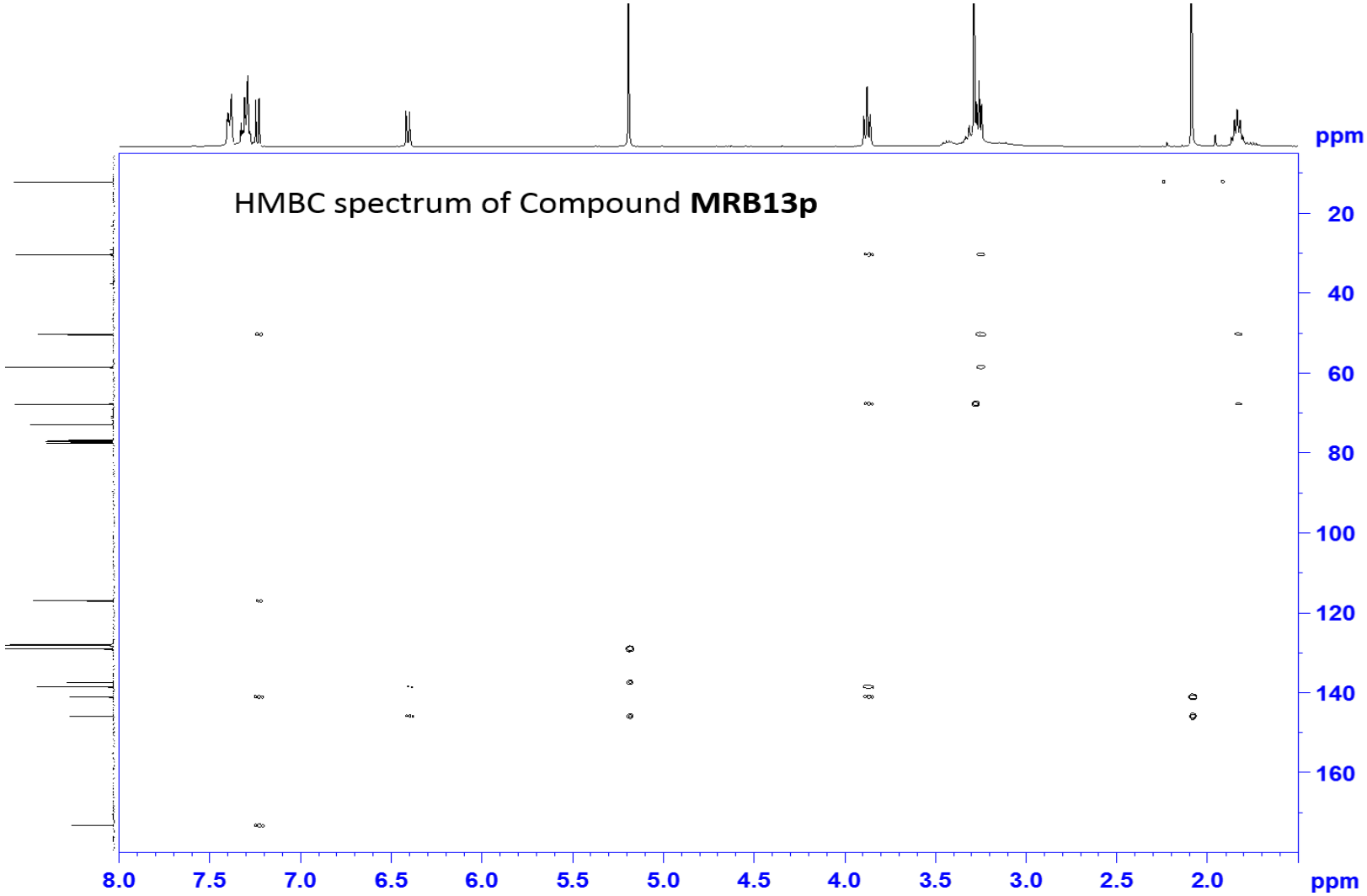

Figure - S5 $^{1}H/^{13}C$ HMBC spectrum of compound **MRB13p**.

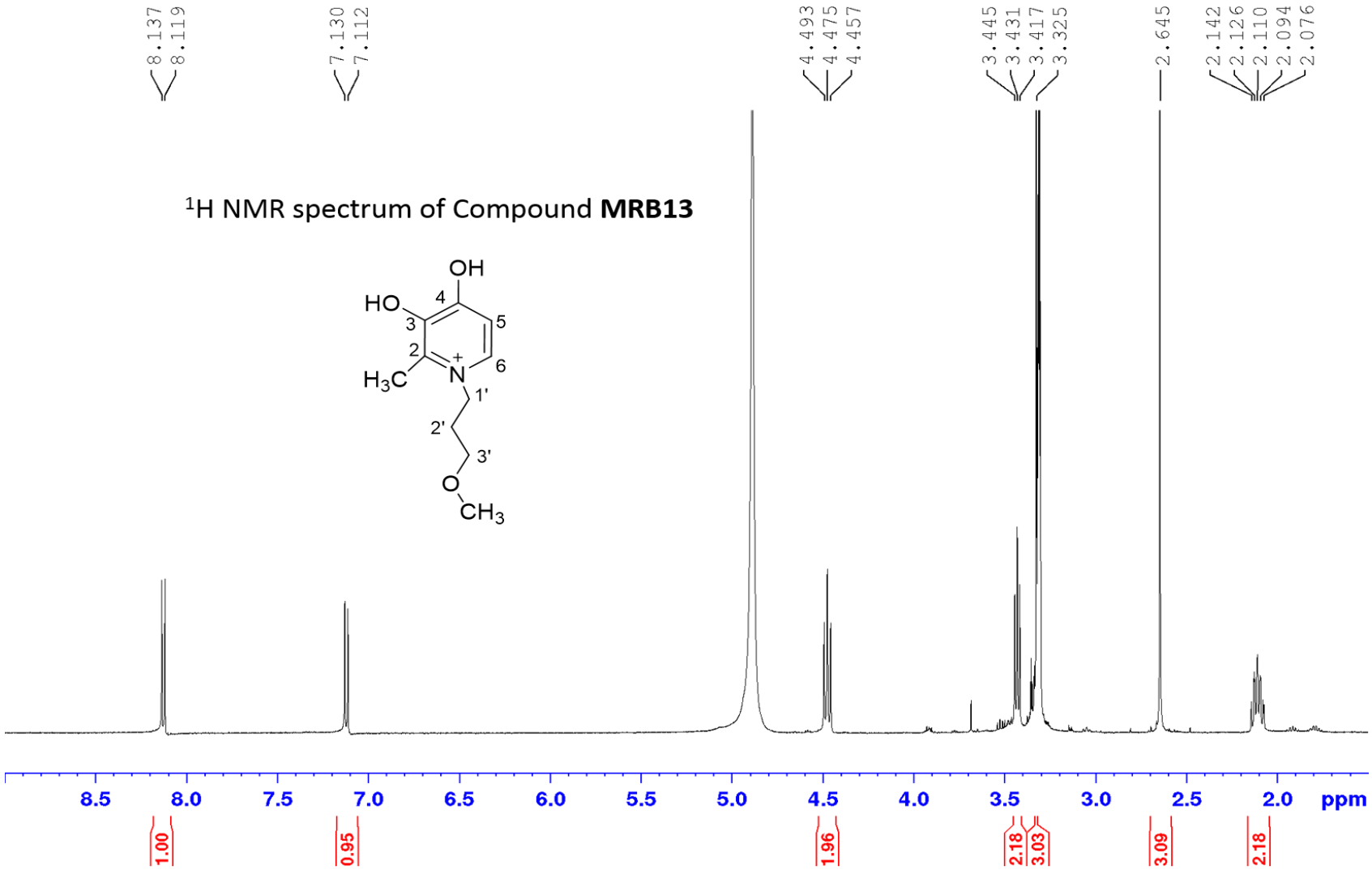

Figure - S6 400.15 MHz ^{1}H spectrum of compound **MRB13**.

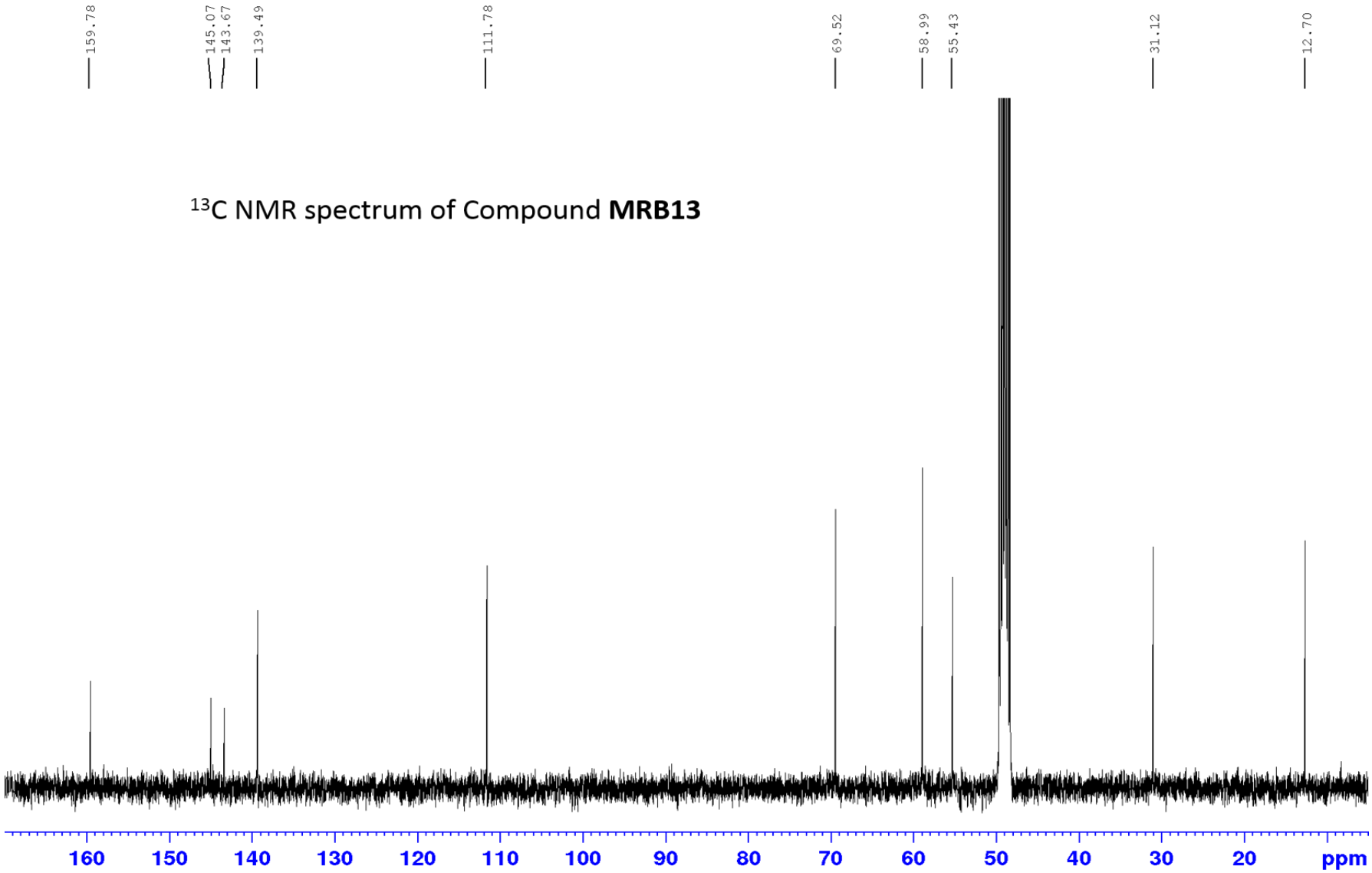

Figure - S7 100.62 MHz ^{13}C spectrum of compound **MRB13.**

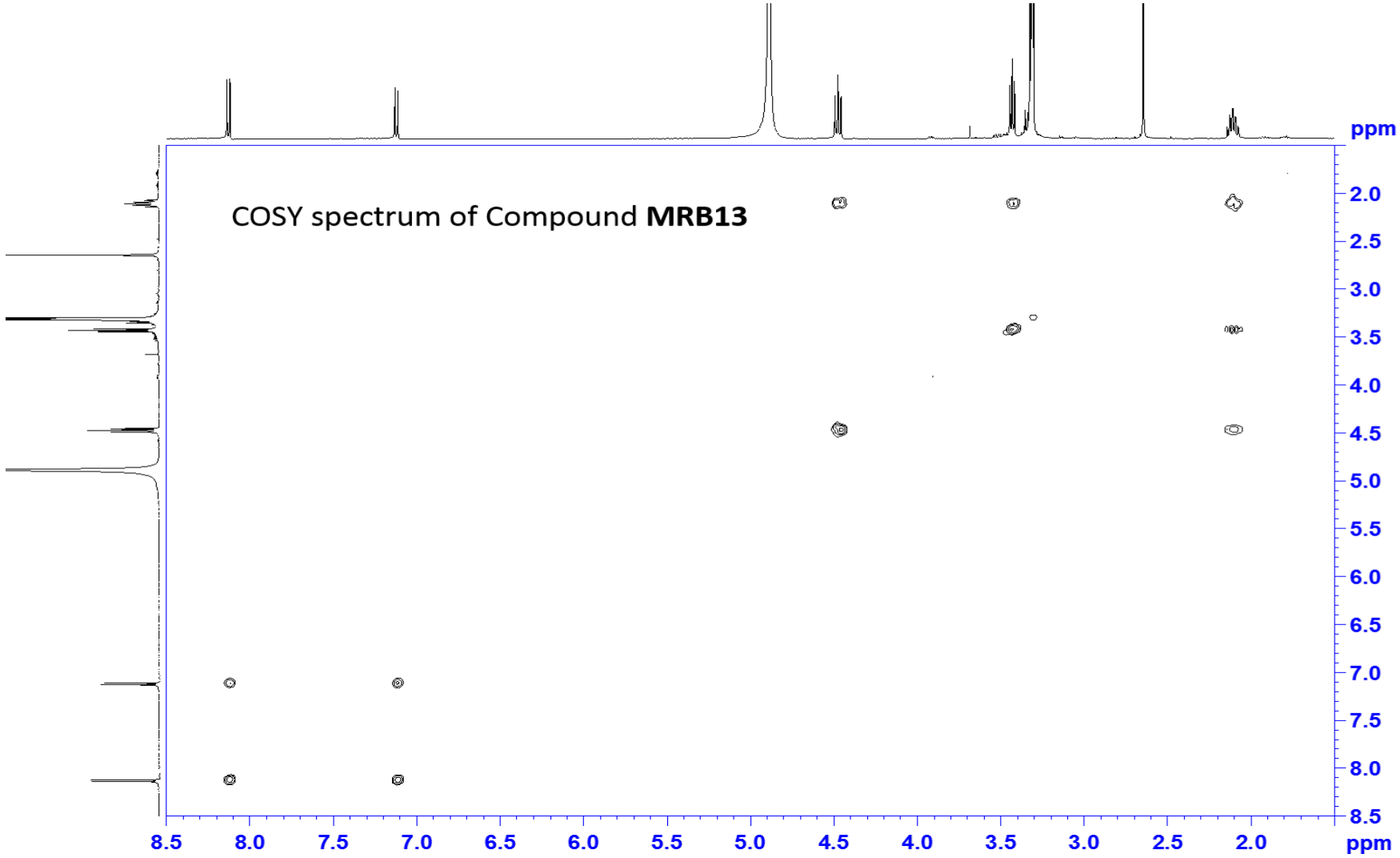

Figure - S8 $^{1}H/^{1}H$ COSY spectrum of compound **MRB13**.

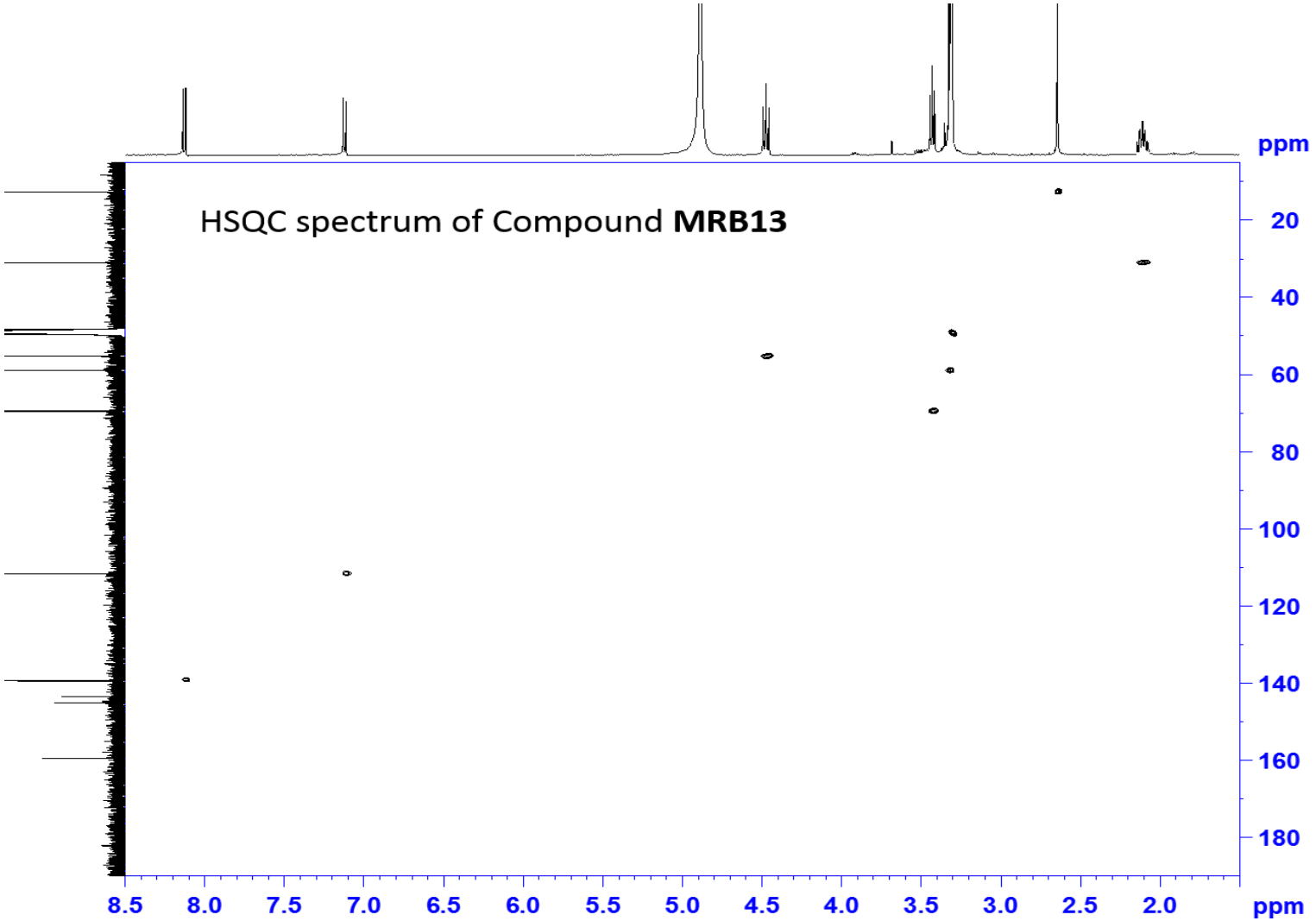

Figure - S9 $^{1}H/^{13}C$ HSQC spectrum of compound **MRB13**.

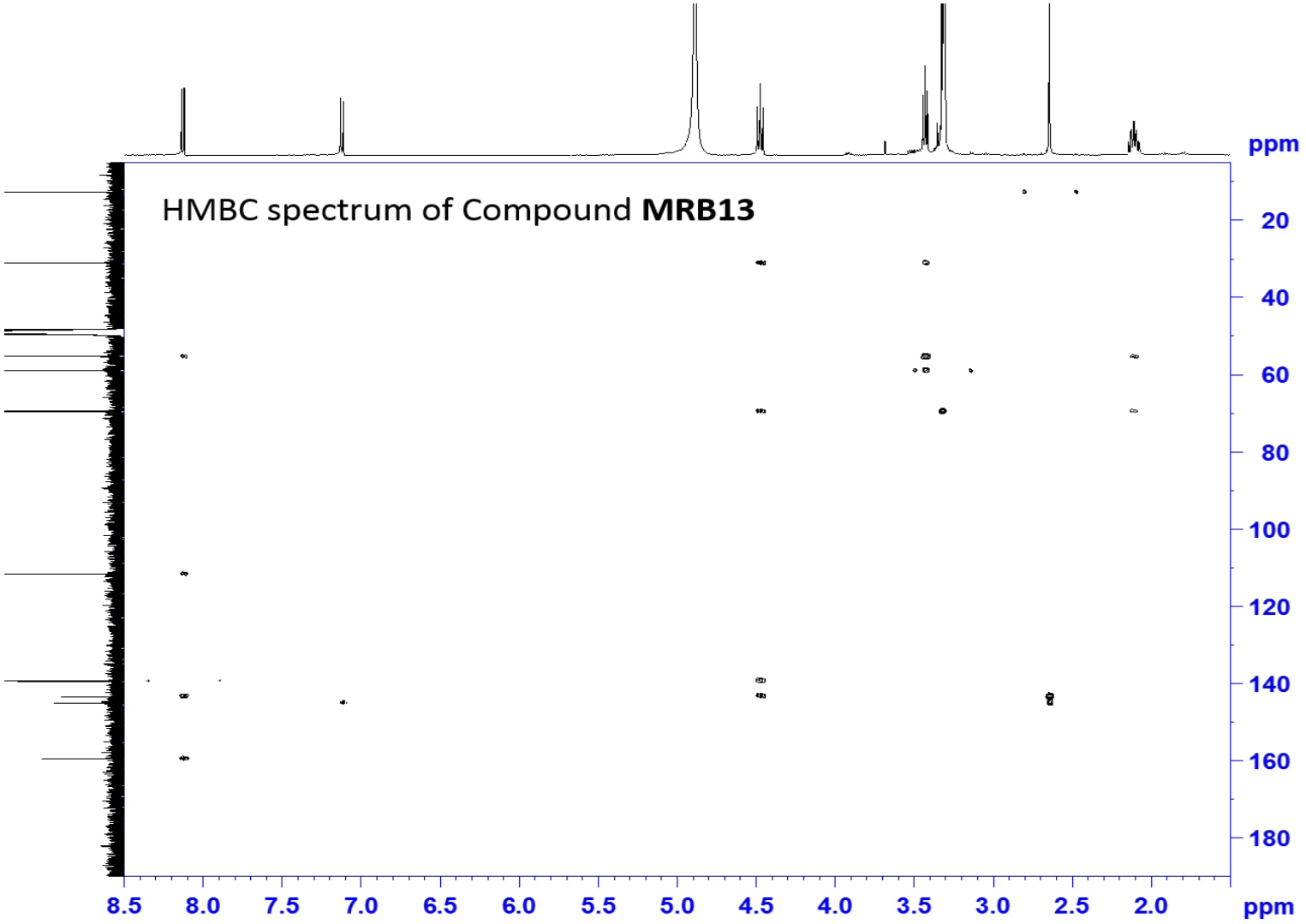

Figure - S10 $^{1}H/^{13}C$ HMBC spectrum of compound **MRB13**.

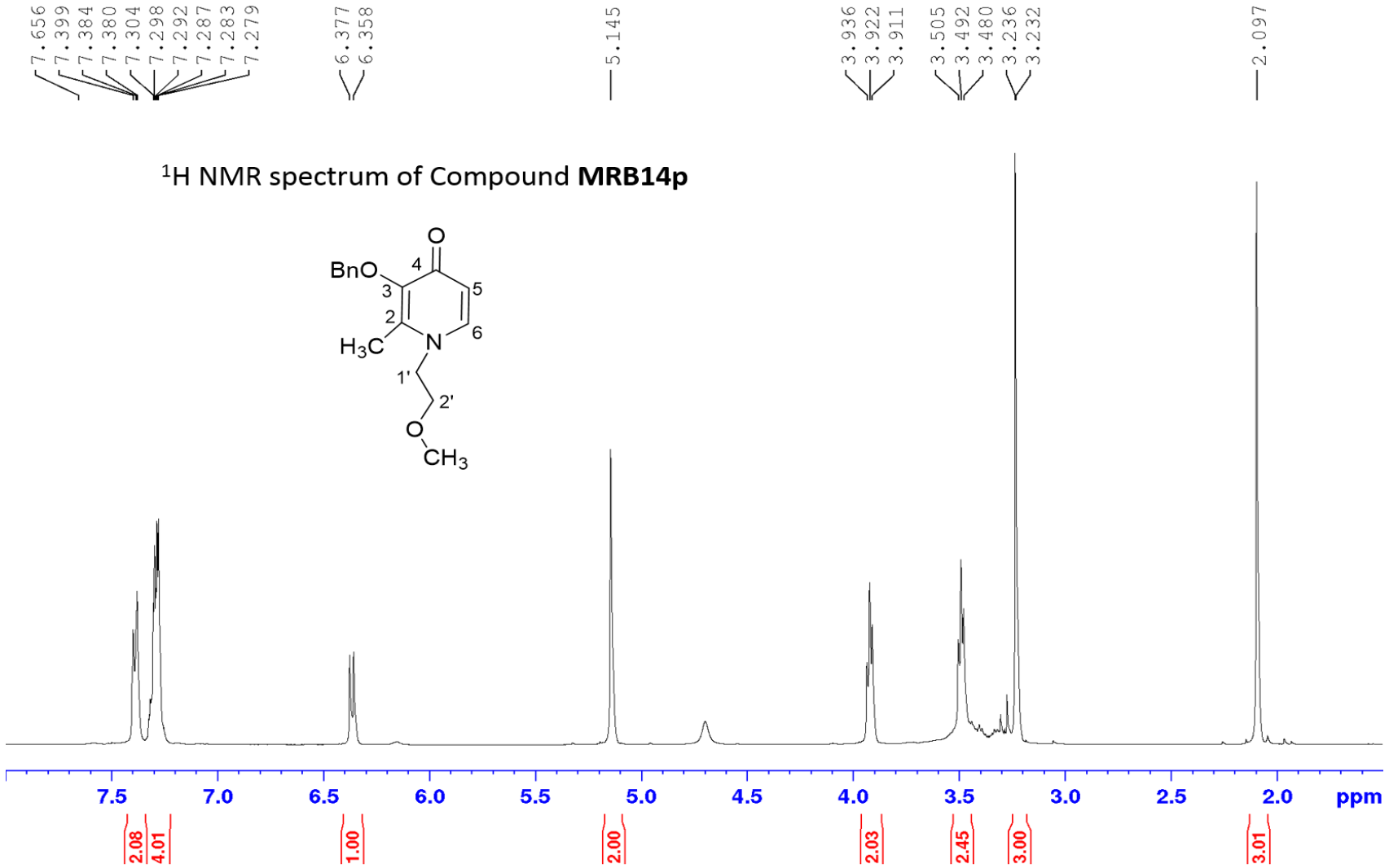

Figure - S11 400.15 MHz ^{1}H spectrum of compound **MRB14p**.

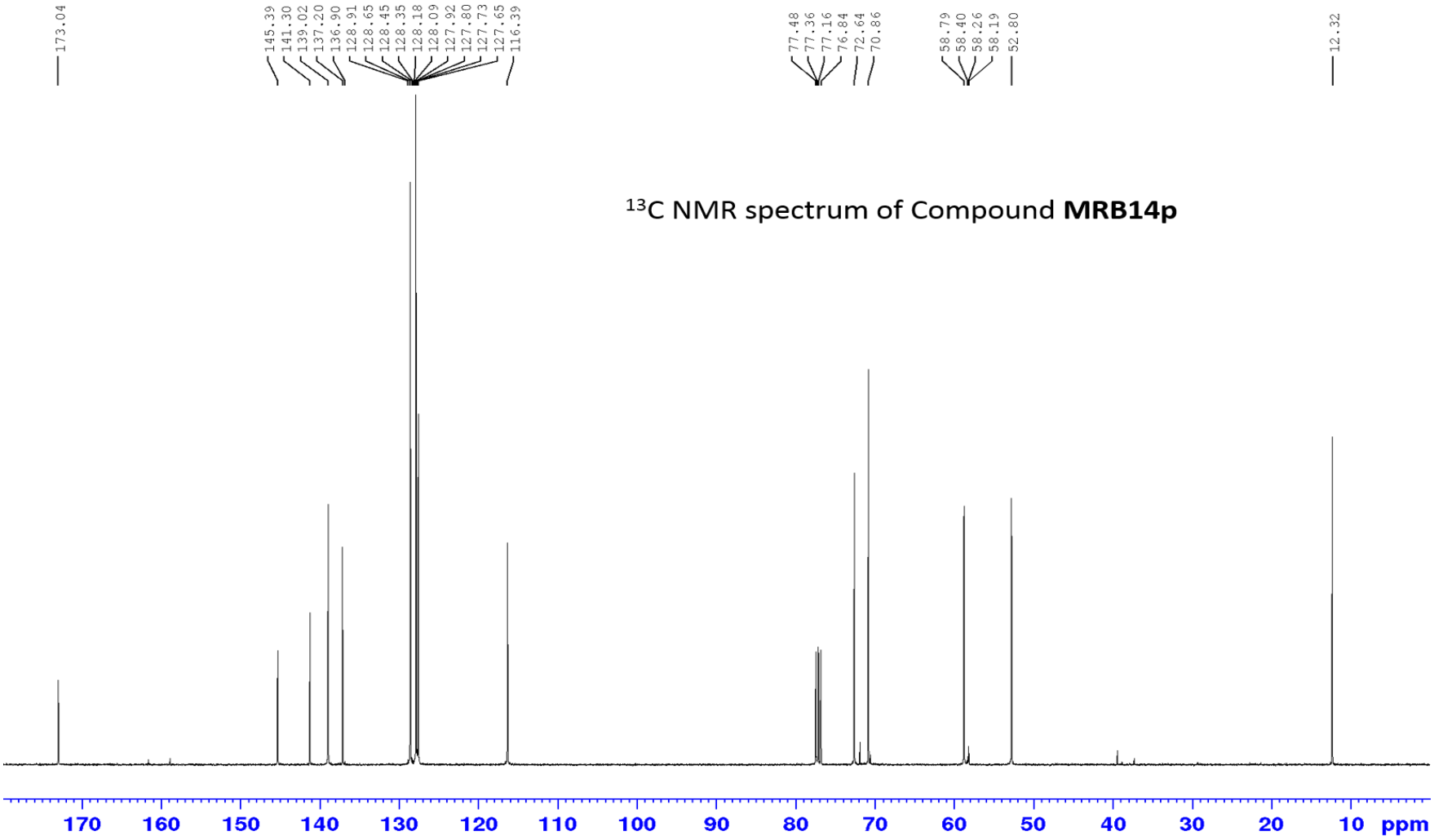

Figure - S12 100.62 MHz ^{13}C spectrum of compound **MRB14p.**

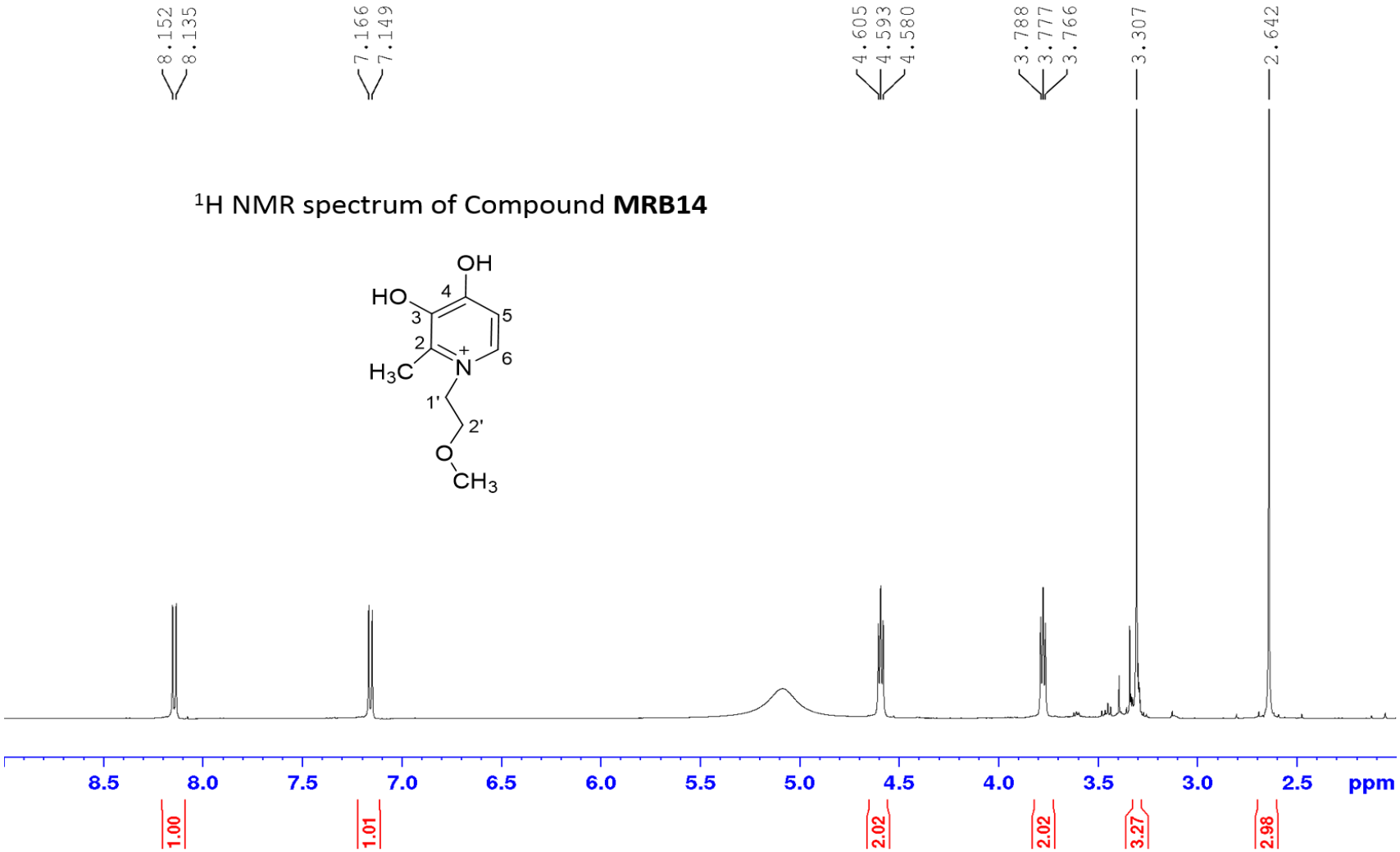

Figure - S13 400.15 MHz ^{1}H spectrum of compound **MRB14**.

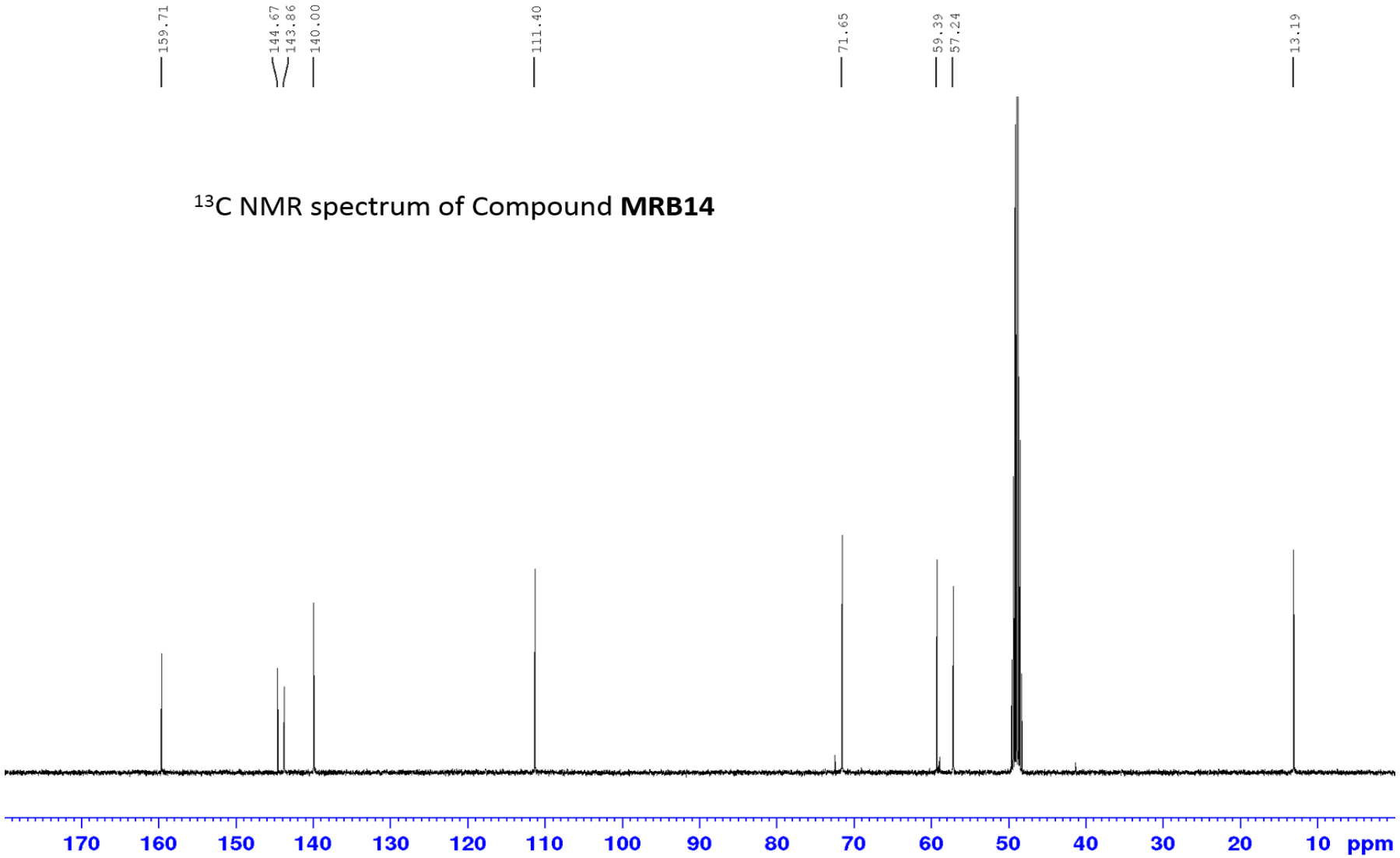

Figure - S14 100.62 MHz ^{13}C spectrum of compound **MRB14.**

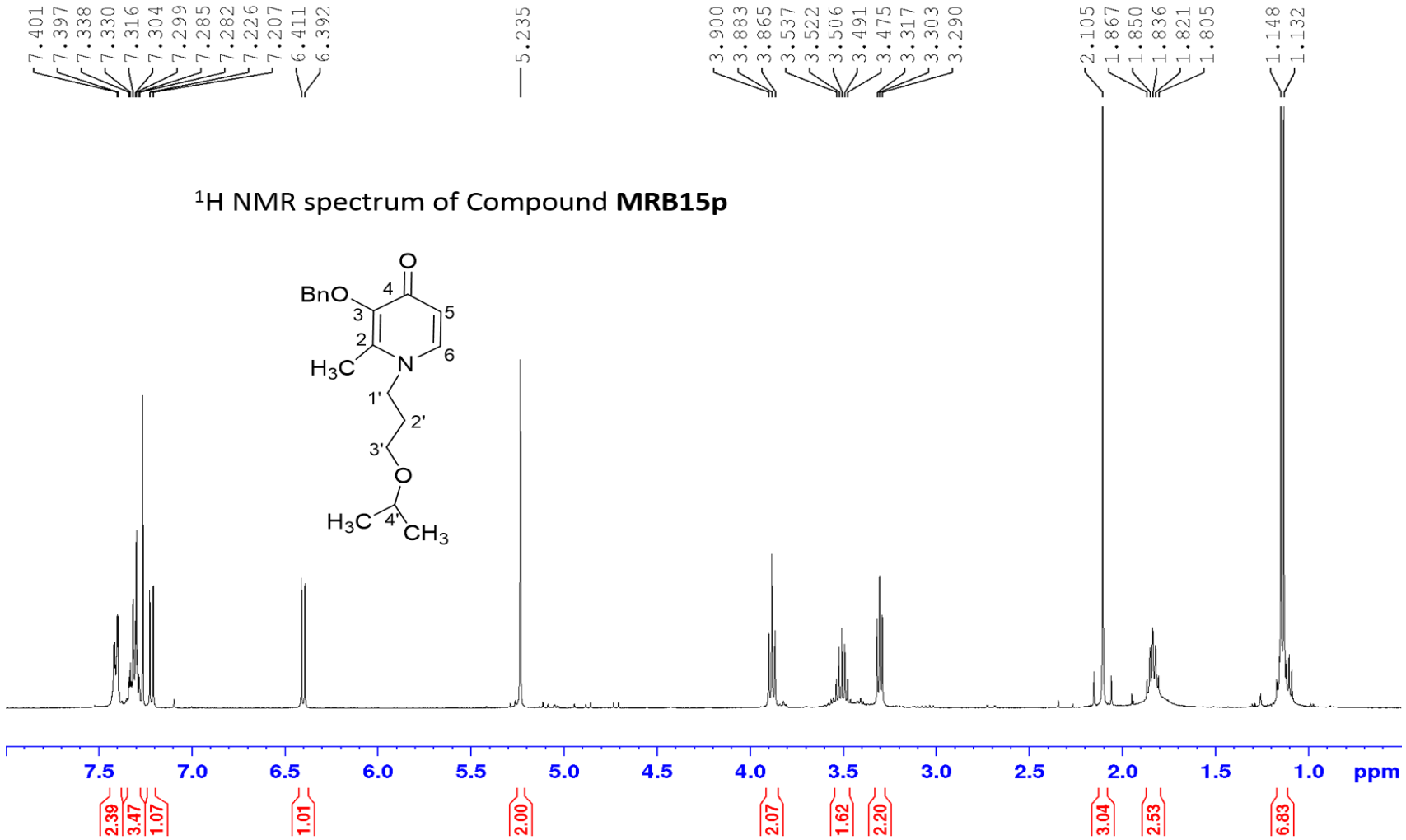

Figure - S15 400.15 MHz ^{1}H spectrum of compound **MRB15p**.

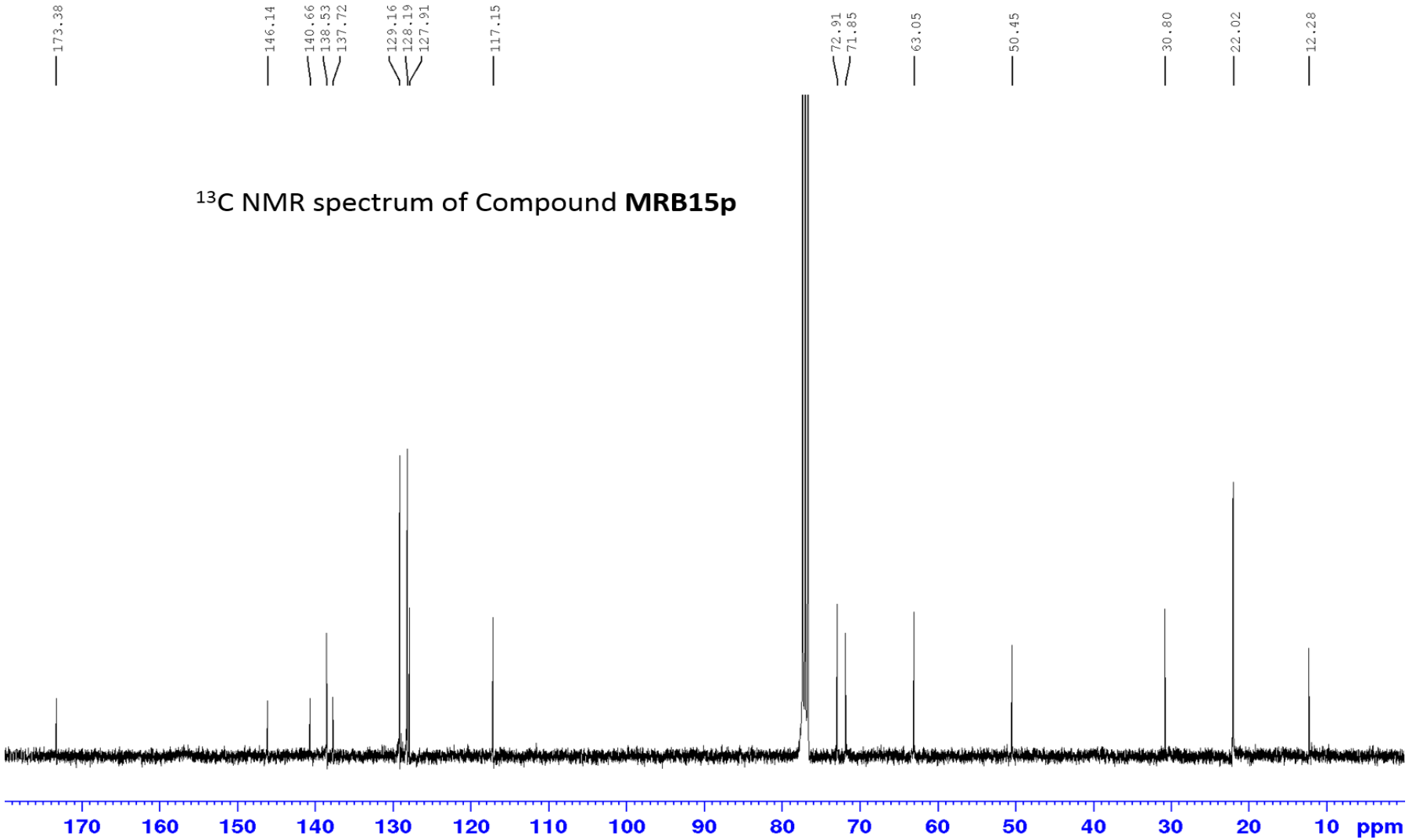

Figure - S16 100.62 MHz ^{13}C spectrum of compound **MRB15p.**

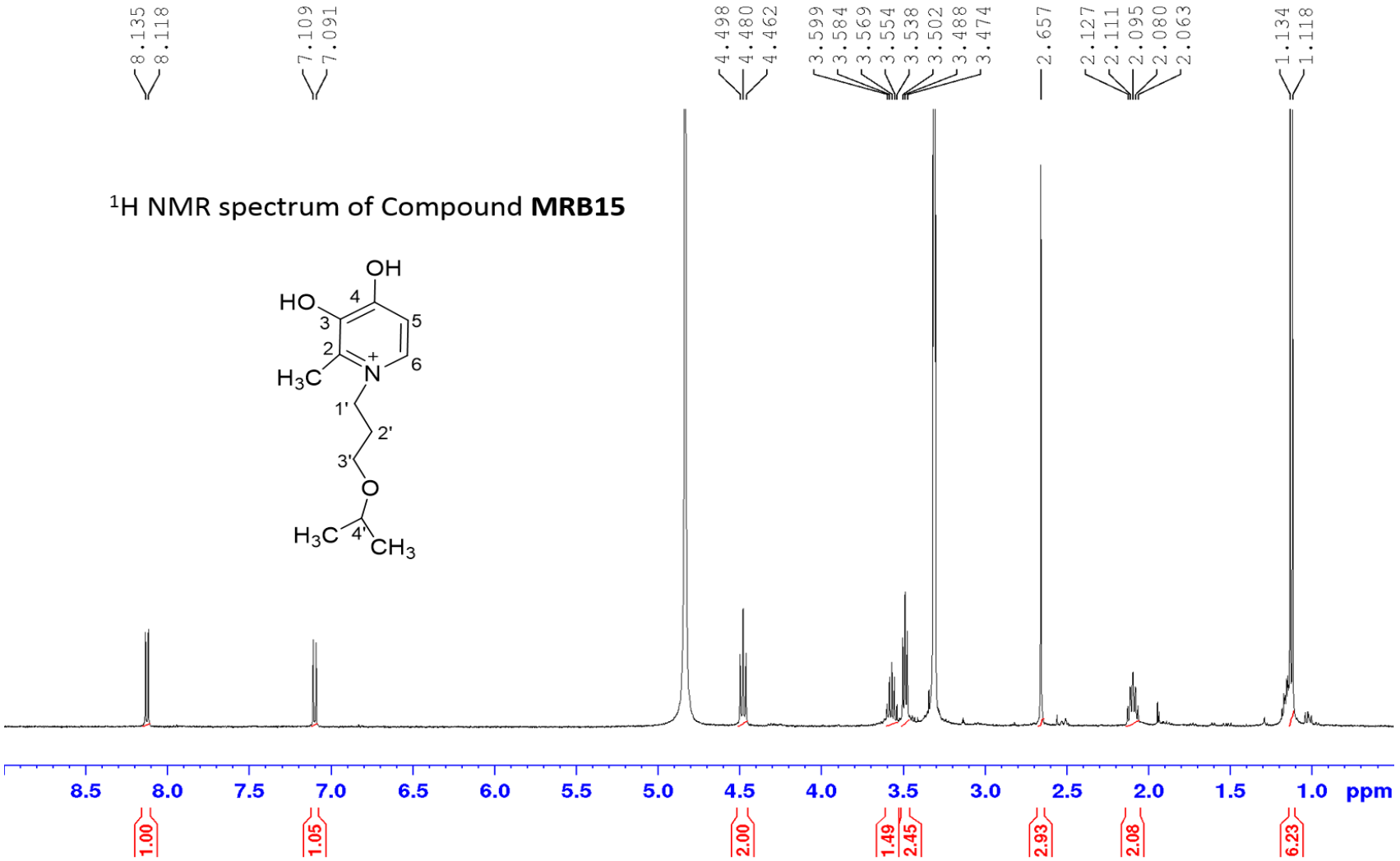

Figure - S17 400.15 MHz ^{1}H spectrum of compound **MRB15**.

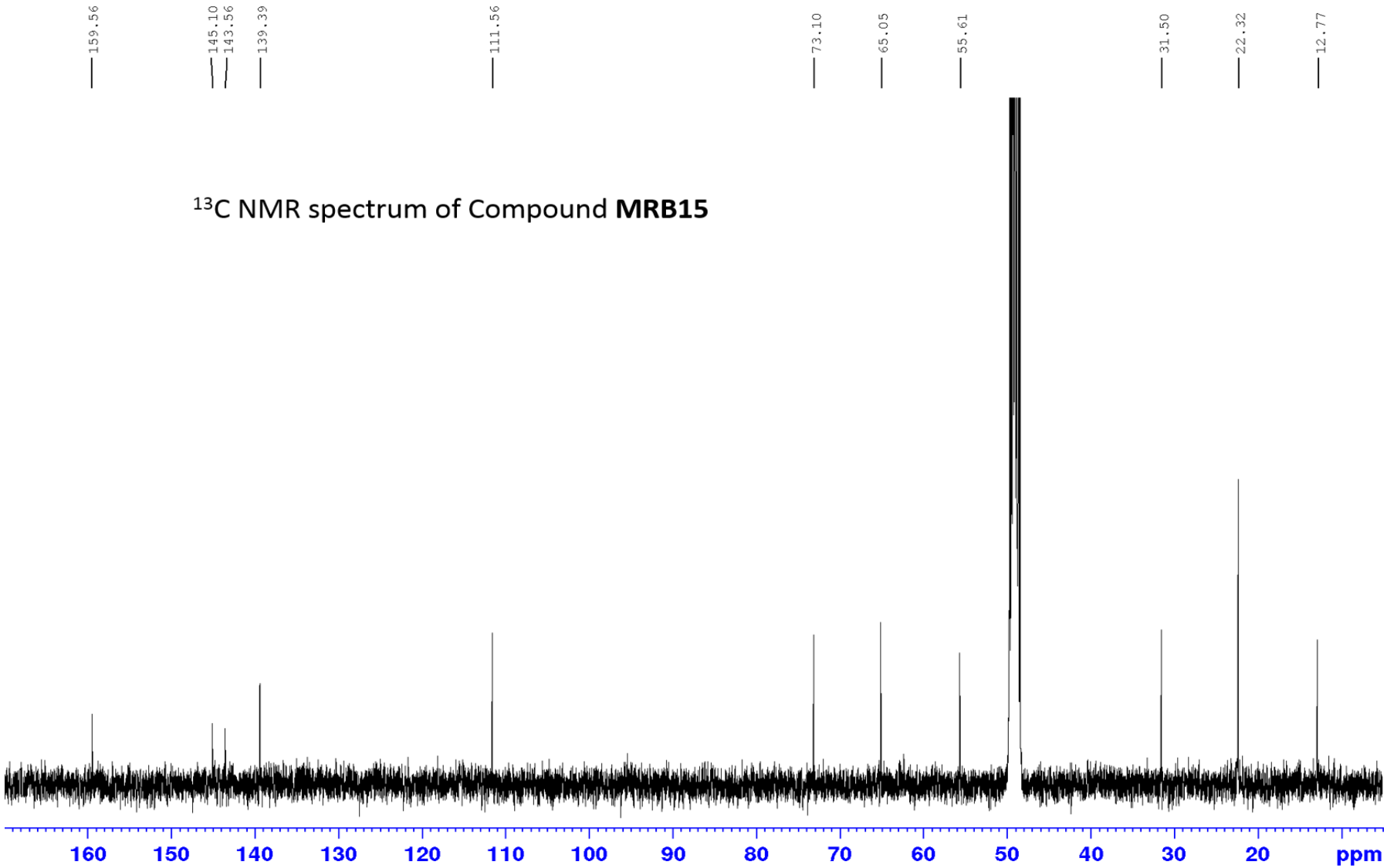

Figure - S18 100.62 MHz ^{13}C spectrum of compound **MRB15.**

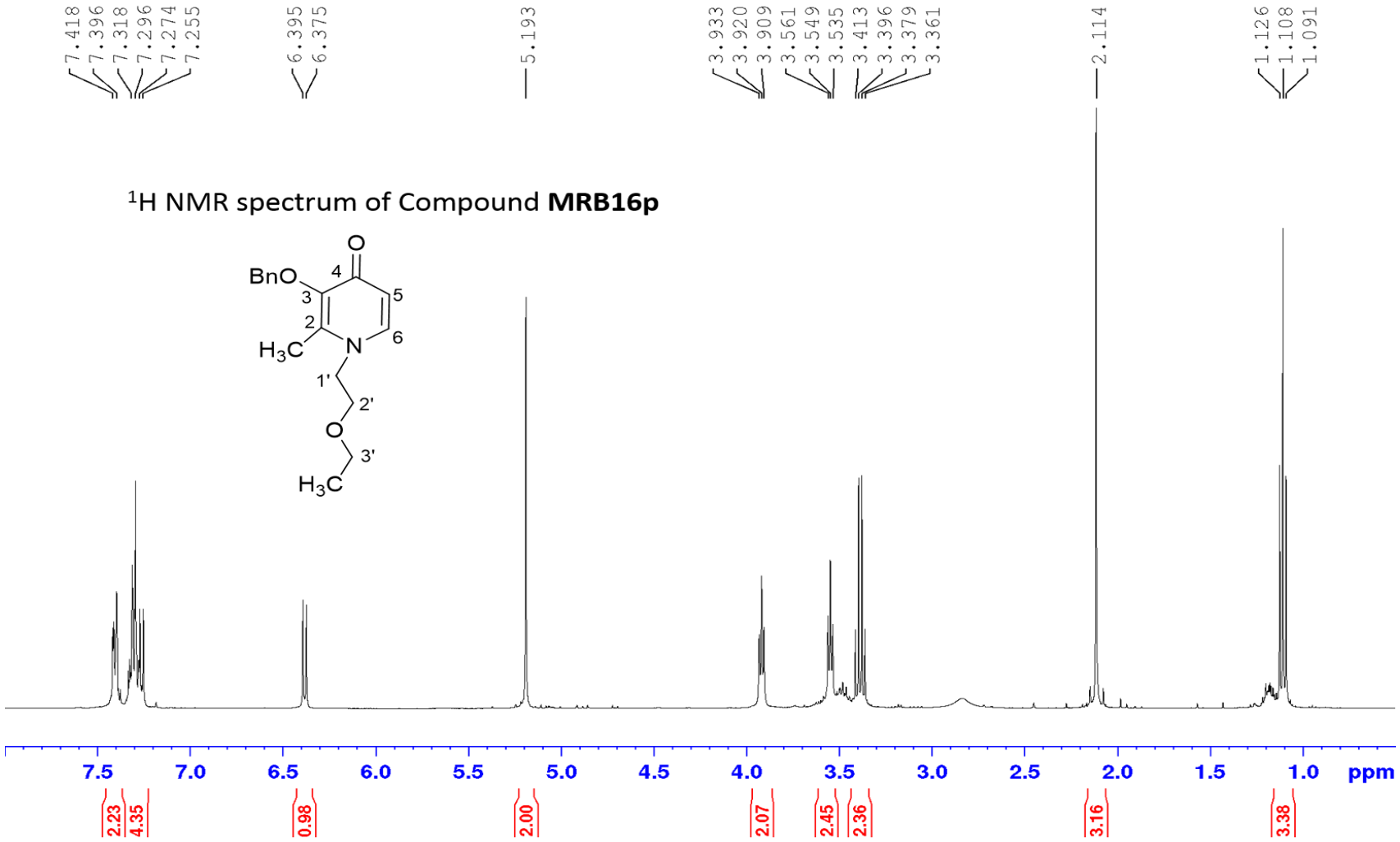

Figure -- S19 400.15 MHz ^{1}H spectrum of compound **MRB16p**.

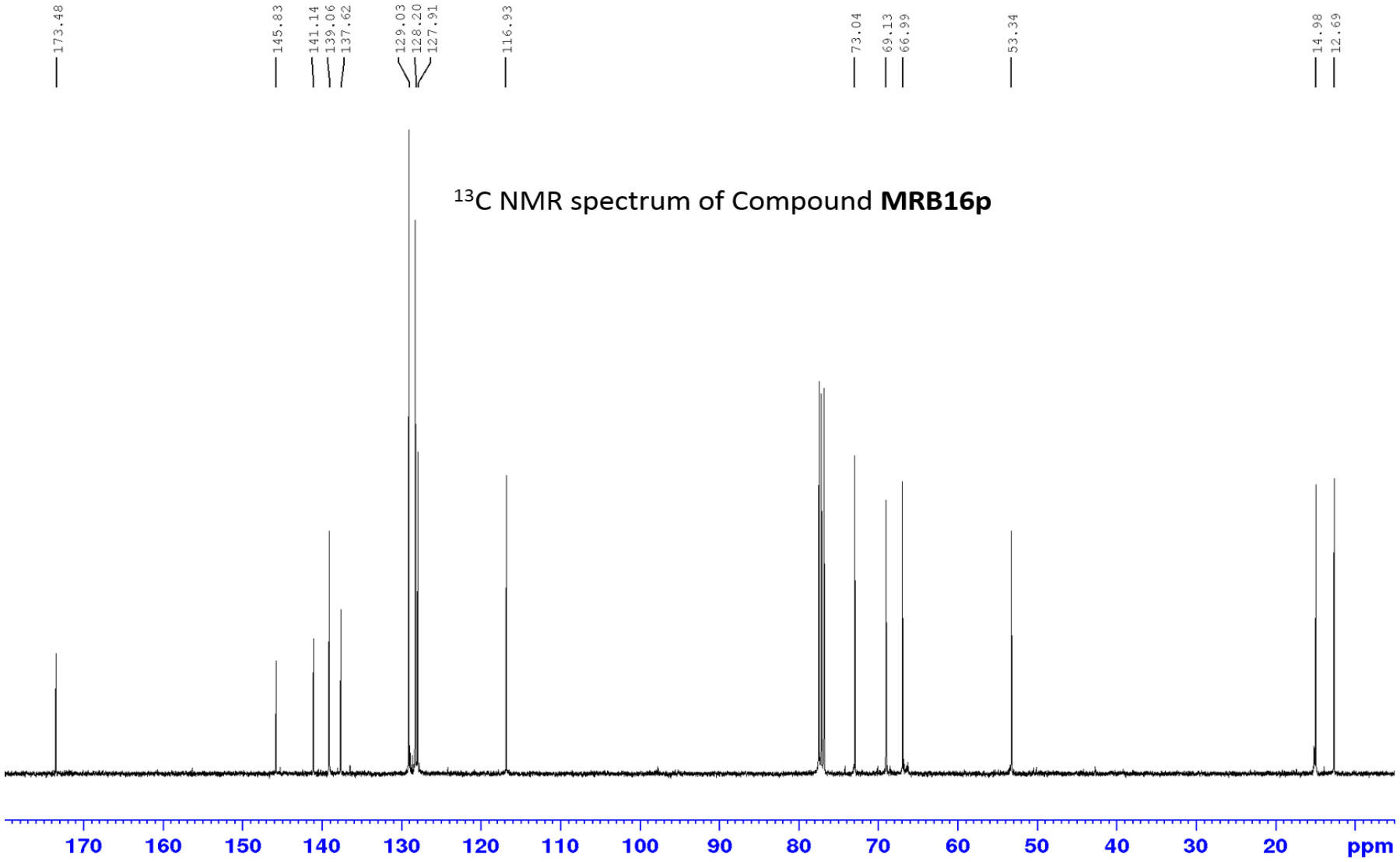

Figure - S20 100.62 MHz ^{13}C spectrum of compound **MRB16p.**

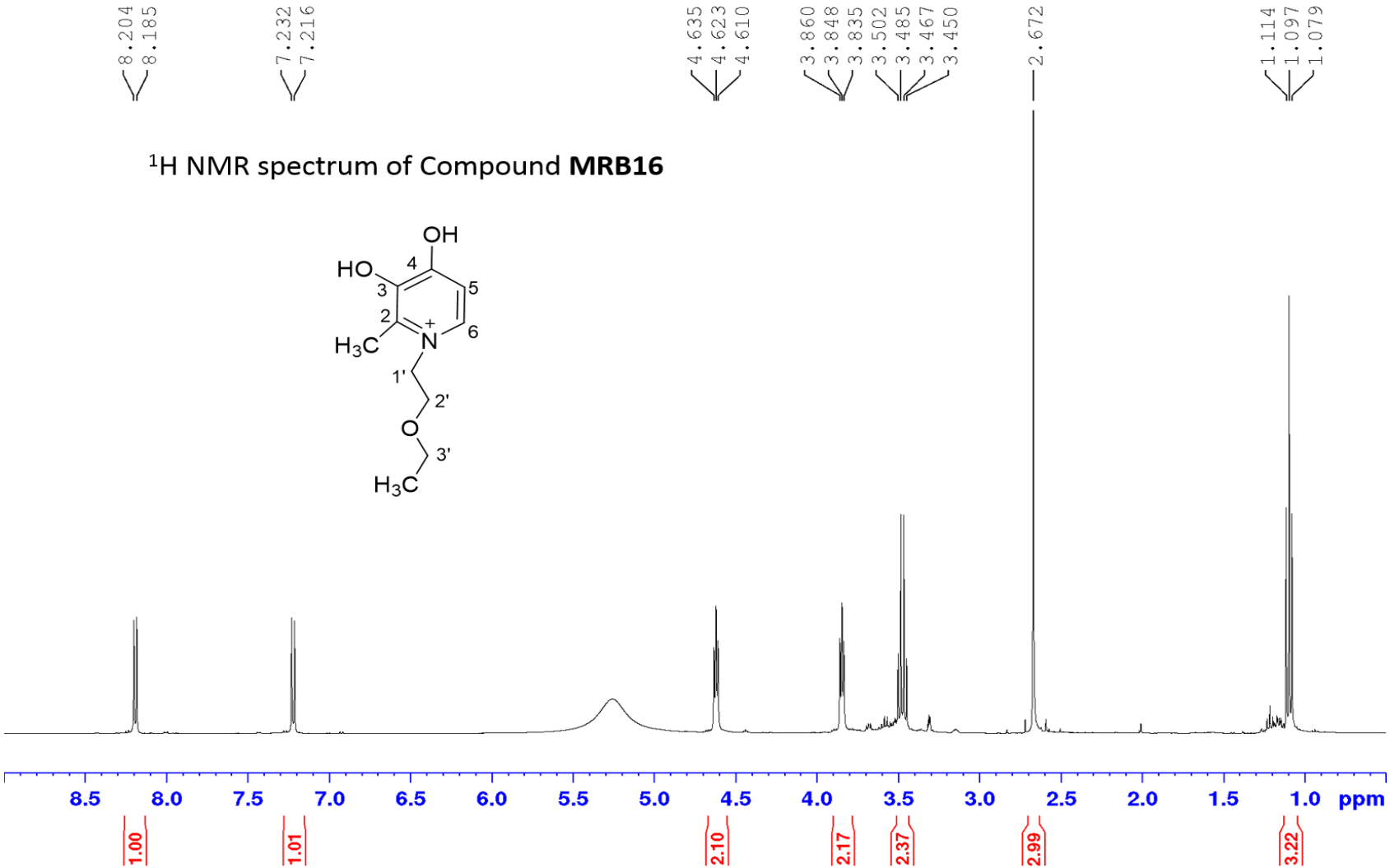

Figure - S21 400.15 MHz ^{1}H spectrum of compound **MRB16**.

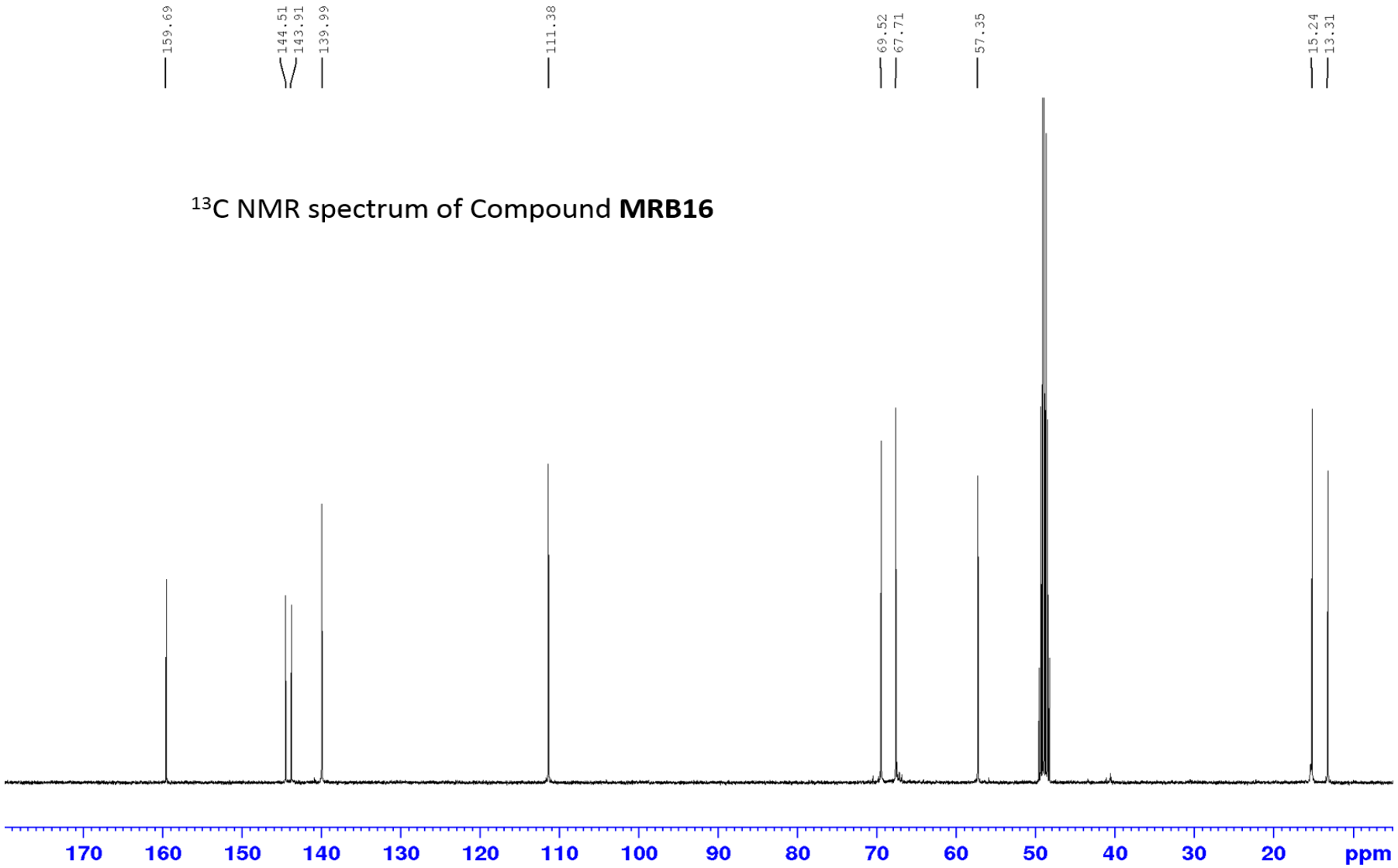

Figure - S22 100.62 MHz ^{13}C spectrum of compound **MRB16.**

NMR spectroscopy discussion for compounds MRB14-MRB16 (protected and deprotected forms)

In the NMR spectra of ligand **MRB14p**, the aliphatic signals at 3.49 and 3.92 ppm were assigned as protons H2' and H1', respectively and C2' and C1' appear at 70.9 and 52.8 ppm. The resonance signal of -OC$\underline{H}_3$ group appears at 3.24 ppm and the related carbon (-O$\underline{C}H_3$) appears at 58.8 ppm and shows HSQC correlation. Carbon C1' has also shown long range HMBC correlation with protons H6 and H2', allowing the assignment performed. After the deprotection (**MRB14)** significantly differences in the ^{1}H and ^{13}C spectra were also noticed, as described above for **MRB13**. In a similar mode, the peak of H1' protons varied from 3.92 to 4.59 ppm and signal of H2' protons shifted from 3.49 to 3.78 ppm. In the carbon spectra, the signal of C1'shifted from 52.8 to 57.2 ppm, respectively in protected and deprotected forms. The signal at 57.2 ppm exhibited HMBC correlation with H6 and H2' and was attributed to C1' while the signal 71.6 ppm was assigned as carbon C2' due to its correlations with H1' and O-C$\underline{H}_3$.

The characteristic aliphatic signal of ligand **MRB15p** appears in the NMR spectra at 1.14 ppm corresponds to both -CH_3 groups attached to terminal carbon of the amine chain. The quintet at 1.83 ppm was attributed to the proton H2' and exhibited correlation in the HMBC spectra with carbons C1' and C3', respectively at 50.5 and 63.1 ppm. The triplets at 3.30 and 3.89 ppm were assigned as protons H3'and H1', respectively, and the signal at 3.51 ppm corresponds to -CH proton of carbon C4' which appears at 71.9 ppm in the ^{13}C spectra. This signal presented HMBC correlation with protons H3' and protons of the terminal groups (4'-(C$\underline{H}_3)_2$) allowing the assignment performed. In the spectra of the deprotected form (**MRB15)** the most shifted pick corresponds to H1' proton, which appears after deprotection at 4.48 ppm. Their respective carbon, C1', presents HSQC correlation and is also shifted from 50.5 to 55.6 ppm. Considering HMBC spectrum, the resonance signal at 31.5 ppm was attributed to C2' due to its correlations with H1' and H3' protons. Also, the signal at 73.1 ppm has shown correlations with protons H3' and 4'-(C$\underline{H}_3)_2$ and therefore was attributed as C4' carbon.

Regarding the NMR studies of ligand **MRB16p**, it was possible to register a triplet at 1.11 ppm that corresponds to protons of terminal -CH_3 group (H4') in the amine chain and the quartet at 3.39 was

attributed to proton H3'. Their respective carbons, C4' and C3', appear at 15.0 and 67.0 ppm, respectively. The signals at 3.55 and 3.92 ppm refers to the other protons of -CH_2 groups in the chain, H2' and H1', respectively. Carbon C1' (53.3 ppm) exhibited correlation in the HMBC spectra with protons H2' and H6, and carbon C2' (69.1 ppm) presented correlation in the HMBC spectra with protons H1' and H3'. Upon the deprotection (**MRB16)**, again several differences in the spectra confirmed the success of the reaction. Some relevant deviations in the chemical shift of the protons of ligand in the protected *vs* the deprotected forms were verified as for protons H2' and H1', which varied from 3.55 and 3.92 to 3.85 and 4.62 ppm, respectively. The signal of carbon C1', also moved from 53.3 to 57.3 ppm. This signal was attributed to C1' due to the HMBC correlation with H6 and H2' protons. The pick at 67.7 ppm was attributed as carbon C3' as it has shown HMBC correlations with H2' and H4'.

Chapter 6

A new approach for NTBI determination in blood serum using microsequential injection solid phase spectrometry

A new approach for NTBI determination in blood serum using microsequential injection solid phase spectrometry

In this chapter, a micro sequential injection lab-on-valve (μSI-LOV) method in a solid phase spectrophotometry (SPS) mode was developed for the quantification of non-transferrin-bound iron (NTBI), using a bidentate 3,4–hydroxypyridinone (3,4-HPO) ligand anchored to sepharose beads as a chromogenic reagent. To attain SPS, elimination of the sample matrix and retention of the analyte (iron(III)), a packed functionalized beads column directly in the flow cell was used. The dynamic concentration range was 1.62 – 7.16 μmol/L of iron(III), with a limit of detection of 0.49 μmol/L and limit of quantification 1.62 μmol/L. The proposed μSI-LOV-SPS method was a contribution to the development of an automatic method for the quantification of the NTBI in serum samples.

Keywords: bidentate 3,4-hydroxypyridinone ligand; iron(III) quantification; solid phase spectrophotometry; functionalized beads; NTBI; serum samples

6.1. Introduction

Iron is an essential metal in the body, for its role in oxygen transport and participation in redox reactions (1). Intestinal absorption is the main step for body iron homeostasis, as there is low iron excretion (2). When iron intake is higher than iron requirements, there is free, unbound iron, precipitating or damaging the cellular environment. The iron overload causes organ damage through free radical production (3) and is developed when the mechanisms responsible for regulating the iron absorption are altered (genetic mutations, ineffective erythropoiesis) or bypassed (red blood cell transfusion, intravenous iron application) (4).
Non-transferrin-bound iron (NTBI) occurs when iron influx into the plasma compartment exceeds iron efflux (5). The term NTBI denotes the forms of iron in serum that are bound to ligands other than transferrin (a carrier protein, responsible for the extracellular transport of iron within the body). This “free” iron can be bound to serum albumin, citrate and other undefined negatively charged ligands (6). Several clinical stages of NTBI have been reported, such as in cases of thalassemia, hemochromatosis and in patients receiving chemotherapy (7). Hemochromatosis is a high prevalence disease in the population (8,9), so it is important to have methods that can quantify the NTBI. Being able to determine the NTBI value is important to understand different pathophysiological conditions but can also be potentially useful in the management of iron-overloaded patients (5).
NTBI is normally present at concentrations up to 10 µmol/L (10). The methods already developed for the NTBI quantification present several potential problems (11); the most common method for the determination employs nitrilotriacetic acid as a ligand, chelating NTBI, followed by ultrafiltration, that could lead to false positive errors (7,10,12). NTBI determination results showed that the amount of quantified iron differed widely between these methods. So, an accurate determination of serum NTBI is difficult to attain employing the available methods (11).

Chelators such as 3-hydroxy-4-pyridinones (3,4–HPO) have been used as chelator therapy in overload iron patients (13). Additionally, these ligands have been recently reported as a ”more sustainable” alternative as chromogenic and selective reagents to quantify iron in flow analysis techniques (14–17).

Aiming for the development of a method for the determination of the NTBI in serum samples, with sample volume limitation, the micro sequential injection platform could be an effective tool. The micro sequential injection lab-on-valve (µSI-LOV) system (18) was designed to integrate all the necessary sample pre-treatment processes and detection at the selection valve. The configuration and small dimensions of the conduits, and the absence of a reactor, minimizes sample and reagents consumption. Moreover, the multipurpose flow cell associated with an additional driving device, provides the possibility of handling solid particles, such as beads (19,20). The combination

of miniaturization, programmable flow and possibility to handle solid particles, makes this platform a potential privileged tool for NTBI determination with a good repeatability (21).

The determination of the NTBI can be a challenge due to the limited amount of serum sample available and for the different forms of “free” iron. Normally, this type of iron is bound to ligands such as serum albumin and citrate. To quantify this complexed iron, it is necessary to displace it from these ligands. Nevertheless, it is still necessary to ensure the transferrin-bound iron stability. To achieve this objective, in this work a μSI-LOV system comprising sepharose beads functionalized with a 3,4–HPO ligand as a reusable sorbent, is proposed for the NTBI quantification. In these conditions, NTBI is retained in the functionalized beads, with colour formation and detection occurring directly at the solid particles surface; then, the beads are washed and conditioned so that they can be reused in the following cycle. As far as we know, this is the first flow-based method for the NTBI determination.

6.2. Experimental

6.2.1. Reagents and solutions

All the solutions were prepared with analytical grade chemicals and Milli-Q water (resistivity 18 MΩ cm, Millipore, Bedford, MA, USA).

A commercially available 0.9% NaCl Labesfal (9 mg/mL, Fresenius Kabi - Laboratórios Almiro, Portugal) was used.

A synthetic serum base solution was prepared by dissolving 1.156 g of MOPS sodium salt (titration ≥99.5%, Sigma-Aldrich, Germany) in 500 mL of 0.9% NaCl solution to final concentration of 0.01 mol/L of MOPS. The solution was adjusted to pH of 7.4 using HCl.

A 5 mmol/L citrate stock solution of sodium citrate dihydrated was prepared by dissolving 0.029 g in 20 mL of Milli-Q water.

A synthetic serum base solution with citrate was obtained by the dilution of the citrate stock solution (5 mM) to a concentration of 100 µmol/L in a synthetic serum base solution.

A synthetic serum base solution with citrate and albumin, was prepared with 20 g/L of Bovine Serum Albumin (BSA) (98%, Sigma-Aldrich, Germany), in synthetic serum base solution with citrate. For a final volume of 20 mL, 0.40 g of BSA was dissolved in synthetic serum base solution with citrate.

An iron(III) stock solution of 10.0 mg/L (0.18 mmol/L) was obtained by dilution of the atomic absorption standard of 1000 mg/L (Fluka, Germany).

An intermediate solution of 1.0 mg/L (0.018 mmol/L) of iron(III) was prepared and left overnight before use, by appropriate dilution of the 10.0 mg/L (0.18 mmol/L) stock solution in the different synthetic serum solutions. The iron(III) working standards were prepared in the range of: 0.025 – 0.40 mg/L (0.45 – 7.2 µmol/L) with the different synthetic serum solutions.

A 1 mol/L nitric acid solution was prepared from a suitable dilution of a 5 mol/L solution, prepared from the concentrated acid (d = 1.4; 65%, Merck, Germany).

6.2.2 Functionalized beads

The functionalized beads consisted in a 3-hydroxy-4-pyridinone (3,4–HPO) ligand, anchored to sepharose beads, with a bead diameter of 70-150 µm. This material was prepared by a group from Requimte, Universidade do Porto.

A suspension of 0.125 g of functionalized beads in 3 mL of Milli-Q water was used for the packing column process.

6.2.3. Sequential injection manifold and procedure

The micro sequential injection lab-on-valve solid phase spectrometry (μSI-LOV-SPS) manifold for iron determination using the 3,4-HPO functionalized beads is presented in Figure 6.1.

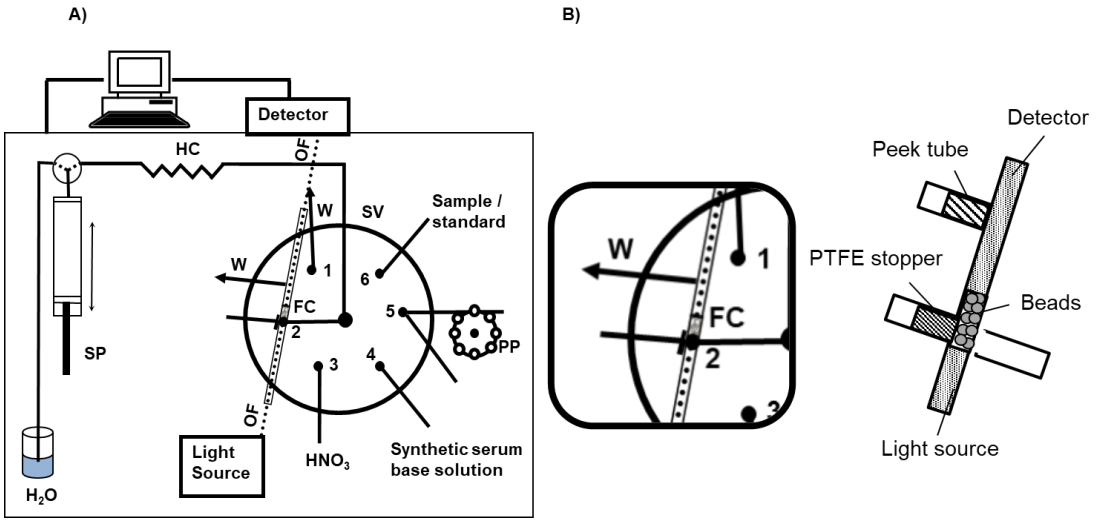

Figure - 6.2 The micro sequential injection lab-on-valve solid phase spectrometry (μSI-LOV-SPS) manifold: **A)** SP, 2.5 mL syringe pump; HC, holding coil, 3 m; FC, 3 mm optical path flow cell packed with functionalized beads; OF, optical fibers; SV, 6 port selection valve; W, waste; HNO_3, 1.0 mol/L nitric acid; Synthetic serum base solution, 0.1 mol/L MOPS and 0.50 mol/L NaCl solution, pH 7.4; PP, peristaltic pump and **B)** flow cell (FC) detail, functionalized beads packed between the two optical fibers.

The μSI-LOV consisted of a FIAlab – 3500 (FIAlab Instruments) equipped with a bi-directional syringe pump (2.5 mL of volume), a holding coil (3 m) and a lab-on-valve head mounted on the top of a six-port selection valve. The detection system comprised a USB 2000 Ocean Optics CCD spectrophotometer, a couple of optical fibers (FIA-P400-SR,400 μm) and a Mikropack DH-2000-BAL deuterium halogen light source. The FIAlab for Windows 5.0 software running on a personal computer (HP Compaq) was used for flow programming and data acquisition.

For the functionalized beads column packing, a peristaltic pump was used as an auxiliary propulsion device to circulate the beads suspension. The beads were injected and packed between the two optical fibers, 3 mm optical path (Figure 6.1, B). To prevent beads loss, a PEEK tube (in the exit port), with inner diameter of 0.06 mm (♯1535 Upchurch scientific) was used, combined with a PTFE stopper, aligned with the central channel (Figure 6.1, B). For the connection of the different components of the flow system it was used tubs of polytetrafluoroethylene (PTFE) with 0.8 mm inner diameter, including a 3 m of holding coil.

The iron(III) determination followed the sequence protocol detailed in Table 6.1.

Table - 6.1 Protocol sequence for the developed micro sequential injection lab-on-valve with SPS method for the NTBI quantification, using functionalized beads with a 3,4-HPO ligand as a colorimetric reagent.

Step	SV position	Flow rate (µL/s)	Volume (µL)	Description
A	-	200	1000	Fill the syringe with carrier
B	4	200	750	Aspiration of synthetic serum base solution
C	6	200	250	Aspiration of sample/standard
D	2	5	170	Propelling to detector and start absorbance measurement
E	2	-	-	Stop propelling 20 seconds
F	2	5	1080	Propelling to detector
G	3	200	500	Stop absorbance measurement and aspiration of nitric acid 1 M
H	2	10	1000	Propelling through the column for analyte removal
I	4	200	250	Aspiration of synthetic serum base solution
J	2	10	500	Propelling through the column for conditioning
K	2	-	-	Reference scan

The initial step consisted of filling the syringe pump to about half capacity (step A). Then, the synthetic serum base solution and the sample/standard were aspirated into the holding coil (steps B and C). The propelling of these plugs through the flow cell comprising the packed functionalized beads column was made in three steps. First, the standard/sample volume was propelled to provide iron(III) retention in the functionalized beads and start the absorbance measurement (step D). Then, a stop period of 20 seconds was made (step E) to promote the complex formation. Finally, the synthetic serum base solution was propelled through the column to ensure the washing of the column (step F). This washing step consisted of propelling a plug of synthetic serum base solution, threefold the sample/standard volume, enabling to wash out the matrix proteins and minimizing interferences. For the analyte removal step, the absorbance measurement was stopped, and a nitric acid solution was aspirated and sent through the functionalized beads column to elute the iron(III) (steps G and H). Finally, a synthetic serum base solution plug was aspirated and sent through the column, conditioning and preparing it for the next cycle (steps I and J). Before starting the following cycle, a reference scan step was accomplished (step K).

6.2.4. Sample collection, preparation and accuracy assessment

Samples were provided by a partner group from Requimte, Universidade do Porto. Blind blood samples were collected without anticoagulant. Serum was separated after clotting, by centrifuging the blood at 3000 rpm, for 30 min. Afterwards, the serum was decanted and immediately frozen at -80ºC, for storage until required (10,12).

Serum samples were analysed using the developed μSI-LOV method and the results compared with those obtained by the method described by Evans *et al*, 2008 (10).

6.3. Results and discussion

This work aimed to be a contribution to the quantification of NTBI in serum samples. The idea was to retain some iron forms in the functionalized beads packed in the flow cell in a solid phase spectrometry (SPS) approach. The iron forms to be retained should mainly correspond to the ones not bound to transferrin, possibly bound to citrate, other proteins, and as “free” iron. Therefore, one of the main challenges was to displace iron from citrate and proteins, with exception of transferrin. At the same time, besides retention, the 3,4-HPO ligand should act as chromogenic reagent and so allow the spectrophotometric measurement at the beads surface.
To study the NTBI determination, a synthetic serum base solution was used as matrix for preparing iron(III) standards. The study of the influence of different iron-complexes forms was achieved by adding citrate and other proteins found in human serum, to this so-called serum base solution.

6.3.1. Preliminary studies

The bidentate ligand 3,4-HPO forms a coloured complex with iron(III) with a stoichiometry of 3:1 as shown in the spectra analysis from previous works (15), with a maximum absorption for the FeL_3 at 460 nm. To minimize the influence of refraction interfaces interference (schlieren effect), the absorbance at 800 nm was measured, and subtracted from the absorbance at the detection wavelength (15).

The quantification of NTBI in blood serum should be necessarily carried out over a limited volume; actually, the sample volume from patients provided to us was around 500 µL. Therefore, the method was designed and studied to cope with such a low volume of sample.
A column of 1.5 mm of functionalized beads was packed in the flow cell and the use of sample volumes in the range of 60 – 250 µL was studied by performing calibration curves in a synthetic serum base solution matrix (0.10 mol/L of NaCl and 0.01 mol/L of MOPS, pH 7.4). The slope increased with the increase of the sample volume up to 250 µL, being this one the chosen sample volume. This allowed to carry out at least two replicas per sample analysis.

6.3.2. Solid phase spectrometry studies

Sepharose based beads (70-150 µm of bead diameter) functionalized with a bidentade 3,4-HPO ligand were used as sorbents.

6.3.2.1. Length of beads column – optical pathlength

The bead column was obtained by packing the functionalized beads between the two optical fibres, with a suspension of 0.125 g functionalized beads in 3 mL of Milli-Q water. This solid phase suspension was propelled until packing a column in the flow cell. The properties of the beads enabled sufficient transparency to set the baseline using the reference scan. Different column lengths were studied, and calibration curves in a synthetic serum base solution matrix (0.10 mol/L of NaCl and 0.01 mol/L of MOPS, pH 7.4), were established with the different configurations, detailed in Figure 6.2.

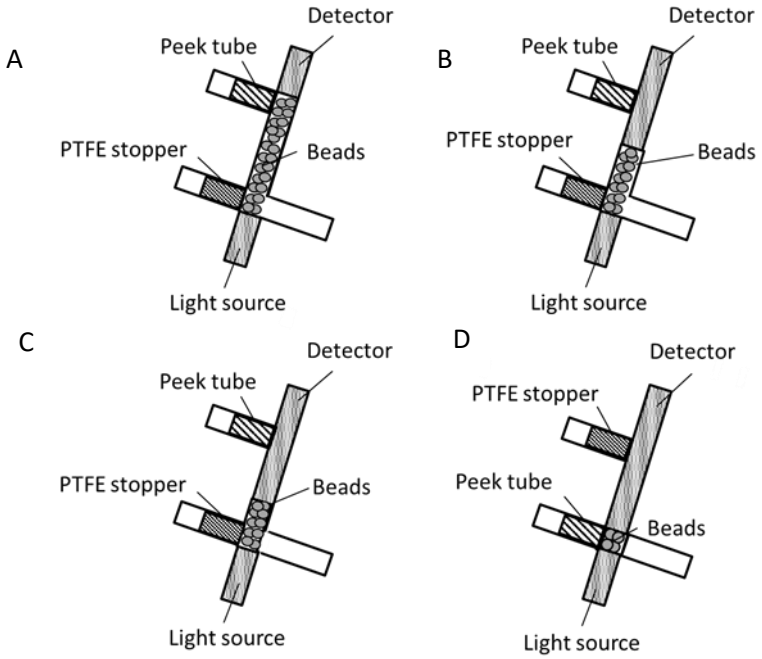

Figure - 6.2 Scheme of functionalized beads packed between the two optical fibres: A) 10 mm, B) 5 mm, C) 3 mm and D) 1.5 mm optical path.

The absorbance measurement was performed directly on the surface of the beads. It was not possible to perform a calibration curve with a column length higher than 3 mm, as the overpacking of the beads blocked the passage of light, not enabling to set the baseline. The optical path/column length chosen was 3 mm, as it was the one that allowed the highest sensitivity and linearity for the determination range of NTBI expected to be found in serum.

The possible influence of the human serum citrate in the NTBI determination, was evaluated. To mimic the average human serum citrate concentration, a final concentration of 100 µmol/L of citrate was added to the standards in a synthetic serum base solution. There was no significant difference

(0.1%) when the slopes of the calibration curves with the two standard matrices solutions (with or without citrate) were compared. Therefore, a final concentration of 100 µmol/L of citrate in the standard matrix solutions was used for further studies.

6.3.2.2. Stoppage time

Considering that the bidentate ligand is anchored to a solid material, there was the possibility of being less accessible for the complex formation and consequently demand a higher complex formation time. So, the addition of a stop period during the signal acquisition was tested. The influence of two stop periods of 10 and 20 seconds were studied; standards in a synthetic serum base solution with citrate were used. The 20 seconds stop propulsion period was selected as it resulted in a two-fold increase in the sensitivity. Longer stop periods were not studied to avoid a significant decrease in the determination rate. Instead, the flow rate of propelling the sample/standard through the column during the determination step was studied. A flow rate of 5 µL/s (the lowest flow rate possible for the µSI-LOV system) was compared with the 10 µL/s rate used initially. The lowest flow rate (5 µL/s) provided the best sensitivity (increase of 21%).

6.3.2.3 Analyte removal

In terms of reagent volume consumption, in principle the immobilization of the reagent in a solid material is advantageous over its use in solution. However, the regeneration of the column before another analytical cycle must be performed. The column regeneration consists in the removal of the analyte complexed with the ligand in the beads surface. This could be performed by using a nitric acid solution. So, the study of the influence of the acid concentration was performed using three different concentrations: 0.5, 1.0 and 1.5 mol/L of nitric acid (Figure 6.3). For this study, iron(III) standards in a synthetic serum base solution with citrate were used.

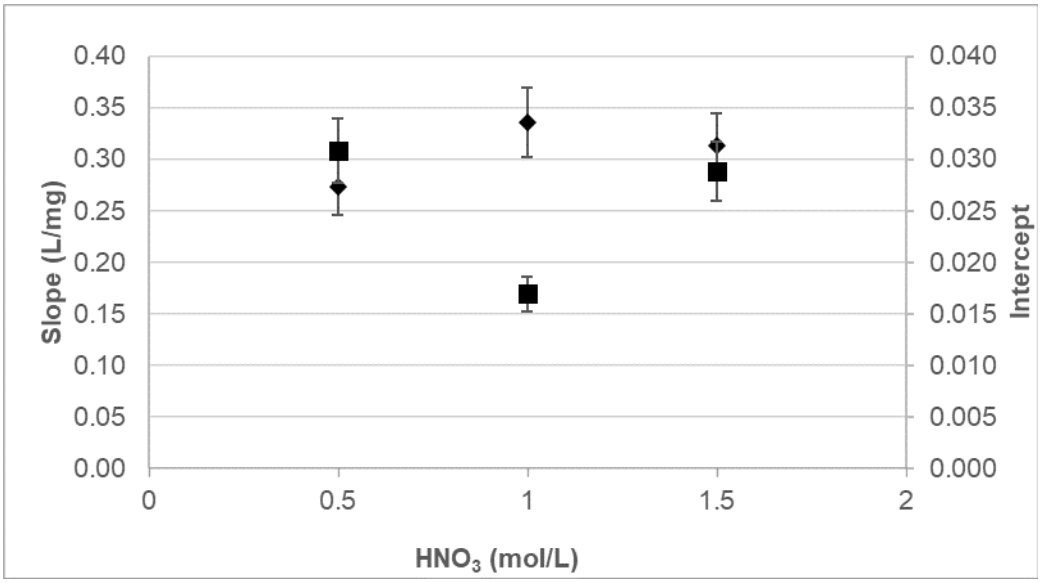

Figure - 6.3 Study of the influence of the HNO_3 concentration in the analyte removal from the functionalized beads on the analytical curve slope (■) and intercept (▲).

The use of a 1.0 mol/L concentration led to a higher slope and lower intercept value (Figure 6.3). Therefore, this concentration was chosen, as the minimum concentration that allowed an efficient cleaning of beads within the standards concentration range. In fact, for the 0.5 mol/L of nitric acid solution, it was observed that, for higher iron concentrations, the analyte removal was not effective, as there was still visible color in the column from the iron(III) – 3,4-HPO ligand complex.

6.3.2.4 Washing and conditioning of the beads

The application of the developed method to the analysis of a complex matrix sample, as human serum, using a solid phase approach, may implicate the undesirable retention of some serum components (like citrate and proteins) on the packed column. So, an efficient column cleaning must be taken into consideration. Additionally, the use of a concentrated acid solution for the analyte removal could lead to the change of pH conditions. To guarantee that the pH conditions are appropriate for the following cycle, a conditioning step should also be considered.

The addition of two plugs, one for washing purposes and another for conditioning, was proposed.

The washing step consisted of including a 250 µL plug of synthetic serum base solution in the determination step, after the sample injection. After the iron removal with nitric acid, a conditioning step was added, consisting of a 250 µL plug of synthetic serum base solution.

To test the efficiency of the inclusion of the different plugs in the sequence method, calibration curves in synthetic serum base solution with citrate were performed (Figure 6.4).

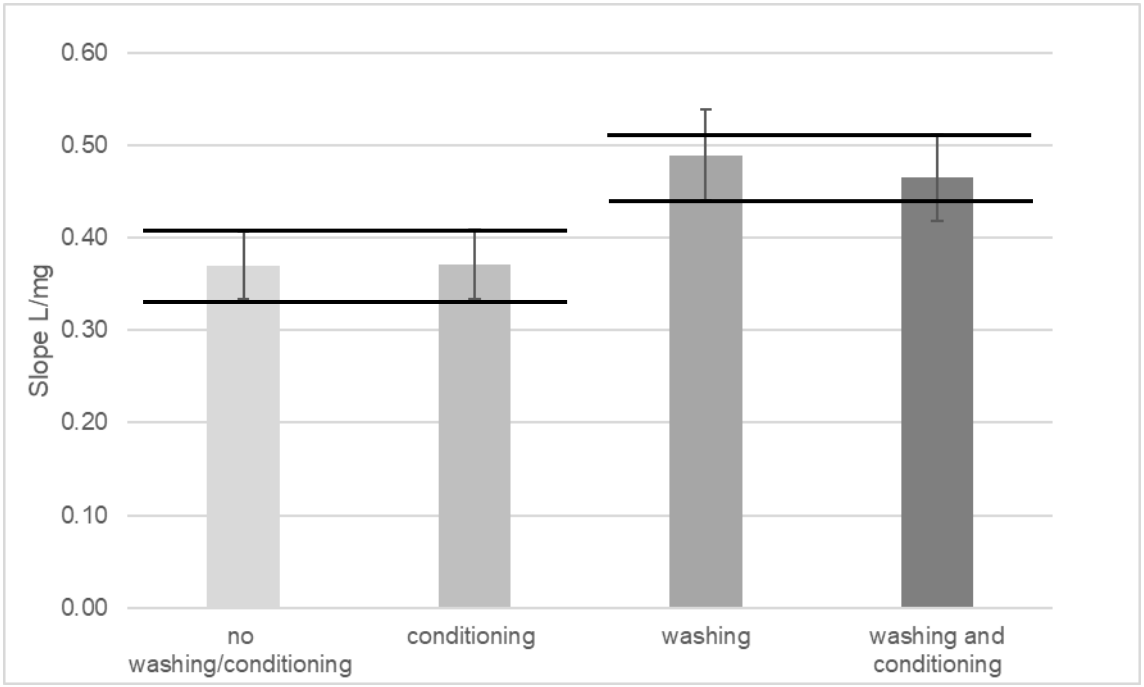

Figure - 6.4 Study of the influence of the different plugs for washing and conditioning the functionalized beads column on sensitivity.

It could be concluded (Figure 6.4) that a washing plug was necessary, but the conditioning plug could be omitted. Therefore, at this point only the use of a washing plug was included to the protocol sequence for the developed method.

6.3.2.5 Test of a renewable sorbent approach

As an alternative to the washing, conditioning, and analyte removal of the functionalized beads steps, the use of a new packed column for each determination was tested. This concept of a renewable approach is called bead injection (BI) (22). To make the packing/removal of the beads easier and avoid excessive sorbent consumption, the optical path was changed to 1.5 mm. Both approaches, with BI and with a reused packed column, were compared by tracing calibration curves with standards in synthetic serum base solution with citrate.
However, the beads diameter was too small, not allowing to remove and clean completely the optical path between determinations. Therefore, the use of a renewable approach was discarded.

6.3.3. Interferences assessment

The interference of the human serum matrix was evaluated. Human serum samples have an ionic strength of around 0.15 mol/L (23,24). Therefore, the previously studied conditions, using a concentration of 0.10 mol/L NaCl for the solutions matrix, was compared to a 0.15 mol/L of NaCl

(commercial sodium chloride 0.9% solution (= 0.15 mol/L of NaCl). Calibration curves using standards in synthetic serum base solution with citrate in both conditions, were compared (Figure 6.5).

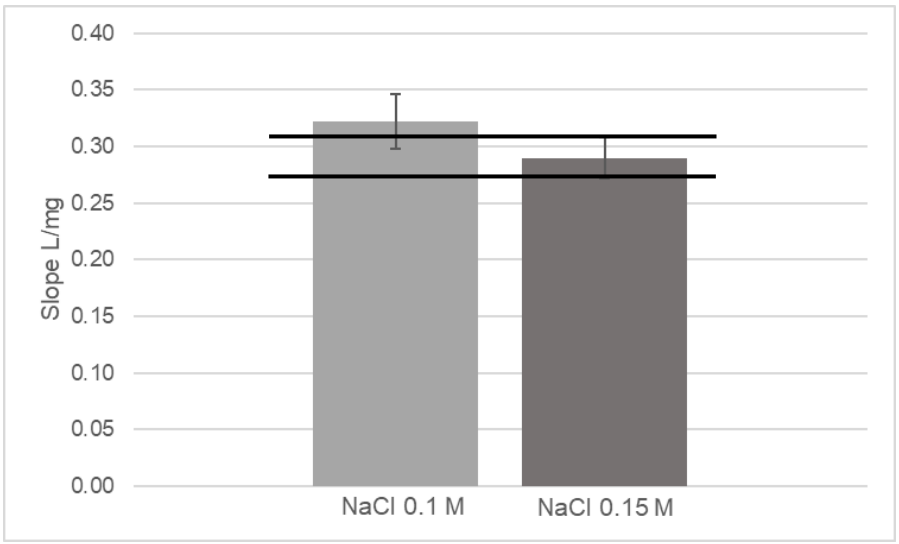

Figure - 6.5 Study of the influence of the ionic strength in the synthetic serum base solution with citrate: comparison between the 0.15 mol/L and the 0.10 mol/L concentration of NaCl.

There was no significant difference (-10%) when calibration curves in both matrices were compared, so the use of the commercial NaCl solution as matrix was set for further experiments.
Aiming to study the potential interference of some of the serum matrix components, solutions with proteins concentrations normally present in human serum (25,26) were tested, as follows.

6.3.3.1 Albumin

An albumin, Bovine Serum Albumin (BSA) (98%, Sigma-Aldrich, Germany), solution was prepared with a concentration corresponding to the average amount present in human serum (40 g/L) (25), in synthetic serum base solution with citrate. For a final volume of 50 mL, 2.0 g of BSA was dissolved in synthetic serum base solution with 100 µmol/L of citrate. Comparing calibration curves with standards in both matrices, with and without the BSA, a decrease of 44 % in the sensitivity was observed when the protein was present. So, this problem had to be tackled by improving washing conditions. Therefore, the volume of the washing plug was increased from 250 to 500 µL, and the results compared (Figure 6.6).

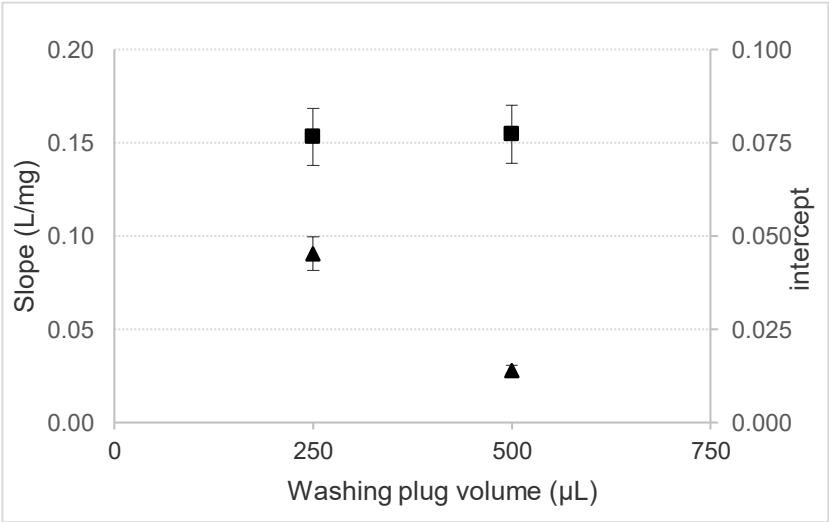

Figure - 6.6 Study of the influence of the volume increase of the washing column step with synthetic serum base solution, on the analytical curve slope (■) and intercept (▲).

The increase of the washing volume led to the decrease of the intercept value (-69%) (Figure 6.6), while the sensitivity was maintained. The 500 µL plug volume allowed a better column washing, and so this was the volume chosen.

6.3.3.2 Serum transferrin

Frequently, patients with “free” iron in serum (with NTBI) present a high saturation percentage of transferrin. This condition can potentially lead to a NTBI determination interference, either by sorption at the beads surface or then part of the iron bound to this protein can be released and affect the determination process,

To study this possibility, a synthetic serum solution containing the average amount of this protein present in human serum (26) was prepared. So, the synthetic serum base with proteins included 2.5 g/L of Human holo-transferrin (≥ 98%, Sigma-Aldrich, Germany) and 40 g/L of Bovine Serum Albumin (BSA) (98%, Sigma-Aldrich, Germany). For a final volume of 20 mL, 50.0 mg of Human Transferrin was dissolved in the synthetic serum base solution with citrate and albumin. Comparing calibration curves with standards in both matrices, synthetic serum without and with saturated transferrin, a decrease of sensitivity of 26% was observed with transferrin. So, further studies were conducted.

6.3.3.2.1 Restudy the washing and conditioning of the beads

The studies on possible interfering constituents of the human serum demanded to restudy the column cleaning and conditioning steps.

Calibration curves in synthetic serum solution with citrate, albumin and transferrin were traced, using two washing plug volumes, 500 and 750 µL. The increase of the washing plug volume led to an increase of 36% in sensitivity, apparently compensating the potential effect of transferrin.

The conditioning plug previously tested and discarded (in section 6.3.2.4), was at this point revisited to recondition the column to a neutral pH; the inclusion of this plug would prevent a pH change after the analyte removal step with an acid solution. This step would also avoid the proteins denaturation and so the possible release of iron from the transferrin. Therefore, the use of a 250 µL conditioning plug was included to the protocol sequence for the developed method.

6.3.3.2.2 Study of the background NaCl concentration in washing and conditioning plugs

To maximize the cleaning of the packed beads, a study of the increase of the NaCl concentration in the washing and conditioning plugs was performed. Four concentrations of NaCl (0.15, 0.20, 0.50, 0.75 mol/L) in the synthetic serum base solution were tested. Calibration curves in synthetic serum base solution with citrate and both serum proteins were used to study the efficiency of the different NaCl concentrations solutions.

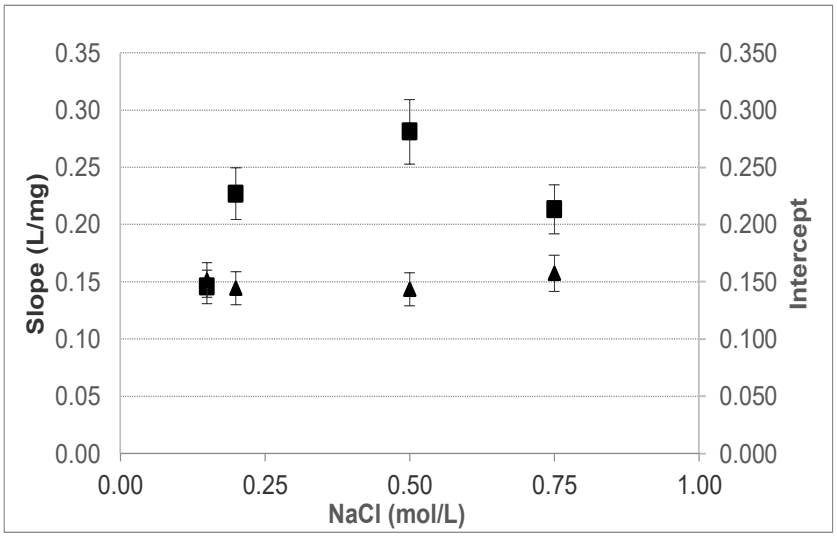

Figure - 6.7 Study of the influence of the NaCl concentration in the washing and conditioning plugs on the analytical curve slope (■) and intercept (▲).

If compared to the previously set NaCl 0.15 mol/L conditions, the sensitivity increased 93% when using a 0.50 mol/L NaCl solution and the intercept did not statistically change (Figure 6.7). This pointed out that the removal of the proteins was more effective for a 0.50 mol/L NaCl solution, and so this concentration was set for further studies.

6.3.4 Accuracy assessment for NTBI determination

The application of the developed method to the NTBI quantification was performed by analysing human serum samples. The limited sample volume was an important aspect to consider. To increase the amount of volume subject to analysis initially available (approximately 500 µL) an option was made to dilute the original sample in synthetic serum base solution with citrate. As such, a final volume of 1 mL would allow to have three replicas per sample analysis.
As the samples were subject to a 1:1 dilution, the composition of the matrix of the standards was adjusted to mimic the sample´s. So, the matrix was set to: for a volume of 20 mL, 0.40 g of BSA was dissolved in synthetic serum base solution with citrate.
The serum samples (kept at-80ºC before used) were defrosted and diluted in synthetic serum base solution with citrate.

The accuracy assessment was carried out by analysing three serum samples with the developed µSI-LOV- SPS method and comparing the results with a NTBI determination method described by Evans *et al*, 2008 (10). The results are presented in Table 6.2.

Table - 6.2 Results obtained with the proposed flow system (µSI-LOV-SPS) and with a comparison method (10) for NTBI determination, for the analysis of three serum samples: RD, relative deviation between the two set of results.

Sample ID	µSI-LOV- SPS [NTBI] (µmol/L)	NTBI conventional method (µmol/L)	RD(%)
#I01	1.26 ± 0.10	1.5	-16%
#I02	7.65± 0.01	5.9	30%
#I018	5.05± 0.57	5.2	-3%

No significant difference was observed for the relative deviation (RD) between the results from both methods for one of the analysed samples, #I018 (RD = -3%). For the other two samples, the relative deviations are relatively high. This could be due to the complexity of the analytical process, and so no definite conclusion can be taken. More analysis should be carried out by both methods.

6.3.5. Figures of merit

To study the characteristics of the developed method, standards prepared in the abovementioned matrix were prepared. The characteristics of the developed method were summarized in Table 6.3.

Table - 6.3 Features of the developed NTBI determination method.

Dynamic range (µmol/L)	**Typical calibration curve[a] A = S x µmol Fe^{3+}/L + b**	**LOD (µmol/L)**	**LOQ (µmol/L)**	**Determination rate (h^{-1})**
1.6 – 7.2	A= 0.013±0.001 x[Fe^{3+}] +0.016 ±0.002 R2= 0.994±0.006	0.5	1.6	7

[a] total of three calibration curves

The limits of detection and quantification, LOD and LOQ, were calculated according to IUPAC recommendations (27) as the concentration corresponding to the average of the blank signal (n=10) plus three (LOD) and ten (LOQ) times its standard deviation. The determination rate was calculated as the time spent per analytical cycle, consisting of the sum of the time needed for each step plus the time necessary for the port selection in the selection valve. One calibration curve took about 1 hour and 40 minutes.

6.4. Conclusions

The use of a microsequential injection lab-on-valve system with a solid phase spectrophotometry approach proved to be an important contribution to the development of an automatic method for the NTBI determination. As far as we know, this is the first flow-based method for NTBI determination, and presents advantages over previously described methods (7,10,28), which are based on manual batch procedures, subject to more operators influence and much more time consuming.

The choice of the μSI-LOV technique enabled to easily handle solid particles (sorbent) inside a flow system and carry out the measurement directly at the beads surface, displaying a relatively good repeatability.

The option to use the bidentate 3,4-HPO ligand, as reagent immobilized in a solid support, enabled to reduce the number of analytical steps, and reduce the reagent consumption, being the solid material reused in successive cycles.

The described μSI-LOV-SPS method was a contribution to the development of an automatized method for the quantification of the NTBI in serum samples. To fully validate the method for the NTBI determination in human serum it is still necessary to analyse a higher number of human serum samples. Anyway, the results presented in this work indicate that the procedure is efficient to discriminate between NTBI and the iron linked to transferrin.

References

1. World Health Organization. Iron Deficiency Anaemia: Assessment, Prevention and Control. Geneva: World Health Organization. Geneva, Switzerland: World Health Organization. 2001.

2. Theil EC, Chen H, Miranda C, Janser H, Elsenhans B, Núñez MT, et al. Absorption of iron from ferritin is independent of heme iron and ferrous salts in women and rat intestinal segments. J Nutr. 2012 Mar 1;142(3):478–483.

3. Ito S, Ikuta K, Kato D, Shibusa K, Niizeki N, Tanaka H, et al. Non-transferrin-bound iron assay system utilizing a conventional automated analyzer. Clin Chim Acta. 2014;437:129–135.

4. Franke GN, Kubasch AS, Cross M, Vucinic V, Platzbecker U. Iron overload and its impact on outcome of patients with hematological diseases. Mol Aspects Med. 2020;75:100868.

5. Garbowski MW, Ma Y, Fucharoen S, Srichairatanakool S, Hider R, Porter JB. Clinical and methodological factors affecting non-transferrin-bound iron values using a novel fluorescent bead assay. Transl Res. 2016;177:19-30.e5.

6. Patel M, Ramavataram DVSS. Non transferrin bound iron: Nature, manifestations and analytical approaches for estimation. Indian J Clin Biochem. 2012;27(4):322–332.

7. Gosriwatana I, Loreal O, Lu S, Brissot P, Porter J, Hider RC. Quantification of non-transferrin-bound iron in the presence of unsaturated transferrin. Anal Biochem. 1999;273(2):212–220.

8. Matos LC, Batista P, Monteiro N, Heriques P, Girão F, Carvalho A de. Genetic Diseases Associated with Iron Overload. Med Interna - Rev Soc Port Med Interna. 2012;48–56.

9. Gouveia S, Ribeiro C, Carrilho F. Sobrecarga de ferro e diabetes mellitus. Rev Port Endocrinol Diabetes e Metab. 2014;9(1):74–78.

10. Evans RW, Roozina AE, Ae R, Zarea A, Chiara AE, Ae R, et al. Nature of non-transferrin-bound iron: studies on iron citrate complexes and thalassemic sera Abbreviations CB-Sepharose Cibacron blue-Sepharose Deferiprone 1,2-Dimethyl-3-hydroxypyridin-4-one DFO Desferrioxamine EPR Electron paramagnetic resonance FO Ferrioxamine HEDTA Hydroxyethylethylenediaminetriacetic acid HEIDA 2-Hydroxyethyliminodiacetic acid. J Biol Inorg Chem. 2008;13:57–74.

11. Makino T, Nakamura K, Takahara K. Potential problems in the determination of serum non-

transferrin-bound iron using nitrilotriacetic acid and ultrafiltration. Clin Chim Acta. 2014 Feb 15;429:12–13.

12. Jacobs EMG, Hendriks JCM, Van Tits BLJH, Evans PJ, Breuer W, Ding YL, et al. Results of an international round robin for the quantification of serum non-transferrin-bound iron: Need for defining standardization and a clinically relevant isoform. Anal Biochem. 2005;341(2).

13. Burgess J, Rangel M. Hydroxypyranones, hydroxypyridinones, and their complexes. Vol. 60, Advances in Inorganic Chemistry. 2008. 167–243 p.

14. Suárez R, Mesquita RBR, Rangel M, Cerdà V, Rangel AOSS. Iron speciation by microsequential injection solid phase spectrometry using 3-hydroxy-1(H)-2-methyl-4-pyridinone as chromogenic reagent. Talanta. 2015;133:15–20.

15. Mesquita RBR, Suárez R, Cerdà V, Rangel M, Rangel AOSS. Exploiting the use of 3,4-HPO ligands as nontoxic reagents for the determination of iron in natural waters with a sequential injection approach. Talanta. 2013;108:38–45.

16. Mesquita RBR, Moniz T, Miranda JLA, Gomes V, Silva AMN, Rodriguez-Borges JE, et al. Synthesis and characterization of a 3-hydroxy-4-pyridinone chelator functionalized with a polyethylene glycol (PEG) chain aimed at sequential injection determination of iron in natural waters. Polyhedron. 2015;101:171–178.

17. Miranda JLA, Mesquita RBR, Nunes A, Rangel M, Rangel AOSS. Iron speciation in natural waters by sequential injection analysis with a hexadentate 3-hydroxy-4-pyridinone chelator as chromogenic agent. Talanta. 2016;148:633–640.

18. Ruzicka J. Lab-on valve: Universal microflow analyzer based on sequential and bead injection. Analyst. 2000;125(6):1053–1060.

19. Vidigal SSMP, Tóth I V., Rangel AOSS. Sequential injection lab-on-valve system for the on-line monitoring of hydrogen peroxide in lens care solutions. Microchem J. 2009;91(2):197–201.

20. Santos IC, Mesquita RBR, Rangel AOSS. Micro solid phase spectrophotometry in a sequential injection lab-on-valve platform for cadmium, zinc, and copper determination in freshwaters. Anal Chim Acta. 2015;891:171–178.

21. Mesquita RBR, Rangel AOSS. A review on sequential injection methods for water analysis. Anal Chim Acta. 2009;648(1):7–22.

22. Vidigal SSMP, Tóth I V., Rangel AOSS. Sequential injection lab-on-valve platform as a miniaturisation tool for solid phase extraction. Anal Methods. 2013;5(3):585–597.

23. Lentner C. Geigy scientific tables. 8th ed. Ciba-Geigy, editor. Vol. 3, Physical Chemistry,

Composition of Blood, Hematology, Somatometric Data. Basle, Switzerland; 1984. 359 p.

24. Covington AK, Robinson RA. References standards for the electrometric determination, with ion-selective electrodes, of potassium and calcium in blood serum. Anal Chim Acta. 1975;78(1):219–223.

25. Hoppe JD, Scriba PC, Klüter H. 5 Human Albumin. Transfus Med Hemotherapy. 2009;36(6):399.

26. Welch S. Transferrin: The Iron Carrier. CRC Press; 1992. 304 p.

27. Currie LA. Nomenclature in Evaluation of Analytical Methods Including Detection and Quantification Capabilities (IUPAC Recommendations 1995). Int Union Pure Appl Chem. 1995;67:1699–1723.

28. Jacobs EMG, Hendriks JCM, Van Tits BLJH, Evans PJ, Breuer W, Ding YL, et al. Results of an international round robin for the quantification of serum non-transferrin-bound iron: Need for defining standardization and a clinically relevant isoform. Anal Biochem. 2005 Jun 15;341(2):241–250.

Chapter 7

General Conclusions

7.1 General Conclusions

This thesis had the objective of developing new flow-based methods for iron and iodine quantification in complex matrices samples (food and biological samples); the multi-syringe and μSI systems proved to be versatile and valuable tools for the development of new methodologies to accommodate all the in-line sample treatment and detection.

A chip-based spectrofluorimetric method was proposed for the determination of total iodine in supplement samples (Chapter 3). The use of a multi-syringe flow system with an in-line UV digestion step demonstrated to be an advantageous process for organo-iodine decomposition. No pre-treatment steps were required, leading to a reduction in reagents consumption and timesaving. One of the main goals was the automation for total iodine determination, leading to a lower operator influence and reagents manipulation. The use of a chip-multi-syringe apparatus flow system combined with spectrofluorimetric detection made this method more sensitive than the classical approach of the Sandell-Kolthoff reaction for iodine determination.

The developed methodologies for iron determination using μSI systems allowed to use different ligands as chromogenic and less toxic reagents (Chapters 4, 5 and 6). The hydroxypyridinone ligands were found as promising to be used as colorimetric reagents for iron(III) determination, in aqueous and biological samples. The study of bidentate and hexadentate ligands, as reagents, reinforced the potential application of these ligands in the monitorization of iron(III), in natural water and serum samples (Chapters 4, 5 and 6).

One of the objectives, transversal to all Chapters, was to minimise the samples off-line treatments; this was successfully achieved by implementing an in-line UV digestion step (in Chapter 3) and solid phase extraction processes (Chapters 4 and 6).

Aiming to reduce sample and reagents volume, a μSI-LOV technique was chosen (Chapter 4 and 6). The detection was successfully performed directly on the solid phase surface, packed in the flow cell, using a solid material for matrix elimination and in-line iron(III) pre-concentration. The iron(III) determination in natural waters, described in Chapter 4, was attained with a solid phase spectrometry (SPS) method, using a NTA (nitrilotriacetic acid) resin column. The work described in Chapter 6 was a contribution to the development of a methodology for the NTBI quantification with the use of a bidentate 3,4–HPO ligand functionalized solid phase. Combining the μSI-LOV technique with a SPS approach, using these functionalized beads, allowed to analyse a complex matrix sample (serum), and quantify NTBI without pre-treatments steps and reduced reagent consumption. Again, the choice of the μSI-LOV technique proved to be a valuable tool for method automation, leading to lower operator influence.

7.2 Suggestions for future work

Several other potentialities could be explored, especially considering the advantages of a μSI-LOV system with a solid-phase extraction approach. Functionalized beads could be used for different analytes quantification and application to various analytical fields. A 3,4–HPO ligand, as a chromogenic reagent, could be used to functionalize a solid phase composed of beads with a higher diameter. These would allow having less pressure in the flow cell with a packed column and allow to perform the bead injection technique, ensuring a more efficient matrix elimination.

The ability to eliminate sample matrix and its interference components is crucial when analyte determination, without pre-treatment steps, is intended. The application of an in-line process for the elimination of other complex biological matrices could be attained with developed methods, using μSI-LOV and multi-syringe systems.

The development of an improved multi-syringe method for total iodine determination in different complex samples analysis, as urine and breast milk, could be explored. The different matrix interference components could be eliminated using an improved method with additional in-line processes.

So, the developed methods using μSI and multi-syringe systems can always be improved, giving new valuable contributions to the current demands in bioanalytical sciences for automation and rapid screening and diagnostics.

List of Publications and Communications

Papers in international scientific journals with referees

Joana L. A. Miranda, Raquel B. R. Mesquita, Ana Nunes, Maria Rangel, António O. S. S. Rangel, *"Determination of iron(III) in water samples by microsequential injection solid phase spectrometry using an hexadentate 3-hydroxy-4-pyridinone chelator as reagent"*, Talanta 191 (2019) 409 – 414. https://10.1016/j.talanta.2018.08.063

Tânia Moniz, Luís Cunha-Silva, Raquel B. R. Mesquita, Joana L. A. Miranda, André M. N. Silva, Ana M. G. Silva, António O. S. S. Rangel, Baltazar de Castro, Maria Rangel, "*New hydrophilic 3-hydroxy-4-pyridinone chelators with ether-derived substituents: Synthesis and evaluation of analytical performance in the determination of iron in waters"*, Polyhedron 160 (2019) 145 – 156. https://10.1016/j.poly.2018.12.005

Communications in international scientific symposiums

Oral communications

Joana L. A. Miranda, Raquel B. R. Mesquita, Ana Nunes, Maria Rangel, António O. S. S. Rangel, *"Measurement of iron (III) in waters by microsequential injection solid phase spectrometry using an hexadentate 3-hydroxyl- 4-pyridinone chelator as a colour reagent"* in the 21st International Conference on Flow Injection Analysis and Related Techniques, September 2017, St Petersburg, Russia.

Joana L. A. Miranda, Edwin Palacio, Raquel B. R. Mesquita, José M. Estela, Víctor Cerdà, António O. S. S. Rangel, *"A miniaturized chip in a multi-syringe flow system for spectrofluorimetric determination of iodide in urine samples"* in the XXIV Encontro Luso-Galego de Química, November 2018, Porto, Portugal.

Poster presentations

Joana L. A. Miranda, Edwin Palacio, Raquel B. R. Mesquita, José M. Estela, Víctor Cerdà, António O. S. S. Rangel, *"Spectrofluorimetric determination of iodide in urine samples without pretreatment using a miniaturized analyzer chip in a multi-syringe flow system"*, in the 14th International Conference on Flow Analysis, 2-7 December 2018, Bangkok, Thailand.

Communications in national scientific symposiums

Oral communications

Joana L. A. Miranda, Raquel B. R. Mesquita, Andreia Leite, André Silva, Maria Rangel, António O. S. S. Rangel, *"Study of 3,4–Hydroxypyridinones Functionalised Beads for Iron(III) Determination in a Microsequential Injection Solid Phase Spectrometry Mode"*, poster pitch in Analítica 2018, in the 9th Meeting of Division of Analytical Chemistry of SPQ, March 26-27 2018, Porto, Portugal.

Poster presentations

Joana L. A. Miranda, Raquel B. R. Mesquita, Andreia Leite, André Silva, Maria Rangel, António O. S. S. Rangel, *"Study of 3,4–Hydroxypyridinones Functionalised Beads for Iron(III) Determination in a Microsequential Injection Solid Phase Spectrometry Mode"*, in Analítica 2018, in the 9th Meeting of Division of Analytical Chemistry of SPQ, March 26-27 2018, Porto, Portugal.

Joana L. A. Miranda, Edwin Palacio, Raquel B. R. Mesquita, José M. Estela, Víctor Cerdà, António O. S. S. Rangel, *"Spectrofluorimetric determination of iodine in urine samples with on-line UV photooxidation using a miniaturized analyzer chip in a multi-syringe flow system"*, in the XXVI National Meeting of Portuguese Chemical Society (SPQ), July 24-26 2019, Porto, Portugal.

Joana L. A. Miranda, Raquel B. R. Mesquita, António O. S. S. Rangel, "Development and application of automatic and miniaturized methods for iodine and iron quantification for thyroid-related disorders", in Meeting Ciência' 20, Meeting of Science and Technology in Portugal, November 3-4 2020, Lisboa, Portugal.